IMPACTS OF HIGH-FAT DIET AND GENOTYPE ON BLOOD-BRAIN BARRIER AND SYNAPTIC INTEGRITY IN MOUSE CEREBRAL CORTEX: AN EXPLORATION OF PERK PATHWAY

A THESIS SUBMITTED TO

THE GRADUATE SCHOOL OF ENGINEERING AND SCIENCE

OF BILKENT UNIVERSITY

IN PARTIAL FULFILLMENT OF THE REQUIREMENTS FOR

THE DEGREE OF

MASTER OF SCIENCE

IN

NEUROSCIENCE

By

Büşranur Şeker

September 2024

IMPACTS OF HIGH-FAT DIET AND GENOTYPE ON BLOOD-BRAIN BARRIER AND SYNAPTIC INTEGRITY IN MOUSE CEREBRAL CORTEX: AN EXPLORATION OF PERK PATHWAY

By Büşranur Şeker

September 2024

We certify that we have read this thesis and that in our opinion it is fully adequate, in scope and in quality, as a thesis for the degree of Master of Science.

_____

Michelle Marie Adams (Advisor)

_____

Burcu Ayşen Ürgen

_____

Elif Tuğce Karoğlu Eravşar

Approved for the Graduate School of Engineering and Science

_____

Orhan Arıkan Director of the Graduate School

ABSTRACT

IMPACTS OF HIGH-FAT DIET AND GENOTYPE ON BLOOD-BRAIN BARRIER AND SYNAPTIC INTEGRITY IN MOUSE CEREBRAL CORTEX: AN EXPLORATION OF PERK PATHWAY

Büşranur Şeker

M.Sc. in Neuroscience

Advisor: Michelle Marie Adams

September 2024

High-fat diet intake can induce hyperlipidemia and result in cognitive decline by causing endoplasmic reticulum stress, decreased blood-brain barrier, and synaptic integrity. The protein kinase R-like endoplasmic reticulum kinase (PERK) pathway is one of the arms of the unfolded protein response, which is activated by endoplasmic reticulum stress. The PERK inhibits the global protein translation while allowing the translation of certain proteins that are involved in inflammation and apoptosis. Due to its apoptotic properties, it is thought that the PERK pathway causes neurodegeneration.

To study the effects of hyperlipidemia, a high-fat diet-fed Apoe knock-out mice model ($Apoe^{-/-}$) is appropriate. Knocking out the Apoe in mice makes the animal model more prone to high-fat diet-induced hyperlipidemia. In the cerebral cortex of these animals, endoplasmic reticulum stress, blood-brain barrier, and synaptic integrity markers are checked at protein and mRNA levels. No changes are observed in the PERK pathway

markers besides phosphorylated eukaryotic Initiation Factor 2α. Additionally, there is a significant increase in blood-brain barrier marker Claudin-5 levels in Apoe$^{-/-}$ mice fed with a high-fat diet. There is also no significant change in synaptic integrity markers. In the second part, the effects of the PERK pathway inhibition are checked with integrated stress response inhibitor and GSK2606414 in the high-fat diet-fed Apoe$^{-/-}$ mice cerebral cortex. There are no significant alterations in BBB and synaptic integrity when the animals are injected with inhibitors.

In conclusion, this study investigates the effects of high-fat diet induced hyperlipidemia in the cerebral cortex of Apoe$^{-/-}$ mice on ER stress, blood-brain barrier, and synaptic integrity. In the cerebral cortex region, the PERK pathway-related ER stress is not observed, and synaptic integrity remained unchanged while the blood-brain barrier is affected. Moreover, the effects of the PERK pathway inhibition are researched, and there is no inhibition effect observed in the cerebral cortex region.

***Keywords**:* High fat Diet, Apoe$^{-/-}$ Mice, ER Stress, BBB and Synaptic integrity, PERK pathway inhibition

ÖZET

YÜKSEK YAĞLI DİYET İLE GENOTİPİN FARENİN SEREBRAL KORTEKSİNDE KAN-BEYİN BARİYERİ VE SİNAPTİK BÜTÜNLÜĞE ETKİLERİ: PERK YOLAĞININ ARAŞTIRILMASI

Büşranur Şeker

M.Sc. in Neuroscience

Danışman: Michelle Marie Adams

Eylül 2024

Kanda dolaşan kolesterol ve trigliseritin artışı hiperlipidemiye neden olur. Yüksek yağlı diyetin yol açtığı hiperlipidemi endoplazmik retikulum (ER) stresine, kan-beyin bariyerinin ve sinaptik bütünlüğünün bozulmasına sebep olarak bilişsel bozulmalar görülür. Protein kinaz R benzeri endoplazmik retikulum kinaz (PERK) yolağı, ER stresi ile aktive edilen katlanmamış protein yanıtı kollarından biridir. PERK apoptotik proteinlerinin translasyonuna yol açarken global protein translasyonunu engeller. Apoptotik özelliklerinden dolayı PERK yolağının nörodejenerasyona neden olduğu düşünülmektedir.

Bu çalışmada hiperlipideminin etkilerini incelemek için yüksek yağlı diyetle beslenen $Apoe^{-/-}$ fare modeli kullanıldı. Farelerde apolipoprotein E'nin (ApoE) devre dışı bırakılması fareleri yüksek yağlı diyetin neden olduğu hiperlipidemiye yatkın hale getirir. Bu hayvanların serebral korteksinde ER stres, kan-beyin bariyeri ve sinaptik bütünlük

belirteçleri protein ve mRNA düzeylerinde kontrol edildi. PERK yolağı belirteçlerinden fosforile olmuş ökaryotik inisiyasyon faktörü 2α dışında herhangi bir belirteçte belirgin bir değişiklik gözlenmedi. Ayrıca, yüksek yağlı diyetle beslenen Apoe$^{-/-}$ farelerinde kan-beyin bariyeri belirteci claudin-5 düzeylerinde önemli bir artış olduğu gözlemlendi. Sinaptik bütünlükte bir değişiklik gözlemlenmedi. Çalışmanın ikinci kısmında, yüksek yağlı diyetle beslenen Apoe$^{-/-}$ farelerin serebral korteksinde PERK yolağı inhibisyonunun etkileri entegre stres tepkisi inhibitörü ve GSK2606414 ile kontrol edildi. Hayvanlar inhibitör enjekte edildiğinde belirgin bir değişiklik gözlemlenmedi.

Sonuç olarak bu çalışma, Apoe$^{-/-}$ farelerin serebral korteksinde yüksek yağlı diyet kaynaklı hiperlipideminin ER stresi, kan-beyin bariyeri ve sinaptik bütünlük üzerindeki etkilerini araştırdı. Serebral korteks bölgesinde PERK yolağına bağlı ER stresi ve sinaptik bütünlükte değişiklik gözlemlenmezken, kan-beyin bariyeri bütünlüğü etkilenmiştir. Ayrıca PERK yolağı inhibisyonunun etkileri de araştırılmıştır. Serebral korteks bölgesinde herhangi bir inhibisyon etkisi gözlemlenmemiştir.

Anahtar Kelimeler: Yüksek yağlı diyet, Apoe$^{-/-}$ fare, ER stres, kan-beyin bariyeri ve sinaptik bütünlük, PERK yolağı inhibisyonu

To all the women in science…

Acknowledgments

Firstly, I want to thank my supervisor, Dr. Michelle Marie Adams. I'm grateful for her supervision over the years. I grow a lot as a scientist thanks to her knowledge and supervision.

I would like to express my gratitude to my jury members, Dr. Burcu Ayşen Ürgen and Dr. Elif Tuğçe Karaoğlu Eravşar, for taking the time to attend my thesis defense.

I would like to thank Gamze Aykut for helping us in our animal experiments. I would like to express my utmost gratitude to Adams lab members Fulya Kızıldağ, Naciye Bozkurt, Narin Ilgım Ardıç Avcı, Naz Mengi Çamur, Sanem Sobacı, Seçil Gülden, Serena Sevdiye Aktürk, and Zeynep Karaer.

I want to thank Naz especially; her guidance helped me get through my master's. Working with her on the same project was my luck, and I cannot be thankful enough for it. I also want to thank Fulya; I could not imagine a better lab partner. Working alongside her was the highlight of my master's.

I would like to thank my family members. My mom and brothers helped and supported me throughout my education; I am lucky to have them as my family. I cannot express my love and gratitude for my little nephews, Pars and Kayra enough. They are the light of my life; their little smiles bring happiness to me when I am at my lowest. I want to thank my grandparents, Fatma and Mehmet. They were the best grandparents a child could ever dream of; I am where I am today because of their love and support.

I want to thank my friends, Sanem and Barış, their friendship helped and guided me in my life. I also want to thank Bilgesu Hezen for being such a good friend to me for over 17 years. She listened to me rambling about my problems non-stop for all my life, I could not be here today without her support and friendship.

I want to thank my cat family, Ceviz, Venüs, Tarçın and Tuzot. Their unconditional love has given me the strength to continue in the times I was so near to giving up everything.

Finally, I want to express my thanks to my partner in crime Seçil Gülden. Whatever I say would be insufficient to express how much she helped me not only in my studies but also in every aspect of my life, so I want to use a song lyric instead: *"I had the time of my life fighting dragons with you."*

This research is funded by the Scientific and Technological Research Council of Turkey (TUBITAK) under grant number 220S079.

Table of Contents

List of Figures

List of Tables

List of Abbreviations

AMPA: α-amino-3-hydroxy-5-methyl-4-isoxazole propionic acid

ANOVA: Analysis of variance

Apo: Apolipoprotein

ApoE: Apolipoprotein E

Apoe$^{-/-}$: Apoe knockout

ATF4: Activating transcription factor 4

ATF6: Activating transcription factor 6

BBB: Blood-brain barrier

BiP: Binding immunoglobulin protein

BSA: Bovine serum albumin

CHOP: CCAAT-enhancer-binding protein homologous protein

CMT: Carrier-mediated transport

eIF2: eukaryotic Initiation Factor 2

ER: Endoplasmic reticulum

ERAD: ER-associated degradation

GABA: Gamma-aminobutyric acid

GADD34: Growth arrest and DNA damage-inducible protein

GAPDH: glyceraldehyde-3-phosphate dehydrogenase

GCN2: General control nonderepressible 2

GDP: Guanosine diphosphate

GTP: Guanosine triphosphate

HDLs: High-density lipoproteins

HMGCR: 3-hydroxy-3-methyl-glutaryl-coenzyme A reductase

IDLs: Intermediate-density lipoproteins

IL-1ß: Interleukin-1ß

IP: Intraperitoneal injection

ISR: Integrated stress response

ISRIB: ISR inhibitor

JAMs: Junction-adhesion molecules

LDLs: Low-density lipoproteins

Marvel D3: Marvel domain containing 3

NMDA: N-methyl-D-aspartate

NVU: Neurovascular unit

PBS: Phosphate-buffered saline

PERK: Protein-kinase R like Endoplasmic Reticulum Kinase

p-eIF2α: Phosphorylated eIF2α

PI: Phosphatase inhibitor

PIC: Protease inhibitor cocktail

PKR: Protein kinase R

p-PERK: Phosphorylated PERK

PSD-95: Post-synaptic density 95

PVDF: Polyvinylidene difluoride

RIPA: Radioimmunoprecipitation assay

RMT: Receptor-mediated transportation

RPL13A: Ribosomal Protein L13a

SDS-PAGE: Sodium dodecyl sulfate-polyacrylamide gel electrophoresis

SNARE: Soluble N-ethylmaleimide-sensitive factor activating protein receptor

SREBP: Sterol regulatory element binding protein

TBS: Tris-buffered saline

TBS-T: TBS-Tween

TG: Triacylglycerols

t-RNA: transfer ribonucleic acid

uORF: short upstream open reading frame

UPR: Unfolded protein response

VEGF: Vascular endothelial growth factor

VLDLs: Very low-density lipoproteins

ZOs: Zonula occludens

CHAPTER 1

INTRODUCTION

1.1 Hyperlipidemia

One of the main building blocks of living beings is lipids. There are two groups of lipids, where they are formed mainly with fatty acids like triacylglycerols and where they are formed mainly with steroids like cholesterols [1]. The metabolism of these lipids is tightly regulated, and disruptions in it might cause health problems. Hyperlipidemia is one such health deficit that occurs when the cholesterol or triglyceride levels circulating in the blood increase above a threshold [2].

1.1.1 Lipids

There are various types of lipids that differ in metabolism mechanisms. Cholesterols, triacylglycerol, and phospholipids are the crucial lipids found in the body [3]. They have their own importance for human health.

Cholesterol is a steroid-based lipid and resides in animal tissues in two forms: esterified and free. Free cholesterol can be found in membranes, whereas esterified cholesterol can be found in the plasma [4]. When cholesterol levels decrease in the plasma, the sterol regulatory element binding protein (SREBP) gets activated and migrates to the nucleus. There, SREBP binds to the sterol regulatory element of the reductase gene, which increases the transcription of 3-hydroxy-3-methyl-glutaryl-coenzyme A reductase (HMGCR). This is important since HMGCR is a catalyzer for cholesterol synthesis. In the event of

cholesterol increase in the plasma, SREBP stays inactive, and the remaining SREBP found in the nucleus gets degraded, which closes off the cholesterol synthesis [5].

Many transporters are involved in the cholesterol transportation. Some of them are engaged in the uptake of cholesterol, and some are to promote the efflux of unesterified cholesterol [6]. The esterification of cholesterol is vital for the storage and transportation of cholesterol, as unesterified/free cholesterol is toxic to the body [7]. Intracellular cholesterol gets esterified at the Endoplasmic Reticulum (ER) with acetyl-coenzyme A acyltransferase 2. After that, it is compacted into lipoproteins [8].

Triacylglycerols (TG) are another lipid type that is important for the body. TGs are vast energy providers to the mammalian body [9]. Dietary TGs are taken up by enterocytes after hydrolyzing them with pancreatic lipases to monoglycerides and free fatty acids and packed into lipoproteins [10].

Phospholipids are lipids that are composed of fatty acids. They are mainly derived from glycerol [11]. They have a hydrophilic head and a hydrophobic tail, which makes them perfect structural lipids for cell membranes [12]. Moreover, due to their amphipathic features, they play an essential role in the transportation of lipids. In lipoproteins, the hydrophobic core is enveloped with phospholipids to create the hydrophilic surface [13].

1.1.2 Lipoproteins

Lipids are hydrophobic by nature, and in order to travel through blood, they need to be coated with hydrophilic components. Therefore, lipoproteins contain both lipids and proteins. At the core of the structure of lipoproteins, cholesteryl esters and triacylglycerols reside. The hydrophilic surface that coats the hydrophobic part contains apolipoproteins

(peripheral and integral), unesterified lipids, and phospholipids [14]. There are different classes of lipoproteins, such as chylomicrons, very low-density lipoproteins, intermediate-density lipoproteins, low-density lipoproteins, and high-density lipoproteins [15]. Each class of lipoproteins differs in terms of size, lipid, and apolipoprotein content. Apolipoproteins not only play structural roles but also act as ligands for lipoprotein receptors and sometimes might activate or inhibit enzymes crucial for lipid metabolism [16].

Chylomicrons are the largest lipoproteins. They transport the dietary cholesterol and TG [17]. It contains apolipoproteins A-I, A-II, A-IV, A-V, B-48, C-II, C-III, and E. Apolipoprotein B-48 must be present in every chylomicron as they are the structural proteins [18]. The size of the chylomicrons depends on the consumed fat, and they have a half-life of less than an hour. After that, they degraded into chylomicron remnants [19]. As the chylomicron remnants are small, they can cross the endothelium and accumulate. This accumulation can contribute to cardiovascular diseases [20].

Very low-density lipoproteins (VLDLs) are responsible for the transportation of TGs. It contains apolipoprotein(apo) B-100, C-I, C-II, C-III, and E [21]. After it is synthesized by the liver and starts circulation, it achieves its mature form by getting apo C and E along with cholesterol esters from high-density lipids (HDLs) [22]. When delipidation of VLDLs occurs, they are converted into intermediate-density lipoproteins (IDLs). Some IDLs circulating are transformed into low-density lipoproteins (LDLs), and others are directly removed from the plasma [23].

Low-density lipoproteins are the major lipoproteins that are responsible for carrying cholesterol. It contains apolipoprotein B-100 [24]. The small, dense LDL particles tend to

accumulate as they have a low affinity to LDL receptors for uptake [25]. They also tend to get oxidized easily and stimulate inflammation in their oxidized form [26].

High-density lipoproteins are also carriers of cholesterol. Apolipoprotein A-I is the structural apolipoprotein of the HDLs [27]. HDLs are highly important because they carry cholesterol, not from the liver to other tissues but rather from peripheral tissues to the liver, through a process called reverse cholesterol transport [28].

1.1.3 Exogenous and Endogenous Lipid Pathways

The exogenous lipid pathway deals with lipids coming from diet. These lipids first undergo pancreatic lipase-mediated lipolysis, then emulsified by bile acids in the small intestine [29]. The fatty acids and monoacylglycerols come from the lipolysis of TGs, and the free cholesterol and fatty acids come from the hydrolyzation of cholesterol esters and are taken up by intestinal enterocytes. In the enterocytes, chylomicrons are formed by the re-esterification of fatty acids and cholesterol. Then, the chylomicron is secreted into the intestinal lymphatics [30]. Chylomicrons get apolipoprotein C from HDLs, and with this act, activation of lipoprotein lipase by apolipoprotein C-II occurs. As a result, fatty acids and glycerol from the TGs are absorbed by the tissues, whereas phospholipids, free cholesterol, and apolipoprotein C are taken up by HDLs. The remaining particles become chylomicron remnants [31].

The endogenous lipid pathway is for transporting TGs and cholesterol that is synthesized in the liver to the peripheral tissues. The free cholesterol is delivered with chylomicron remnants and newly synthesized triacylglycerol from VLDLs to be sent into circulation [32]. To form a mature VLDL, nascent VLDL takes apolipoproteins A, C, and E from HDL

[33]. After TGs and cholesterol are delivered to the peripheral tissues, VLDL remnants form. Then, as the VLDL remnants, IDLs, form, they are either converted into LDLs or removed from circulation [31]. The conversion to LDL is mediated by the activity of the LDL receptors. If the activity of the LDL receptors is high, then the production of LDL is low [34]. HDLs, which are synthesized in the liver, become mature and circulate. Free cholesterol is taken up by HDL and gets esterified, which blocks cholesterol from being released and delivered back to the liver [35].

1.1.4 High-Fat Diet

The term hyperlipidemia usually reflects the high level of LDL in the plasma. When the clearance of LDL by its receptor is defective, LDL levels increase [36], [37]. This might have many causes, like genetic disorders, alcohol consumption, obesity, and such [38]. Diet is one of those causes; increasing the intake of dietary saturated fatty acids causes hyperlipidemia [39].

Hyperlipidemia can cause diseases like atherosclerosis and cardiovascular diseases. It can also cause impairments in neuronal functions [40]. The high-fat diet causes increased levels of circulating lipids, which causes hyperlipidemia, resulting in decreased blood-brain barrier (BBB) integrity [41]. Though prolonged high-fat diet consumption causes neurodegeneration, short-term intake can also cause cognitive deficits [42].

1.2 Apoe Knockout Mice as Hyperlipidemia Model

Mice are widely used animal models due to its many advantages. Besides genetic similarity to humans, their life cycle are suitable for studying many timeframe. They can develop

from 19 to 21 days, and by 7 to 8 weeks, they get sexually mature. Among these, they are smaller and have a short generation time, making them easier to maintain than other mammals [43].

There are also differences between humans and mice. For example, The lipid metabolism in mice differs from that of humans in multiple ways. In humans, 75% of the plasma cholesterol is in the form of LDL [44]. Meanwhile, in mice, the plasma cholesterol is mainly carried by HDL [45]. This is mainly due to the absence of cholesterol ester transferase in mice [46]. This enzyme transfers cholesterol from HDL to LDL and VLDL, and in the absence of it, HDLs are not depleted from cholesterol and continue their function as the leading carrier of cholesterol [47], [48]. There is also a difference in the content of the non-HDL cholesterol fraction. VLDL and chylomicron remnants are the main ones, rather than LDLs [49]. Moreover, apolipoprotein B is active in the liver and the small intestine, resulting in more efficient and faster clearance of LDL [48]. With all that, mice somehow show resistance toward hyperlipidemia [50]. To study hyperlipidemia in mice, in 1992, Apoe knockout ($Apoe^{-/-}$) mice have been produced [51]. Apolipoprotein E (ApoE) is a vital ligand that binds to cell surface LDL receptor and chylomicron remnant receptor with high affinity. This binding allows the clearance of VLDL and chylomicron remnants from the circulation [52]. Thus, the deficiency of this protein holds back the clearance of these remnants and results in a shift towards VLDL and chylomicron remnants from HDLs [53]. Moreover, feeding these mice with a high-fat diet causes hyperlipidemia due to increased VLDL and chylomicron remnants [54].

1.3 Endoplasmic Reticulum

In the cells, most of the protein synthesis and transportation occurs in the organelle called endoplasmic reticulum (ER). Proteins that ER, Golgi, plasma membrane, and lysosome as their determined locations mostly translated on the ribosomes located on the ER membrane [55]. The ER plays more of a role in the cell than protein synthesis; it is involved in the folding and maturation of more than a third of all proteins [56]. Folding and maturation are crucial for the proteins to achieve their final form. At the ER lumen, proteins go through some post-translational modifications, such as disulfide bond formation, to attain the final three-dimensional shape. There are machineries, such as chaperones, that assist these modifications [57]. Even though these modifications are controlled, the success of protein folding is under 20% [58]. The other proteins are misfolded or sometimes aggregated [59]. The process called ER-associated degradation (ERAD) is for these misfolded or aggregated proteins to be disposed of [60]. Through this process, unfolded proteins are marked for ubiquitylation to target proteins for proteasome and degradation [61].

1.3.1. ER Stress

The increase in the misfolded/aggregated protein causes cell stress. This stress is called ER stress [62]. Under stress conditions, the accumulation of misfolded proteins increases, and the unfolded protein response (UPR) is activated [63]. The first aim of the UPR is to restore the normal function of the ER. To do that, it causes an expansion in the size of the ER and increases the number of ER chaperones by upregulating the transcription [64]. If, with these changes, homeostasis is achieved, the misfolded protein number is decreased, UPR is closed, and the functionality of the ER is restored. However, if UPR is proven insufficient

and the cell undergoes chronic stress, apoptosis or cell death may occur [65].

1.3.1.1 PERK Pathway of the Unfolded Protein Response

The UPR has three major signaling pathways. These are Inositol-Requiring Enzyme 1 α, Protein-kinase R like Endoplasmic Reticulum Kinase (PERK) and Activating Transcription Factor 6 (ATF6). PERK is a membrane-bound protein [66]. In its inactive form, PERK is bound to the Binding immunoglobulin Protein (BiP) [67]. When UPR is activated with increased misfolded proteins, BiP is released from PERK due to its high affinity to misfolded proteins. With the release of BiP, PERK gets activated and auto-phosphorylates itself [68].

When PERK is phosphorylated, it initiates a cascade of events. One of the downstream targets of phosphorylated PERK (p-PERK) is eukaryotic Initiation Factor 2 (eIF2) [69]. eIF2 has 3 subunits; α, β, and γ. γ subunit of eIF2 binds to guanosine diphosphate (GDP) or guanosine triphosphate (GTP) [70]. In its inactive form, eIF2 is bound to GDP, and it becomes active when it is bound to GTP [71]. This exchange of GDP to GTP is facilitated by eIF2B [72]. eIF2 bound to GTP (eIF2-GTP) delivers initiator transfer ribonucleic acid (t-RNA) to ribosomes and forms the 43S pre-initiation complex with 40S ribosomal subunit. This pre-initiation complex recognizes the initiation codon, which allows translation to continue [73]. p-PERK causes the phosphorylation of the alpha subunit of the eIF2. This initiates the integrated stress response (ISR) [74]. Phosphorylated eIF2α (p-eIF2α) causes the inhibition of eIF2B, so the exchange of GDP to GTP does not occur. This halts delivery of the initiator t-RNA; as a result, global protein synthesis is inhibited, which buys time for cells to handle all the misfolded proteins (Fig 1.1) [75], [76].

One of the downstream elements of p-eIF2α is Activating Transcription Factor 4 (ATF4). p-eIF2α causes the selective translation of ATF4 while inhibiting the global protein synthesis [77]. Under normal conditions where eIF2-GTP levels are high, and p-eIF2α levels are low, the translation complex is able to continue the translation, and once it translates the inhibitory short upstream open reading frame (uORF), the translation complex dissociates and stops translation before getting a chance to translate ATF4 [78]. However, under stress conditions, where eIF2-GTP levels are low, and p-eIF2α levels are high, delivery of the reinitiation complex is delayed, and the 40S subunit continues to scan through the uORF without translating inhibitory uORF. And the translation reinitiates at the start codon of ATF4, which results in an increase in ATF4 translation [79]. In the attempt to recover the normal condition of the cell, ATF4 activates and causes an increase in some pro-survival factors, such as ER Chaperones [80]. If the stress conditions are relieved, eif2α phosphorylation will end, as well as PERK inhibition. This inhibition will terminate the ISR [81].

On the other hand, under prolonged stress conditions, ATF4 initiates a pro-apoptotic cascade of events. ATF4 allows the transcription of CCAAT-enhancer-binding protein homologous protein (CHOP) [82]. CHOP also contains uORF, which allows for it to be translated under the inhibited global protein synthesis through a mechanism called ribosomal bypass mechanism, in which inhibitory uORF is scanned through by ribosome and translates CHOP [83]. When the CHOP is upregulated, it causes the activation of apoptotic mechanisms (Fig 1.2) [84]. First of all, the expression of the gene that encodes the anti-apoptotic B-cell lymphoma 2 that blocks cell death is inhibited by CHOP [85]. Moreover, CHOP also activates the growth arrest and DNA damage-inducible protein

(GADD34), and GADD34 causes the dephosphorylation of eIF2α through protein phosphatase 1, thereby allowing the synthesis of pro-apoptotic proteins [86]. Also, CHOP causes caspase-3 activation and if the activation passes the threshold, it would end in cellular death [87].

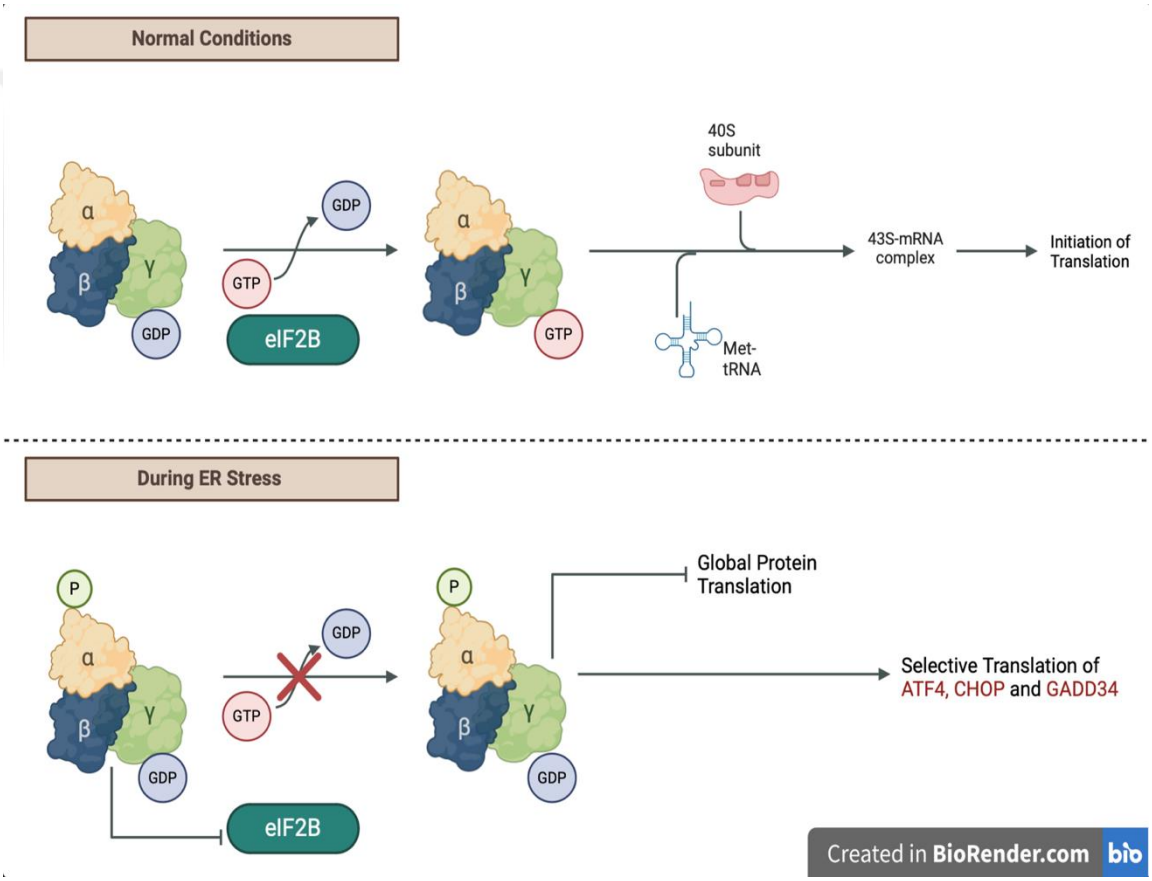

Figure 1.1. eIF2 and eIF2B interaction. The upper part of this scheme represents how eIF2 and eIF2B interact under normal conditions. In normal conditions, eIF2B initiates the activation of eIF2 by providing an exchange of GDP to GTP. GTP-bound eIF2 forms an initiation complex with 40S subunit of ribosome and initiator met-tRNA. This complex

initiates the translation. The lower part of this scheme shows how ER stress and phosphorylation of eIF2 affect the eIF2B and translation. When eIF2 is phosphorylated from its α subunit, it blocks the exchange of GDP-GTP by inhibiting eIF2B. This halts the global protein translation while allowing the selective translation of ATF4, CHOP, and GADD34. The figure is created with BioRender.com.

Excess amounts of misfolded proteins caused by ER stress have been dictated as a pathology in several neurodegenerative diseases. Moreover, apoptosis induced by CHOP results in neuronal cell death, which might contribute to neurodegenerative diseases [88]. ER can detect metabolic changes and excessive nutrients caused by high-fat diet-induced hyperlipidemia, leading to the disruption of ER homeostasis. Disruption in the homeostasis of ER results in ER stress [89].

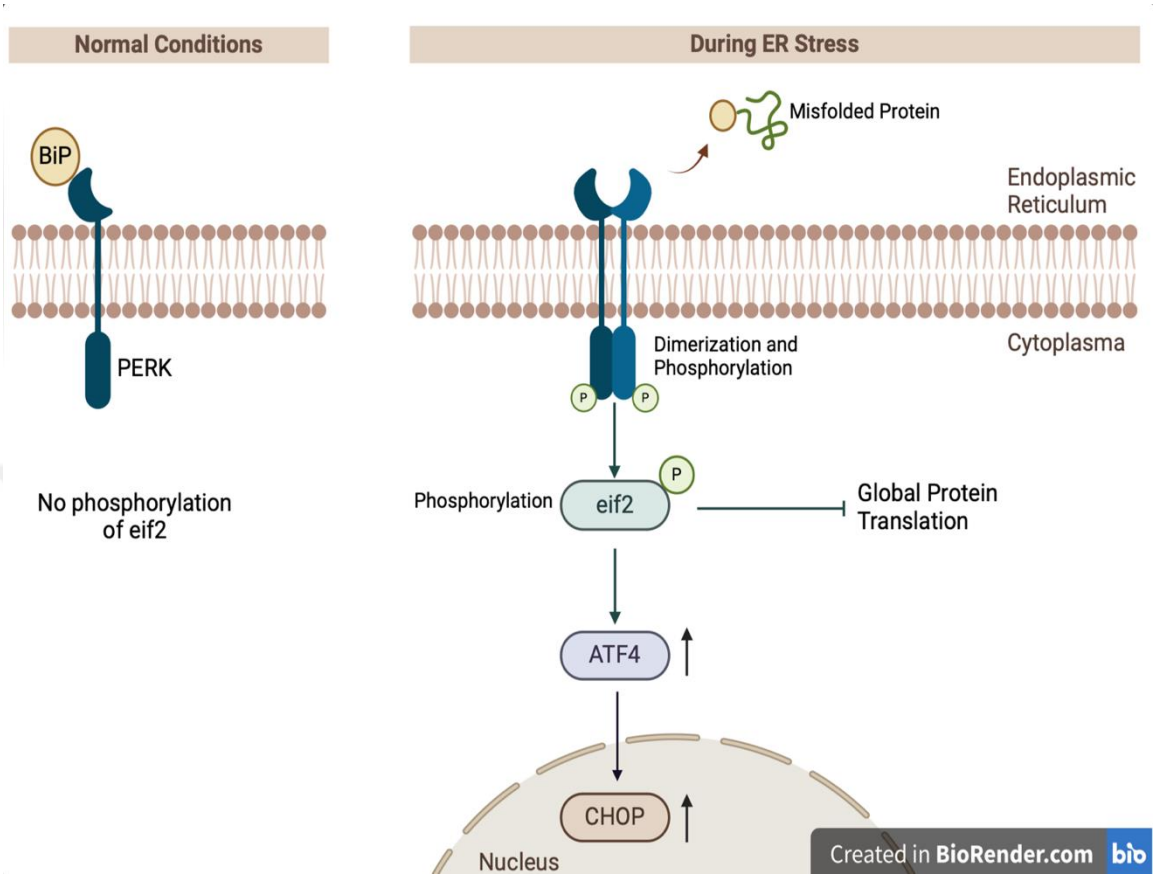

Figure 1.2. The PERK Pathway. The left side of the figure shows the normal state of PERK. Normally, PERK is found in monomer form bound with BiP. The right side of the figure shows the PERK pathway activated with ER Stress. BiP has a high affinity to unfolded proteins; under ER stress, when the unfolded proteins increase, BiP is released from PERK. This initiates the dimerization and phosphorylation of PERK. p-PERK causes the phosphorylation of eIF2 and, therefore, inhibits the global protein translation while selectively upregulating the translation of ATF4. ATF4 when it is upregulated, it activates CHOP. The figure is created with BioRender.com.

1.4 Blood-Brain Barrier

The limited capacity of regeneration requires neurons to have extra protection from the materials circulating in the blood that can harm them. There are many neurotoxins in the blood coming from endogenous sources such as metabolites or exogenous sources. On the other hand, the brain needs nutrients and oxygen to execute the neuronal functions. The blood-brain barrier (BBB) limits the entry of harmful substances while allowing a nutrient exchange between blood and the brain (Fig 1.3) [90].

1.4.1 The Neurovascular Unit

Brain endothelial cells that form the BBB form a unit together with astrocytes, mural cells like pericytes, microglia, neurons, and extracellular matrix components called the neurovascular unit (NVU). Interaction between the components of the NVU is critical for an efficient barrier that protects the brain [91]. Each of these components have their own functions in the NVU.

Pericytes are essential elements of the NVU. They have roles in the maintenance of the integrity of BBB, disposing of toxic derivatives of cellular processes through phagocytosis, and controlling the entrance of the immune cells [92]. Moreover, they can modulate the cerebral blood flow by adjusting the capillary diameter. Pericytes can also synthesize vascular endothelial growth factor (VEGF) and participate in angiogenesis, a process that causes the formation of new blood capillaries [93].

Astrocytes are the glial cells that are abundant in the central nervous system. They have several crucial uses in the brain, such as regulating homeostasis and modulating

neurotransmitter uptake. Its function in the NVU is to conduct the communication between neurons and vasculature [94].

The endothelial cells are the main components of the NVU that serve as a barrier. However, pericytes and astrocytes both can act as defense mechanisms as well in case of damage to the endothelial cells [95]. Through this function, pericytes and astrocytes are also crucial for the protection of the brain.

1.4.2 Tight-Junctions

The brain endothelial cells are firmly connected to each other by the tight junction proteins. They are crucial as they seal the junctions between epithelial cells, sustaining the integrity of the BBB [96]. Tight junction proteins establish cell-to-cell adhesion by connecting the neighboring tight junction proteins. Claudins, occludin and junction-adhesion molecules (JAMs) and cytoplasmic accessory proteins such as cingulin and Zonula occludens-1, -2, -3 (ZO-1, -2, -3) are the main tight-junction proteins [97].

1.4.2.1 Claudins

Claudins have four transmembrane domains with two extracellular loops. Through these loops, they bind to other tight junction proteins, including other claudins on the adjoining endothelial cells. Claudins-1 and -5, along with occludin, are the primary building blocks of the BBB [98]. The scaffolding ZO proteins can arrange the spatial organization of Claudin strands by jointing with the actin proteins in the cytoskeleton [99]. Claudin-5 can regulate the paracellular ionic selectivity and endothelial permeability [100]. Claudin-5 expression is regulated by many pathways and by its interaction with other tight-junction

proteins. For instance, phosphorylation of Claudin-5 decreases its expression [101]. Also, VEGF causes the downregulation of Claudin-5 and increases the BBB permeability [102].

1.4.2.2 Occludin

Occludin, tricellulin, and marvel domain containing 3 (marvel D3) are the tight junctions associated marvel proteins. Tricellulin adjusts the permeability for macromolecules, and marvel D3 has a compensatory role in the sealing of the BBB [103]. Occludin has four transmembrane domains with two extracellular loops. They are integral parts of the selective permeability of the BBB. It can bind to ZO proteins that regulate their trafficking [104]. With Claudins, they can form intramembranous strands that contain fluctuating channels to allow selective diffusion [94].

1.4.2.3. Junctional Adhesion Molecules and Cytoplasmic Accessory Proteins

JAMs are part of the immunoglobulin superfamily that has a single transmembrane domain. The extracellular part has two loops formed by disulfide bonds. They are crucial for cell-to-cell adhesion. Moreover, JAMs are involved in the trafficking of the occludin to the tight-junction proteins. Also, they engage in the transmigration of monocytes upon BBB [105].

The other important proteins in the BBB are cytoplasmic accessory proteins. These proteins create a bridge between cell cytoskeleton and tight-junction proteins [106]. ZO proteins have an actin-binding region at the C-terminus where actin filaments interact. This interaction created by ZO proteins via cingulin between actin and tight junctions like

claudins and occludin is crucial for the structural support of endothelial cells [107].

1.4.3 Transportation Across Blood-Brain Barrier

One of the crucial functions of BBB, besides protection of the neurons from toxins, is to sustain a homeostatic environment using ion channels. It also allows the passage of nutrients that are required by the brain [108]. Moreover, BBB regulates the amount of neurotransmitters by separating the central and peripheral neurotransmitters. Furthermore, it keeps the macromolecules outside of the brain [109]. These functions of the BBB are strictly regulated by the activity of the transportation mechanisms in the BBB. There is passive diffusion, active efflux, carrier-mediated transport, and receptor-mediated transport [94].

1.4.3.1. Passive Diffusion and Active Efflux

Entry to the brain through passive diffusion is dependent on lipid solubility and the molecular weight of the molecules. Also, the area of the polar surface is another limiting factor. Lipid-soluble molecules that have a molecular weight smaller than 400 kDa might diffuse across BBB. The pores that have been formed in the phospholipid bilayer for the diffusion of the molecules have limited sizes. Therefore, molecules that have higher spherical volume than the pore size might not pass to the brain [110].

The active efflux requires ATP to transport substrates. On the blood side of the endothelium membrane of the BBB, there are ATP-driven efflux pumps and ATP-binding cassette proteins. These transporters are for the endogenous metabolites, which can be transported substrate from endothelium to blood, or this transportation might be bidirectional [111].

1.4.3.2. Carrier-mediated Transport and Receptor-mediated Transport

There are some essential nutrients that the brain requires, like glucose, whose entry has been blocked by the BBB. Carrier-mediated transport (CMT) is part of the Solute Carrier Transporters, which enables the transcellular movement of molecules such as amino acids, carbohydrates, fatty acids, and such. These transporters may carry molecules from blood to brain and brain to blood [112].

Although the CMT can carry amino acids, the proteins, due to their size, cannot use as transporters to the brain. In that case, neuroactive peptides, hormones, and growth factors use receptor-mediated transportation (RMT) [113]. There are ligand-specific receptors to which macromolecules bind to promote endocytosis. Macromolecules bind to their receptors, and then they are internalized into endothelial cells, and through the cytoplasm, they are exocytosed to the other side. To avoid degradation by the lysosomal component in the cytoplasm, the endosome and its contents are guided away from the lysosome [114].

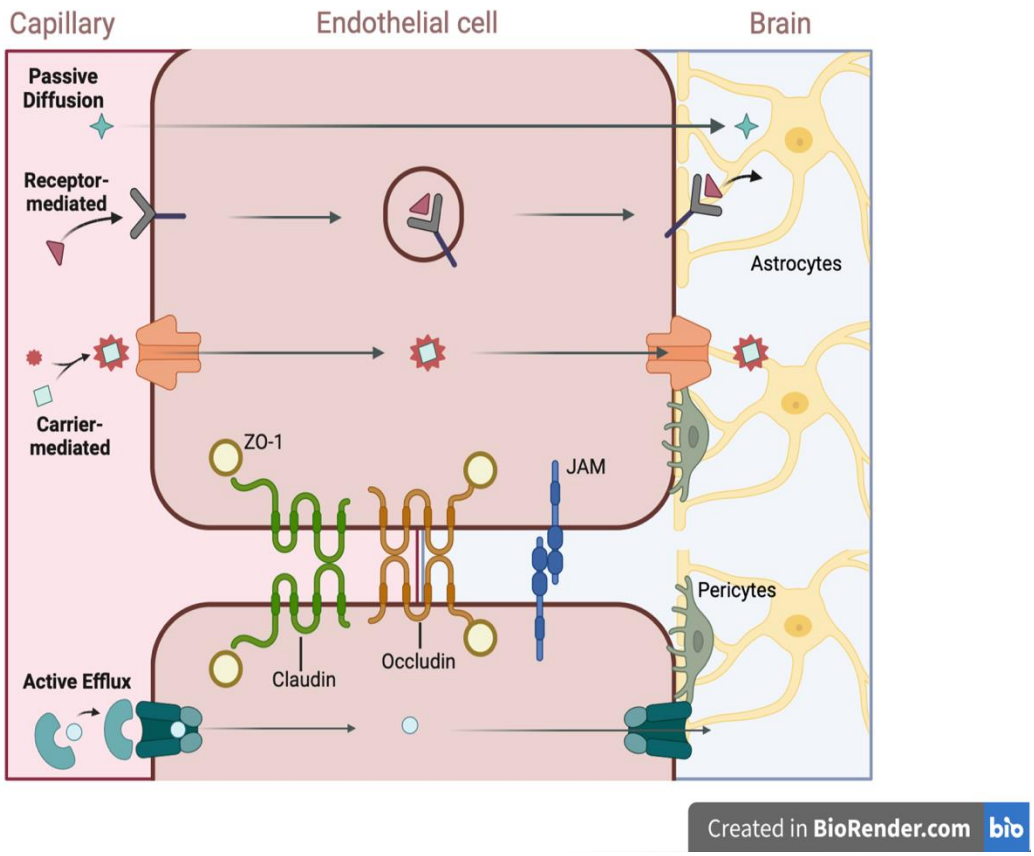

Figure 1.3. The Blood-Brain Barrier. The figure shows the tight junctions and cells that are associated with endothelial cells to create a blood-brain barrier. Both Occludin and Claudin-5 are bound to ZO-1 so that they can attached to the cytoskeleton. JAMs also bind each other to provide more adhesion between cells. At the brain side of the endothelial cells, pericytes and astrocytes interact with endothelial cells to regulate BBB. Transportation across the endothelial cells also can be seen in the figure. Transportation can be active efflux, passive diffusion, receptor-mediated, or carrier-mediated. *Adapted from "Endothelial Junctions in the Blood Brain Barrier" by BioRender.com (2024). Retrieved from https://app.biorender.com/biorender-templates*

.

Previously, it has been shown that hyperlipidemia causes BBB integrity disruptions. These includes such as increased permeability due to the altered expression of the related mRNAs, like the expression of tight-junction proteins [115]. As the BBB protects the brain from the neurotoxins circulating the blood, increased permeability leads to damage to the brain[116].

1.5 Synapses

One neuron's axon and the other neuron's dendrite form a junction called the synapse (Fig 1.4). The synapses are for neurons to communicate with each other. Presynapse, the axon of the neuron, is responsible for neurotransmitter release, and the postsynapse, the dendrite of the opposite neuron, has receptors for neurotransmitters to bind [117].

The synapses can be excitatory or inhibitory depending on the receptors they carry or the neurotransmitters that they release. Excitatory synapses express ionotropic channels (α-amino-3-hydroxy-5-methyl-4-isoxazolepropionic acid (AMPA) receptors and N-methyl-D-aspartate (NMDA) receptors) or metabotropic channels on their post-synaptic region for glutamate that has been released from the presynapse [118]. Inhibitory synapses, on the other hand, express glycine or gamma-aminobutyric acid (GABA) receptors on their post-synapses for GABA and glycine that is released from presynapse to bind [119].

1.5.1 Synaptic Transmission

When an action potential reaches the axon, it activates the voltage-gated calcium channels and allows calcium entry to the presynapse. Calcium triggers the release of synaptic vesicles that contain neurotransmitters from the synapsin. Synapsin is a protein that binds synaptic vesicles to the cytoskeleton of the cell, so when the synaptic vesicles are released

from the synapsin, they become mobile and transported to the presynaptic membrane. Each vesicle contains synaptobrevin protein on its membrane. Synaptobrevin interacts with syntaxin and Synaptosomal-Associated Protein, 25kDa, and forms a complex called soluble N-ethylmaleimide-sensitive factor activating protein receptors (SNARE) complex. SNARE complex allows for synaptic vesicles to fuse with the presynaptic membrane and release the neurotransmitters to the synaptic cleft. After the release, neurotransmitters bind their receptors on the post-synapse and excite or inhibit the cell accordingly. Synaptic vesicles get recycled after the release, so SNARE complex dissembles, and, through endocytosis, synaptic vesicles are taken up to be filled with neurotransmitters again [119]. The excitation or the inhibition of the postsynapses is determined by the ratio of excitation and inhibition that a postsynapse receives. If the balance is shifted towards excitation, the cell excites, and if it is shifted towards inhibition, the cell is inhibited [121].

1.5.1.1 Synaptophysin

Synaptophysin is an integral membrane glycoprotein, and it is one of the swarming proteins found in the synaptic vesicles, along with synaptobrevin. Although it is not directly involved in the neurotransmitter release, synaptophysin establishes the precise re-uptake of synaptobrevin after the synaptic vesicle fusion [122]. Diet-derived cholesterol causes the decreased expression of synaptophysin. Due to its interaction with synaptobrevin, synaptophysin is important for synapse formation and stability. As it decreases due to increased cholesterol intake, synaptic connections weaken [123].

1.5.2 Scaffold Proteins in the Postsynapses

1.5.2.1 Postsynaptic Density Protein 95

On the postsynapses of the excitatory synapses, there is an electron-dense region called the postsynaptic density. In this region, there are high numbers of receptors and the cells that accompany receptors. A major scaffold protein that resides in the postsynaptic density is the postsynaptic density protein 95 (PSD-95). It has several protein-protein interaction domains, and due to this, PSD-95 plays an important role in the regulation of synaptic strength. PSD-95 associates with transmembrane proteins and organizes their locations. It also stabilizes the protein at the synapses [124].

PSD-95 can interact various proteins. For instance, it binds to the transmembrane AMPA receptor regulatory protein, stargazin, and regulates the trafficking of AMPA receptors. Moreover, through its interaction with the NR2 subunit, it also regulates NMDA receptors [125].

Another protein that PSD-95 interacts which is also crucial for the strength of the synapses, are neuroligin. Neuroligins are the adhesion proteins found in the postsynapses that make connections with other adhesion protein neurexins found in the presynapse. PSD-95 packs neuroligin at excitatory synapses and translocates the ones found in the inhibitory synapses to the excitatory synapses. Through this, it changes the balance of excitation and inhibition towards excitation [126]. Dysregulation of the cholesterol mechanism results in cognitive decline and PSD-95 reduction. As it is an important protein that regulates the stability of the excitatory synapses, loss of PSD-95 causes declined synaptic plasticity [127].

1.5.2.2 Gephyrin

Gephyrin is a scaffold protein that is located at the inhibitory synapses. Similar to PSD-95 at the excitatory synapses, gephyrin interacts with many proteins. Gephyrin stabilizes and regulates the inhibitory synapses, glycine, and GABA receptors [128].

Gephyrin can bind to the glycine receptors and to the tubulin at the cytoskeleton. It is crucial clusterization of the glycine receptors at the postsynaptic membrane. In GABAergic synapses, during the inhibitory signaling, gephyrin accumulates. Gephyrin also binds to neuroligins to facilitate the maturation of inhibitory synapses. Thus, it can change the balance of excitation and inhibition ratio towards inhibition [129]. High cholesterol causes the reduction of gephyrin expression. Through reduced gephyrin, cholesterol intake actually affects the organization and the number of inhibitory receptors and negatively affects the integrity of inhibitory synapses [130].

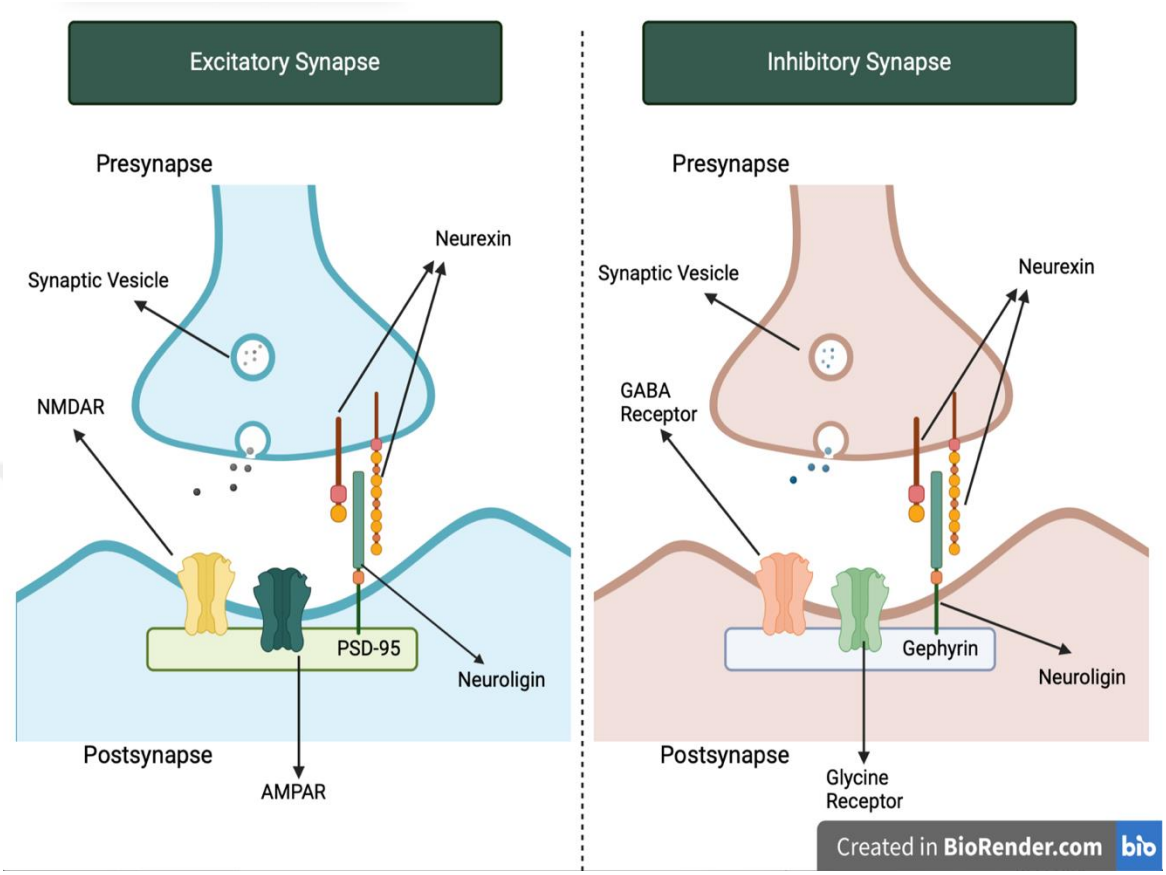

Figure 1.4. The excitatory and inhibitory synapses. The left side of the figure shows the excitatory synapse components and their interactions. The main scaffold protein at the excitatory postsynapse is PSD-95. It interacts with receptors (NMDAR, AMPAR) and neuroligins. Through these interactions, it stabilizes the synapse. The right side of the figure shows the inhibitory synapse components and their interactions. Gephyrin is the main scaffold protein found in the postsynapse of the inhibitory synapse. It binds to receptors (GABA, Glycine Receptors) and neuroligins to stabilize the synapse. The figure is created with BioRender.com.

Synapses can be affected from metabolic changes. A high-fat diet and hyperlipidemia affect the synapses by changing the expression of various associated genes [131]. Moreover, ER stress resulting from hyperlipidemia also leads to synaptic dysfunction. ER stress

causes the halt of global protein translation, and due to this, there would be decreased translation of synaptic proteins. [132].

1.6 GSK2606414 and Integrated Stress Response Inhibitor

1.6.1 GSK2606414, PERK Inhibitor

GSK2606414 is an inhibitor that binds to the cytosolic kinase domain of the PERK protein. After the binding, it inhibits the auto-phosphorylation of PERK. Once the phosphorylation of PERK is inhibited, the PERK pathway of UPR is inhibited. This means that there is no phosphorylation of eIF2, so global protein translation continues without activating ATF4 and CHOP. Resulting in no translation of apoptotic proteins because of CHOP activation. It has been confirmed that GSK2606414 could pass the BBB, and previous studies done on prion-disease mice models showed that GSK2606414 allows global protein translation upon the inhibition of PERK phosphorylation. However, they also showed that GSK2606414 causes pancreatic toxicity [133]. Also, in another study, GSK2606414 protected the brain against cerebral ischemia by altering the PERK pathway [134].

1.6.2 ISRIB, eIF2B activator

Integrated stress response inhibitor (ISRIB) acts allosterically to stabilize the active conformation of eIF2B. This form is resistant to p-eIF2α. Therefore, ISRIB is able to inhibit the downstream of p-eIF2α and allows the global protein translation to continue. This reduces ATF4 and CHOP activation without inhibiting the phosphorylation of eIF2. It has been confirmed that ISRIB could pass the BBB, and previously, it has been shown

that it reduces the ATF4 levels and somewhat restores global protein synthesis in prion-diseased mice models. It has been shown to be neuroprotective without causing pancreatic toxicity [135].

1.7 Aim of The Study

Hyperlipidemia caused by a high-fat diet is the alteration of the lipid content circulating in the blood and the increase in the cholesterol and triglyceride levels in the blood. Metabolic changes such as hyperlipidemia are linked to ER Stress and the activation of the PERK pathway of the UPR signaling. Moreover, hyperlipidemia has been associated with alterations in the blood-brain barrier integrity and synaptic integrity.

The PERK pathway is taught to be one of the inducers of neurodegenerative diseases. As hyperlipidemia is linked to neurodegenerative diseases, the PERK pathway inhibition is thought to be the potential therapeutic target.

The first part of this study is to understand how a high-fat diet affects the cerebral cortex of the Apoe knockout mice compared to C57BL/6 mice by investigating ER stress, blood-brain barrier integrity, and synaptic integrity. The aim of the second part of the study is to investigate the same alterations of the previous part after the inhibition of the PERK pathway with Trans-ISRIB and GSK2606414.

CHAPTER 2

MATERIAL & METHODS

2.1. Animal Study

2.1.1. Animal Subjects

In the study, two genotypes, C57BL/6 (WT) and Apoe$^{-/-}$ animals, have been used. Apoe$^{-/-}$ strain mice (C57BL/6.129P2-Apoetm1Unc/J) are from Jackson Laboratory, Bar Harbor, Maine, and have been created by Nabuyo Maeda, University of North Carolina. Both WT and Apoe$^{-/-}$ mouse strains were already present at Bilkent University Animal Facility. The kept conditions of the animals were 20-22°C and controlled humidity around 45-50%, 12 hours light/dark cycle. All experiments were approved by the Animal Care and Use Committee at Bilkent University (Decision Number: 2020/18). Animal numbers for feeding experiments are 7-8 for each group, and for injection experiments, they are 8 (for Trans-ISRIB) and 4 (for GSK2606414) for each group.

2.1.1.1. Feeding

For the feeding experiments, both WT and Apoe$^{-/-}$ animals were given either a chow diet with 4.5% fat or a western diet with 0.21% cholesterol and 21% butterfat (TD.88137 #E15721, Ssniff Spezialdiaten, Germany) for 16 weeks starting from 6-8 weeks old (Fig 2.1). Animals' access to food and water was *ad libitum*. Their weights were checked weekly.

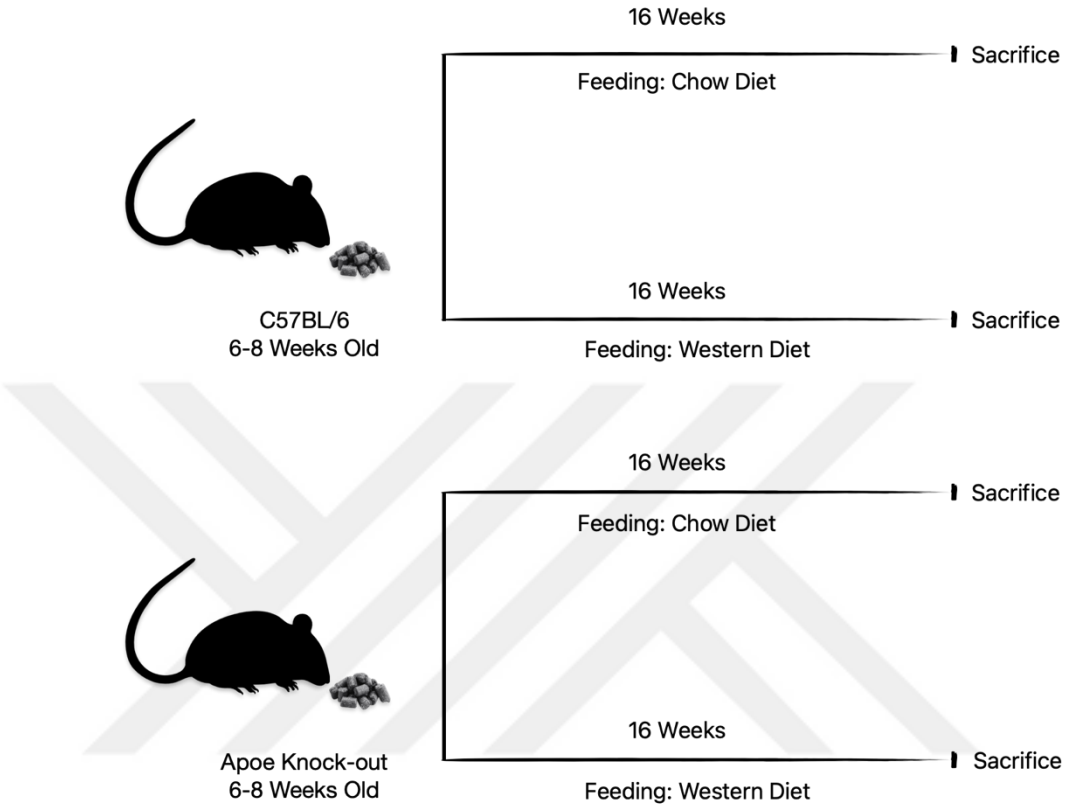

Figure 2.1. Experimental Setup for Feeding Experiments. Experimental design of feeding experiments. Both genotypes of animals have been started on the western or chow diet at 6-8 weeks old, and the diet period lasts for 16 weeks.

2.1.1.2. Injections

There were two different small molecules that were used to inhibit the PERK pathway. Apoe$^{-/-}$ subjects were given western diet for 16 weeks. During the last six weeks of the 16-week feeding experiment, animals were intraperitoneally (IP) injected with either Trans-ISRIB or GSK2606414 (Fig 2.2).

GSK2606414 (HY-18072, MedChemExpress, NJ, USA) was dissolved in DMSO, and then, before administrating to the animal, it was prepared with a 12.5% Cremophor-EL-Saline

(238470-1, Merck, Darmstadt, Germany). It was calculated as 30 mg inhibitor per kg in a day. The vehicle for GSK2606414 contained DMSO and 12.5% Cremophor-EL-Saline. Trans-ISRIB (HY-12495, MedChemExpress, NJ, USA) was dissolved in DMSO and administered with 16% Cremophor-EL-Saline as 1 mg of inhibitor per kg in a day. The vehicle for Trans-ISRIB contained DMSO and 16% Cremophor-EL-Saline. These dosage amounts have been chosen according to the published paper of Dr. İnci Onat and Dr. Ebru Erbay, where they showed the optimal dose for these inhibitors to avoid pancreatic toxicity [136].

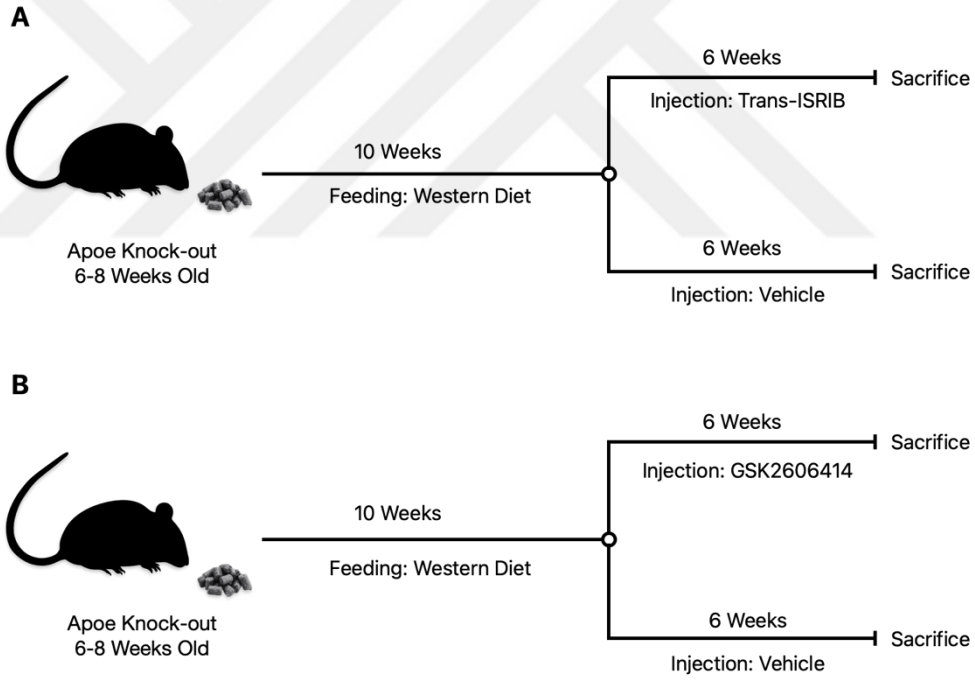

Figure 2.2. Experimental setup for I.P. injections. The experimental design for I.P. injections. Apoe$^{-/-}$ animals have been fed with the western diet for 16 weeks, and in the last 6 weeks of the feeding experiments, they were injected with inhibitors or their vehicles.

2.1.2. Dissections

For both non-injection and injection groups, animals were sacrificed at 22-24 months old. Before the sacrifice, the subjects were fasted for 12 hours. Subjects were anesthetized with isoflurane using the open-drop method, where isoflurane-dropped cotton and the animal were put in a box together. Then, the effectiveness of the anesthetizer was controlled with a toe-pinch response. After confirming that the animal was under anesthesia, the thoracic and abdominal viscera were opened. For checking the blood parameters, ~1 mL of blood was collected from the heart, and then 10 mL of ice-cold 1X phosphate-buffered saline (PBS) perfusion was used to clean the remaining blood.

After the decapitation of the subjects, the thalamus, cerebellum, olfactory bulb, amygdala, hippocampus, and hypothalamus were separated from the brain, and the right and left cerebral cortex regions were collected into separate eppendorf tubes to be used in the experiments.. The samples that were spared for the total protein and RNA isolation were first put into liquid nitrogen and then in a fridge at -80°C for long-term storage. The samples that would be used in synaptosome isolation waited on the ice and then were put in a fridge at -80°C for long-term storage to avoid damaging the synaptosomes.

2.2. Western Blot Analysis

2.2.1. Total Protein Isolation

The cerebral cortex was mechanically homogenized with dounce homogenizer for ~10 strokes, in 1000 µl 1X ice-cold PBS solution. After that, each homogenate was passed through 1 mL syringe to make sure all the tissue was homogenized. Then, 500 µl of

homogenate was reserved for RNA isolation. The remaining 500 µl was centrifuged at 14000 rpm for 10 minutes at 4°C. An inhibitor cocktail (Protease Inhibitor Cocktail (PIC) (P8340-1ML, Sigma-Aldrich, St. Louis, MO, USA), Phosphatase Inhibitor (PI) (P0044-1ML, Sigma-Aldrich, St. Louis, MO, USA), Sodium orthovanadate (Na_3VO_4), PMSF, 5 µl for each inhibitor) was added to 500 µl Radioimmunoprecipitation Assay (RIPA) buffer (Table 2.1), and the pellet has been suspended in this buffer after supernatant is discarded. The suspension was ultrasonicated with a sonicator at 50 amplitude, 0.5-1 cycle for 9 times. The suspension rested on ice for 30 minutes and then centrifuged at 13000 rpm for 20 minutes at 4°C.

Table 2.1. Recipe of RIPA Buffer

RIPA Buffer Recipe	For 100 mL
Materials	Amounts
1 M Tris-HCL pH 8.8	2.5 mL
NaCl	0.876 g
Sodium deoxychalate	0.25 g
NP-40	1 mL
EDTA	0.029 g

2.2.2. Synaptosome Isolation

The cerebral cortex was mechanically homogenized with dounce homogenizer for ~10 strokes, the same for all samples in 800 µl of homogenization buffer (1.0 mM EDTA, 250 mM sucrose, 10 mM Hepes, pH=7.4). After that, the homogenates passed through a 1 mL syringe to make sure all the tissue was homogenized. The homogenates were centrifuged

at 1200 x *g* for 10 minutes at 4°C. The pellet was discarded, and 10 µl of homogenate was preserved for use in experiments later. The remaining supernatant was centrifuged at 15000 x *g* for 20 minutes at 4°C. The supernatant was reserved as cytosol, which will be used in experiments later. The pellet was suspended in 125 µl Syn-PER™ Synaptic Protein Extraction Reagent (#87793, ThermoScientific, Rockford, IL, USA). Before the experiments, synaptosome confirmations were done using NMDAR-2B (LS-C25797, LSBio, Washington, USA), ß-actin and Synaptophysin. (Appendices A.1.)

2.2.3. Bradford Assay

The protein amounts were measured with Bradford Assay. To a 96-well plate, standards, blanks, and samples were loaded. As a standard, Bovine Serum Albumin (BSA) (A7906, Sigma-Aldrich, St. Louis, MO, USA) was used in concentrations of 0.1, 0.2, 0.4, 0.6, 0.8, and 1 µg/µl. For each well, 0.5 µl sample and 4.5 µl dH_2O have been loaded. Later, 250 µl Bradford Reagent (B6916, Sigma-Aldrich, USA) was loaded into each well. The 96-well plate was shaken on the plate shaker at 240 rpm for 45 seconds. The plate was incubated in the dark at room temperature for 10 minutes before the absorbances were measured. Biotek Synergy HT Multi-Mode Microplate Reader (BioTek® Instruments, Inc., Winooski, VT, USA) was used to measure the absorbances at 595 nm. The standard curve was plotted according to the absorbances, and the protein amounts were measured accordingly.

2.2.4. Western Blot Analysis

For protein experiments, sodium dodecyl sulfate (SDS)-polyacrylamide gel electrophoresis was used. For the resolving part of the gel, a 12% and 15% gel composition were used (Table 2.3-4). As a stacking part of the gel, a 5% gel composition was used (Table 2.2).

Firstly, the resolving gel was poured into the casting system, and to avoid bubble formation, a thin layer of isopropanol was poured onto the resolving gel. After the resolving gel was polymerized, isopropanol was cleaned with dH2O. Then, stacking gel was carefully poured to avoid bubbles, and the combs were inserted.

Samples and dH2O were mixed to obtain the desired amount of protein that was aimed to be loaded onto the gel. Later, 2X Loading dye (Table 2.5) was added to the mixture and heated at 95°C in a heater for 10 minutes. Analysis of Claudin-5 was done with non-boiled samples as suggested by the manufacturer.

The SDS Running Buffer (Table 2.6) was used to run the proteins in the gel. The gel was placed in the electrophoresis unit, and the apparatus was filled with 1X Running Buffer. The comb was removed, and prepared proteins containing loading buffer were loaded into the wells. Running started at 80 volts; once the proteins were out from the stacking gel and passed to the resolving gel, the amper was increased to 100 volts to run for ~2 hours.

Polyvinylidene difluoride (PVDF) membrane (88518, ThermoScientific, Rockford, IL, USA) was used to transfer the proteins from the gel. The PVDF membrane was wetted in 100% methanol for 2 minutes before being contacted with gel for activation. Sponge, Whatmann paper, PVDF membrane, and gel were placed in the cassette (Fig 2.4). The cassette was placed in the tank, and the tank was filled with a cold 1X Transfer Buffer (Table 2.7-8). It was transferred at a constant 100 V for 90 minutes.

For preparation of blocking and primary solutions, 1 mL Tween-20 (TWN508.500, BioShop, Burlington, ON, Canada) was added to 1X Tris-Buffered Saline (TBS) (Table 2.9). Before the primary incubation, membranes were blocked in 5% Non-fat Dry Milk in

TBS-Tween (TBS-T) or 5% BSA in TBS-T for 1 hour at room temperature. After blocking, all membranes were washed with TBS-T twice for 5 minutes.

The antibodies that were used during the experiments are listed in Table 2.10. The primary antibody incubation was performed overnight at four °C on a shaker. After ~18 hours, the membranes were washed with TBS-T 3 times for 10 minutes. Then, Anti-Rabbit HRP-Linked (#7074S, Cell Signalling Technology, Danvers, MA, USA) or Anti Goat HRP-Linked (ab97100, Abcam, Cambridge, UK) secondary antibodies were added (Table 2.10), and the membranes were incubated for 1 hour at room temperature on a shaker. After that, the membranes were washed with TBS-T 3 times for 10 minutes.

SuperSignal™ Femto (34095, ThermoScientific, Rockford, IL, USA) was used for imaging. The membranes were incubated with Femto for 2 minutes in the dark and then imaged on ChemiDoc™ XRS Imaging System (Bio-Rad, CA, USA).

Figure 2.3. Placement of Transfer Sandwich. At the bottom part (anode side), there is a sponge, and following that, Whatman paper and PVDF membrane. Above the membrane, there is polyacrylamide gel, Whatman paper, and a sponge that closes with the cathode side.

Table 2.2. 5% Stacking Gel Recipe

5% Stacking Gel Recipe	For 1 gel
Reagents	**Amounts**
Water	2.83 mL
1 M Tris-HCl pH 6.8	0.47 mL
10% SDS	37.5 µl
Bis-Acrylamide 29:1 40% Solution	0.375 mL
10% Ammonium Persulfate (APS)	37.5 µl
Tetramethylethylenediamine (TEMED)	3.75 µl

Table 2.3. 12% Resolving Gel Recipe

12% Resolving Gel Recipe	For 1 gel
Reagents	**Amounts**
Water	2.63 mL
1 M Tris-HCl pH 8.8	3.28 mL
10% SDS	87.5 µl
Bis-Acrylamide 29:1 40% Solution	2.63 mL
10% APS	87.5 µl
TEMED	8.75 µl

Table 2.4. 15% Resolving Gel Recipe

15% Resolving Gel Recipe	For 1 gel
Reagents	**Amounts**
Water	2.4 mL
1 M Tris-HCl pH 8.8	3.75 mL
10% SDS	100 µl
Bis-Acrylamide 29:1 40% Solution	3.75 mL
10% APS	100 µl
TEMED	10 µl

Table 2.5. 2X Loading Buffer Recipe

2X Loading Buffer Recipe	For 20 mL
Reagents	**Amounts**
Tris-HCl pH 6.8	2 mL
10% SDS	8 mL
Glycerol	4 mL
4% Bromophenol Blue	250 µl

Table 2.6. 10X SDS-Page Running Buffer Recipe

10X SDS-Page Running Buffer	For 1 L
Reagents	**Amounts**
Tris Base	30 g
Glycine	144 g
10% SDS	100 mL

Table 2.7. 10X Transfer Buffer Recipe

10X Transfer Buffer	For 1 L (storage 4°C)
Reagents	**Amounts**
Tris Base	30 g
Glycine	144 g

Table 2.8. 1X Transfer Buffer Recipe

1X Transfer Buffer	For 1 L (storage 4°C)
Reagents	**Amounts**
10x Transfer Buffer	100 mL
Methanol	200 mL

Table 2.9. 10X TBS Recipe

10X TBS	For 1 L pH 7.6
Reagents	**Amounts**
Tris-base	24.2 g
NaCl	80 g

Table 2.10. Antibody List Used for Western Blot

Primary Antibodies	Blocking Solution	Primary Dilution	Secondary Dilution
p-PERK (16F8, Cell Signalling Technology, Danvers, MA, USA)	5% BSA in TBS-T	1:250, 5% BSA in TBS-T	1:5000, Rabbit HRP 5% Non-Fat Dry Milk in TBS-T
PERK (C33E10, Cell Signalling Technology, Danvers, MA, USA)	5% Non-fat Dry Milk in TBS-T	1:1000, 5% BSA in TBS-T	1:10000, Rabbit HRP 5% BSA in TBS-T

p-eif2a (STJ11102562, St John's Laboratory, London, UK)	5% BSA in TBS-T	1:8000, 5% BSA in TBS-T	1:10000, Rabbit HRP 5% BSA in TBS-T
eif2a (5324S, Cell Signalling Technology, Danvers, MA, USA)	5% Non-fat Dry Milk in TBS-T	1:10000, 5% BSA in TBS-T	1:10000, Rabbit HRP 5% BSA in TBS-T
Occludin (ab216327, Abcam, Cambridge, UK)	5% Non-fat Dry Milk in TBS-T	1:1000, 5% Non-Fat Dry Milk in TBS-T	1:10000, Rabbit HRP 5% Non-Fat Dry Milk in TBS-T
Claudin-5 (ab131259, Abcam, Cambridge, UK)	5% Non-fat Dry Milk in TBS-T	1:1000, 5% Non-Fat Dry Milk in TBS-T	1:10000, Rabbit HRP 5% Non-Fat Dry Milk in TBS-T
PSD-95 (ab18258, Abcam, Cambridge, UK)	5% Non-fat Dry Milk in TBS-T	1:10000, 5% Non-Fat Dry Milk in TBS-T	1:10000, Rabbit HRP 5% Non-Fat Dry Milk in TBS-T
Gephyrin (sc-6411, Santa Cruz	5% Non-fat Dry Milk in TBS-T	1:1000, 5% Non-Fat Dry Milk in TBS-T	1:20000, Goat HRP 5% Non-Fat Dry Milk in TBS-T

Biotechnology, Dallas, TX, USA)			
Synaptophysin (ab32594, Abcam, Cambridge, UK)	5% Non-fat Dry Milk in TBS-T	1:128000, 5% Non-Fat Dry Milk in TBS-T	1:10000, Rabbit HRP 5% Non-Fat Dry Milk in TBS-T
Tubulin (2146S, Cell Signalling Technology, Danvers, MA, USA)	5% Non-fat Dry Milk in TBS-T	1:5000, 5% Non-Fat Dry Milk in TBS-T	1:10000, Rabbit HRP 5% Non-Fat Dry Milk in TBS-T
ß-Actin (ab1801, Abcam, Cambridge, UK)	5% BSA in TBS-T	1:4000, 5% BSA in TBS-T	1:10000, Rabbit HRP 5% BSA in TBS-T

2.3. RT-qPCR Experiments

2.3.1. RNA Isolation

500 µl of homogenate was preserved for RNA isolation experiments. The homogenate was centrifuged at 11000 x *g* for 10 minutes. The supernatant was discarded, and 500 µl TRIzol® Reagent (code, Ambion, CA, USA) was added to the pellets. Samples were incubated at room temperature for 10 minutes. 125 µl chloroform was added, and the mixture was vigorously shaken and left to rest at room temperature for 2-5 minutes. After a clear phase separation was the mixture was centrifuged at 15000 rpm for 15 minutes at

4°C. After the centrifuge, there was a 3-phase in the tube. The bottom pink part was the organic phase, the white interphase was DNA, and the upper part, where the clear solution was RNA. Without disrupting the bottom layers, RNA was collected into a new tube. 250 µl isopropanol was added and left for the RNA clamp to appear at room temperature for 10 minutes. Then, it centrifuged at 15000 rpm for 35 minutes at 4°C. The supernatant was discarded, and the pellet was suspended in 500 µl 70% ethanol. The sample was centrifuged at 5000 rpm for 5 minutes at 4°C. The supernatant was discarded, and the pellets were left to air dry for 15 minutes. Finally, the pellets were suspended in 35 µl nuclease-free water (AM9937, Ambion, Carlsbad, CA, USA). The concentration of RNA was measured with NanoDrop 2000 (ThermoScientific, Rockford, IL, USA).

2.3.2. cDNA Synthesis and RT-qPCR

Using the iScript™ cDNA Synthesis Kit (1708891, Bio-Rad, CA, USA), cDNA was synthesized from RNA. As a first step, the amount of cDNA was calculated according to the RNA concentrations of the samples. The calculation is done by dividing RNA concentration into 500 ng of cDNA. Then, the RNA amount was completed to 15 µl with nuclease free water. Then, 4 µl of 5X Buffer and 1 µl reverse transcriptase was added. Using C1000™ Thermal Cycler (Bio-Rad, CA, USA), conditions were arranged as follows: 5 minutes at 25°C, 30 minutes at 42°C, 5 minutes at s at 42°C, 5 minutes at 85°C, and then finally at 4°C. The cDNA was stored at -80°C for long-term storage and -20°C for short-term storage. Later, cDNA, reverse and forward primers, and LightCycler® 480 SYBR Green I Master (04887352001, Roche Diagnostics, Mannheim, Germany) mix were added to each well of A 96-well plate. The plates were run in The LightCycler® 480 (Roche

Diagnostics, Mannheim, Germany). Running conditions were an initial heating step of 15 minutes at 95°C, and then a cycle repeated 45 times: 10 seconds at 95°C, 30 seconds at 60°C, and 30 seconds at 72°C. For the results, cycle threshold (ct) values were considered, and there were 2 technical replicates for the primers (Table 2.11). Normalizations were done with housekeeping genes Glyceraldehyde-3-phosphate dehydrogenase (GAPDH) for injection experiments and Ribosomal Protein 13A (RPL13A) for the experiments exploring the effect of high-fat and genotype.

Table 2.11 Primer List Used for RT-qPCR

Primers	Forward	Reverse
CHOP	5' CCTAGCTTGGCTGACAGAGG 3'	5' CTGCTCCTTCTCCTTCATGC 3'
ATF4	5' TCGATGCTCTGTTTCGAAATG 3'	5' AGAATGTAAAGGGGGCAACC 3'
VEGF	5' CGCAAGAAATCCCGGTTTAA 3'	5' CAAATGCTTTCTCCGCTCTGA 3'
GAPDH	5' GTGAAGGTCGGTGTGAACG 3'	5' GGTCGTTGATGGCAACAATC TC 3'
RPL13A	5'AGCCTACCAGAAAGTTTGCTT AC 3'	5'GCTTCTTCTTCCGATAGTGC ATC 3'

2.5. Statistical Analysis

Western Blot Images were arranged at Image Lab 6.1 (Bio-Rad, CA, USA). Later, all the band quantifications were done in ImageJ (National Institute of Health, Bethesda, MD, USA). Each band was selected separately with the same sized selection, and then plots of the band intensity were produced. Analysis of the bands was done using 2 normalizations. First, within gel normalization, the intensity of each band is divided by the average of the same blot's band intensity to remove imaging biases. Second is standard normalization, in which each band is divided by its housekeeping band (Tubulin and ß-actin). For phosphorylated antibodies where total protein and phosphorylated protein were imaged from the same gel, firstly, a gel normalization and standard normalization were performed, and then the phosphorylated one was divided by total protein. If the phosphorylated and its total protein were imaged from different gels, each protein was normalized to its own housekeeping protein, and then the phosphorylated protein was divided by its total protein. All the statistical analyses were done using IBM SPSS Statistics 28.0.0.0 (IBM, SPSS Inc., USA), and the graphs were formed using GraphPad Prism 8 (GraphPad, Boston, MA, USA). The assumptions of a two-way analysis of variance (ANOVA) and t-test were checked with the Shapiro-Wilk and Levene test. For the normally distributed and homogenous samples, a two-way ANOVA was performed to investigate the diet and genotype effect, and to investigate the effect of inhibitors, a Student t-test was performed. Mann-Whitney U Tests were applied to investigate the diet and genotype effect, The Kruskal-Wallis, and the effect of inhibitors in non-parametric situations. The partial-

correlations were performed for testing the correlation between body weight and the markers.

CHAPTER 3

RESULTS

3.1. Body Weights of the Subjects

3.1.1. The Effect of High-fat Diet on the Mouse Cerebral Cortex

3.1.1.1. Total Protein Studies

For analysis the last body weight measurements have been used. The normality tests were done using the Shapiro-Wilk test, and the homogeneity was checked using the Levene's Test. As the parameters for two-way ANOVA are not met, Kruskal-Wallis have been used to look at main effects, then Mann-Whitney U have been used to compare within groups. The Kruskal-Wallis analysis revealed that diet has a significant effect on body weight ($H(1) = 18.531$ $p = <.001$, Table 3.1.) whereas genotype has no significant effect on body weight (($H(1) = 0.954$ $p = <0.329$, Table 3.1.). It also has been revealed that there is a significant increase of body weight in wild type animals with western diet ($U(16) = .000$ $p = <.001$, Table 3.1.). There is also significant increase of body weight between wild-type animals and Apoe knock-out animals fed with chow diet ($U(16) = 2.500$ $p = <.001$, Table 3.1.). Moreover, there is also significant increase with western diet feeding in Apoe knockout animals ($U(15) = 8.000$ $p = <0.017$, Table 3.1.).

Table 3.1 Last Body Weight Measurement Comparisons. In the table, there is the mean of the last body weight measurements of the animals that have been used for total protein isolation and further experiments of it. There is a significant body weight increase with western diet. Also, there is a significant body weight increase between wild-type and Apoe knock-out animals fed with chow diet.

	C57BL/6 Chow Diet	**C57BL/6 Western Diet**	**Apoe$^{-/-}$ Chow Diet**	**Apoe$^{-/-}$ Western Diet**
n	8	8	8	7
Body Weight	27.625	36.25	29.625	35.714

3.1.1.2. Synaptic Integrity Studies

For analysis the last body weight measurements have been used. The normality tests were done using the Shapiro-Wilk test, and the homogeneity was checked using the Levene's Test. A two-way ANOVA is performed and revealed that there is a significant diet effect (F (1,30) =70.406, p =<.001, Table 3.2), there is no genotype (F (1,30) = 0.836, p = 0.368, Table 3.2) or interaction effect (F (1,30) =0.387, p = 0.539, Table 3.2) observed. There is also significant body weight increase in both wild-type (p = <.001) and Apoe knock-out (p = <.001) animals when they fed with western diet.

Table 3.2. Last Body Weight Measurement Comparisons. In the table, there is the mean of the last body weight measurements of the animals that have been used for synaptosome isolation and further experiments of it. There was a significant increase in body weight with diet.

	C57BL/6 Chow Diet	**C57BL/6 Western Diet**	**Apoe$^{-/-}$ Chow Diet**	**Apoe$^{-/-}$ Western Diet**
n	9	9	9	7
Body Weight	28.333	38.111	30	38.428

3.1.2. PERK Pathway Inhibition on the Mouse Cerebral Cortex

3.1.2.1. Total Protein Studies

For analysis the last body weight measurements have been used. The normality tests were done using the Shapiro-Wilk test, and the homogeneity was checked using the Levene's Test. For Trans-ISRIB, t-test revealed that body weight is significantly increased with Trans-ISRIB ($t(14) = -3.574$ $p = 0.003$, Table 3.3) and for GSK2606414 injections, Mann-Whitney U test revealed that body weight is significantly decreased with GSK2606414 ($U(8) = 0.000$ $p = 0.019$, Table 3.3).

Table 3.3 Last Body Weight Measurement Comparisons. In the table, there is the mean of the last body weight measurements of the animals that have been used for total protein isolation and further experiments of it. There is a significant increase of body weight with Trans-ISRIB, and a significant decrease of body weight with GSK2606414. n=8 for Trans-ISRIB and its control group, n=4 for GSK2606414 and its control group.

A	Vehicle	Trans-ISRIB
n	8	8
Body Weight	30.5	38.125

B	Vehicle	GSK2606414
n	4	4
Body Weight	36.5	23.5

3.1.2.2. Synaptic Integrity Studies

For analysis the last body weight measurements have been used. The normality tests were done using the Shapiro-Wilk test, and the homogeneity was checked using the Levene's Test. For Trans-ISRIB, student t-test revealed that there is no significant body weight change ($t(14) = 0.524$ $p = 0.073$, Table 3.4). For GSK2606414, student t-test revealed there is significant decrease in body weight with the injections ($t(6) = 0.524$ $p = <.001$, Table 3.4).

Table 3.4 Last Body Weight Measurement Comparisons. In the table, there is the last body weight measurements of the animals that have been used synaptosome isolation and further experiments of it. There is a significant decrease of body weight with GSK2606414. n=8 for Trans-ISRIB and its control group, n=4 for GSK2606414 and its control group.

A	Vehicle	Trans-ISRIB
n	8	8
Body Weight	39.5	37.75

B	Vehicle	GSK2606414
n	4	4
Body Weight	40	22.5

3.2. The Effect of High-fat Diet on the Mouse Cerebral Cortex

3.2.1. ER Stress – The PERK Pathway

To investigate how a high-fat diet affected the PERK pathway, the following markers have been used for Western blot analysis: p-PERK, p-eIF2α.

3.2.1.1. p-PERK

The ratio of p-PERK to PERK expression has been considered to investigate the phosphorylation levels of PERK. The normality tests were done using the Shapiro-Wilk test, and the homogeneity was checked using the Levene's Test. A two-way ANOVA test has revealed that diet (F (1,27) = 0.170 p= 0.683, Figure 3.1) and genotype (F (1,27) = 2.207 p= 0.149, Figure 3.1) do not have a significant effect on the expression level of p-PERK. Moreover, there is no significant interaction between diet and genotype (F (1,27) =

0.889 p= 0.354, Figure 3.1). The partial correlation analysis is done to see the correlation between body weights. Spearman's correlation revealed that there is no significant correlation between body weights and p-PERK/PERK ratio ($r(27) = 0.094$ $p = 0.626$).

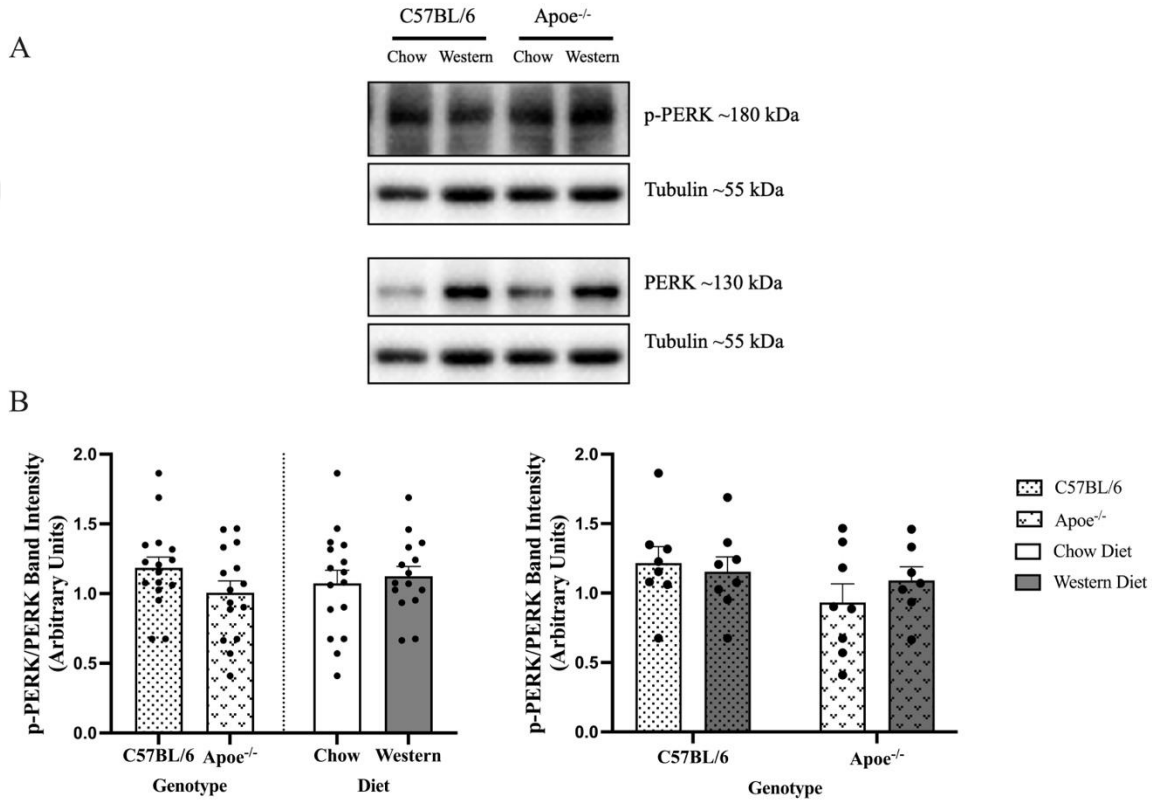

Figure 3.1. Observed Bands and Expression of p-PERK Across Genotype and Diet in the Cerebral Cortex. The A part of the image shows the representative band image for p-PERK, PERK, and Tubulin. The left side of the B part shows the graphs of the normalized quantified bands of the p-PERK/PERK ratio normalized to Tubulin band intensity for the main effects of diet and genotype. The right side of the B part shows the interaction effect between diet and genotype. The expression of p-PERK did not change significantly with diet or genotype and there was no interaction between these main effects. The error bars

represent mean +1 SEM and statistical significance was set at $p < 0.05$. n= 8 for C57BL/6 animals and Apoe$^{-/-}$ Chow diet-fed animals, and n= 7 for Apoe$^{-/-}$ Western diet-fed animals.

3.2.1.2. p-eIF2α

The ratio of p-eIF2α to eIF2α expression has been considered to investigate the phosphorylation levels of eIF2α. The normality tests were done using the Shapiro-Wilk test, and the homogeneity was checked using the Levene's Test. A two-way ANOVA test has revealed that diet (F (1,27) =3.644, p = 0.067, Figure 3.2) does not have a significant effect on p-eIF2α. However, genotype (F (1,27) =13.749, $p < 0.001$, Figure 3.2) has a significant effect; C57BL/6 animals have higher p-eIF2α intensity compared to Apoe$^{-/-}$. And diet, genotype interaction (F (1,27) =11.708, p = 0.002, Figure 3.2) is significant. Moreover, post-hoc analysis revealed that there is a significant increase in the C57BL/6 Western diet when compared to the Chow diet fed C57BL/6 animals ($p < 0.001$, Figure 3.2). Also, the levels of p-eIF2α are higher in C57BL/6 Western diet-fed animals when compared to Apoe$^{-/-}$ Western diet-fed animals ($p < 0.001$, Figure 3.2). There was no significant interaction between the Chow diet-fed C57BL/6 animals and Apoe$^{-/-}$ animals (p = 0.838, Figure 3.2). There was also no significant interaction effect between Apoe$^{-/-}$ animals (p = 0.302). The partial correlation analysis is done to see the correlation between body weights. Spearman's correlation revealed that there is no significant correlation between body weights and p-eIF2α/eIF2α (r(27) = 0.280 p = 0.141).

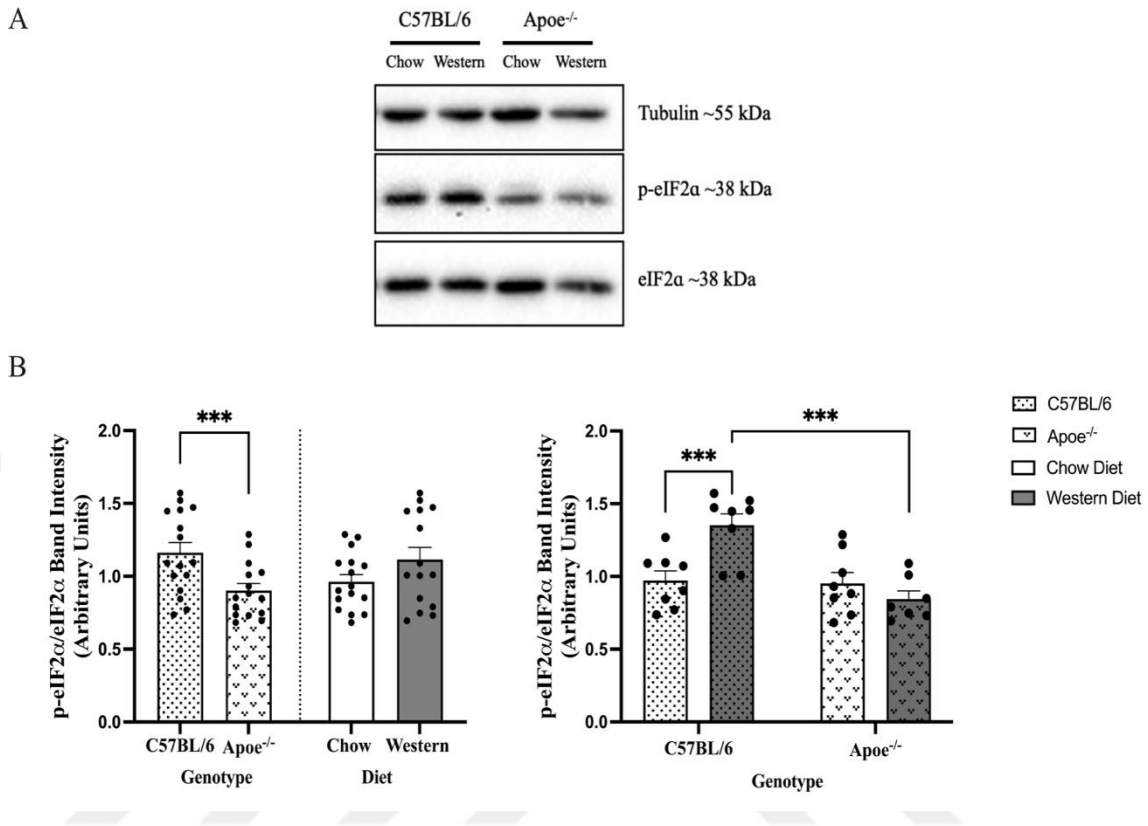

Figure 3.2. Observed Bands and Expression of p-eIF2α Across Genotype and Diet in the Cerebral Cortex. The A part shows the representative images of p-eIF2α, eIF2α and tubulin. The left side of the B part shows the graphs of the normalized quantified bands of the p-eIF2α/eIF2α ratio for the main effects of diet and genotype. The right side of the B part shows the interaction effect between diet and genotype. The expression of p-eIF2α changed significantly with genotype, however, not with diet. There was a significant interaction effect, while western diet increased p-eIF2α protein levels in C57BL/6 mice compared to the C57BL/6 subjects fed with chow diet and Apoe$^{-/-}$ subjects fed with western diet. The error bars represent mean +1 SEM and statistical significance was set at $p < 0.05$, *** $p \leq 0.001$. n= 8 for C57BL/6 animals and Apoe$^{-/-}$ Chow diet-fed animals, and n= 7 for Apoe$^{-/-}$ Western diet-fed Animals.

3.2.2. Blood-Brain Barrier Integrity

To investigate how a high-fat diet affected the blood-brain barrier integrity, the following markers have been used for Western blot analysis: claudin-5 and occludin. For the RT-qPCR analysis vegf has been used.

3.2.2.1. Claudin-5

The normality tests were done using the Shapiro-Wilk test, and the homogeneity was checked using the Levene's Test. A two-way ANOVA test has revealed that diet does have a significant effect on Claudin-5 (F (1,27) = 8.596, p = 0.007, Figure 3.3). Moreover, the effect of genotype (F (1,27) =12.934, p = 0.001, Figure 3.3) and diet and genotype interaction (F (1,27) =7.368, p = 0.011, Figure 3.3) were significant. Moreover, the post-hoc analysis revealed that the expression of Claudin-5 significantly increased in $Apoe^{-/-}$ Western compared to the C57BL/6 Western group ($p < 0.001$, Figure 3.3), and the effect of diet in the $Apoe^{-/-}$ genotype was significant, the expression of Claudin-5 did significantly increase in the $Apoe^{-/-}$ Western group compared to the $Apoe^{-/-}$ Chow group ($p < 0.001$, Figure 3.3). The partial correlation analysis is done to see the correlation between body weights. Spearman's correlation revealed that there is no significant correlation between body weights and Claudin-5 ($r(27) = -0.127$ $p = 0.510$).

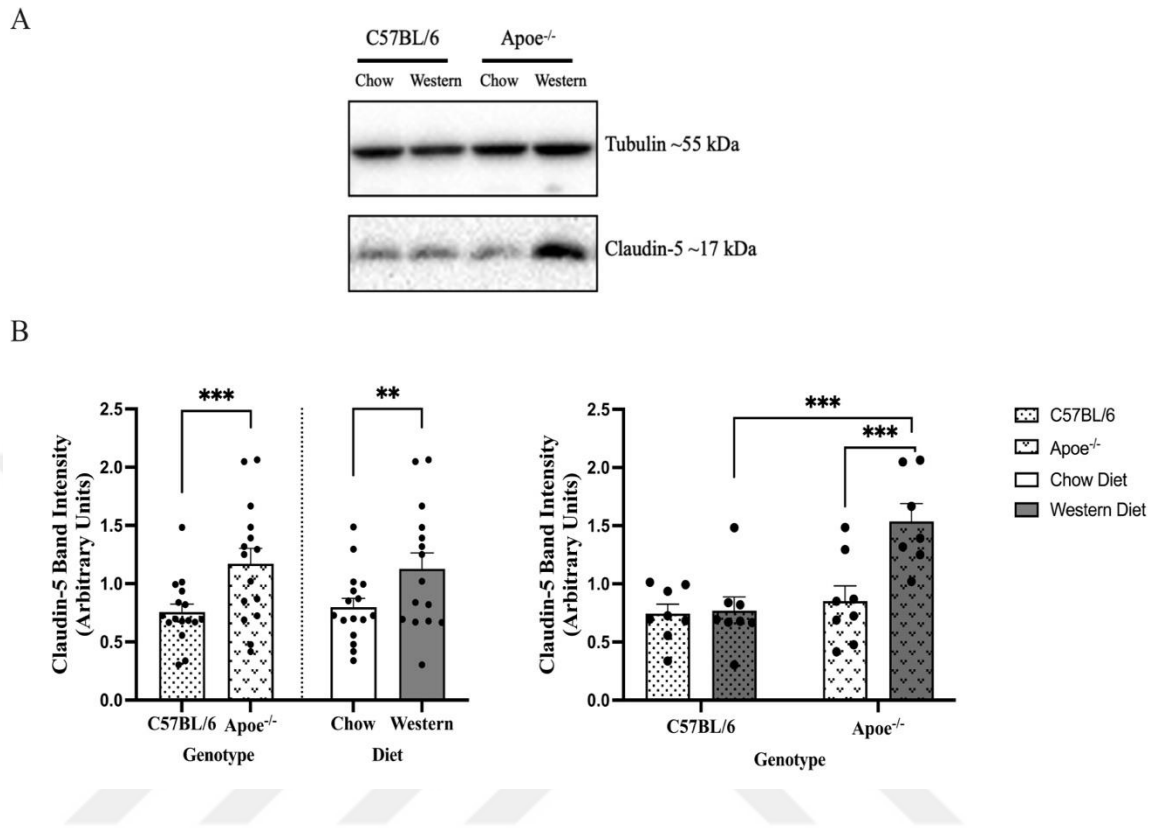

Figure 3.3. Observed Bands and Expression of Claudin-5 Across Genotype and Diet in Cerebral Cortex. The A part shows the representative images of Claudin-5 and Tubulin. The left side of the B part shows the graphs of the normalized quantified bands of Claudin-5 for the main effects of diet and genotype. The right side of the B part shows the interaction effect between diet and genotype. The expression of Claudin-5 significantly increased with the western diet and in Apoe knock-out mice, and there was a significant effect of interaction. Expression of Claudin-5 was higher in Apoe$^{-/-}$ animals fed with the western diet when compared to C57BL/6 animals fed with the western diet and Apoe$^{-/-}$ animals fed with the chow diet. The error bars represent mean +1 SEM and statistical significance was set at $p < 0.05$, ** $p \leq 0.01$, *** $p \leq 0.001$. n=8 for C57BL6 Chow group, C57BL6 Western, Apoe$^{-/-}$ Chow groups and n=7 for Apoe$^{-/-}$ Western groups.

3.2.2.2. Occludin

The normality tests were done using the Shapiro-Wilk test, and the homogeneity was checked using the Levene's Test. Kruskal-Wallis test has revealed that diet (H (1) =0.306, p = 0.580, Figure 3.4) and genotype (H (1) =0.100, p = 0.752, Figure 3.4) do not have a significant effect on Occludin. The partial correlation analysis is done to see the correlation between body weights. Spearman's correlation revealed that there is no significant correlation between body weights and Occludin (r(27) = - 0.071 p = 0.713).

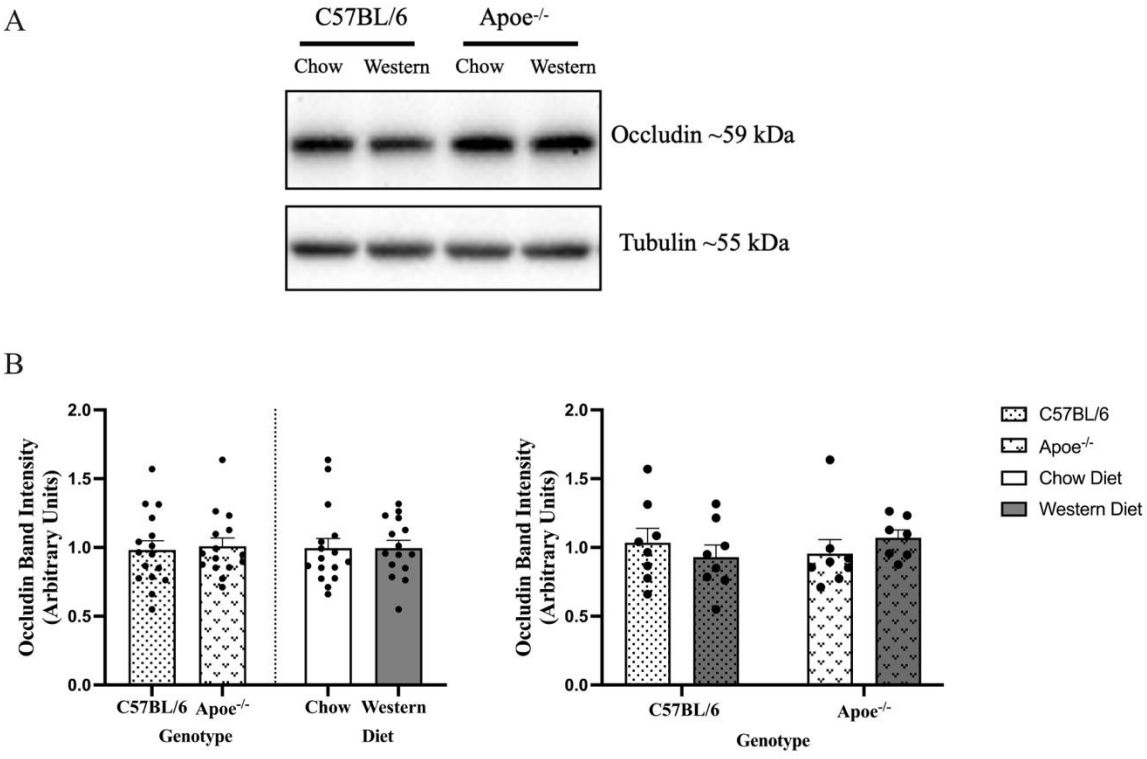

Figure 3.4. Observed Bands and Expression of Occludin Across Genotype and Diet in the Cerebral Cortex. The A part shows the representative images of Occludin and Tubulin. The left side of B part shows the graphs of the normalized quantified bands Occludin for the main effects of diet and genotype. The right side of the B part shows the

interaction effect between diet and genotype. The expression of Occludin did not change significantly with diet or genotype. The error bars represent mean +1 SEM and statistical significance was set at $p < 0.05$. n=8 for C57BL6 Chow group, C57BL6 Western, $Apoe^{-/-}$ Chow groups and n=7 for $Apoe^{-/-}$ Western groups.

3.2.2.3 VEGF

The normality tests were done using the Shapiro-Wilk test, and the homogeneity was checked using the Levene's Test. A two-way ANOVA test has revealed that diet (F (1,8) = 1.718 p = 0.226, Figure 3.5) and genotype (F (1,8) = 0.661 p = 0.440, Figure 3.5) do not have a significant effect on the VEGF mRNA expression levels. Moreover, there is no significant interaction between diet and genotype (F (1,8) = 0.000 p = 0.991, Figure 3.5). The partial correlation analysis is done to see the correlation between body weights. Spearman's correlation revealed that there is no significant correlation between body weights and VEGF (r(8) = -0.221 p = 0.540).

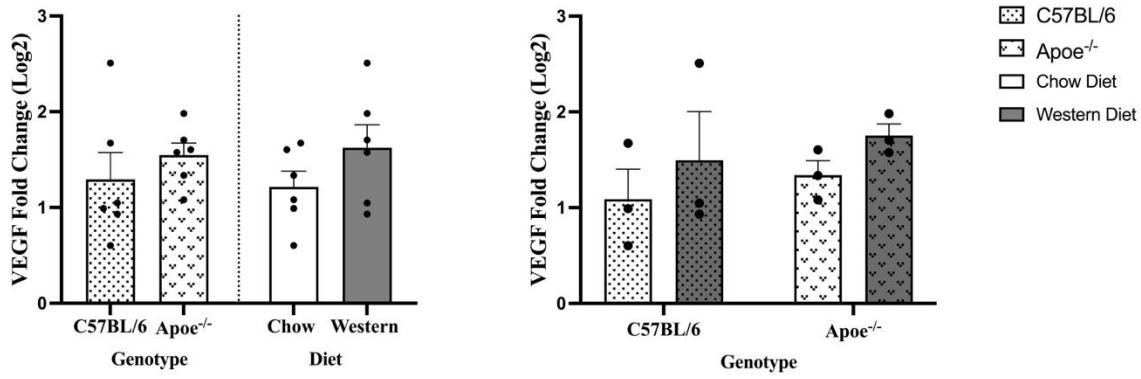

Figure 3.5. VEGF mRNA Expression Levels Across Diet and Genotype in the Cerebral Cortex. The Left side of the figure shows the main effects of genotype and diet and the right side shows the interaction effect between the diet and genotype. The mRNA expression levels of VEGF did not change significantly with diet or genotype. And there was no significant interaction between diet and genotype. The error bars represent mean +1 SEM, and statistical significance was set at $p < 0.05$. n=3 for all groups.

3.2.3. Synaptic Integrity

To investigate how a high-fat diet affected the synaptic integrity, the following markers have been used: PSD-95, Gephyrin and Synaptophysin. To confirm the synaptosome isolation, confirmation experiments have been done. The images can be found at the Appendix section.

3.2.3.1. PSD-95

The normality tests were done using the Shapiro-Wilk test, and the homogeneity was checked using the Levene's Test. A two-way ANOVA has revealed that the main effects of diet (F (1,30) =3.806, p = 0.060, Figure 3.6) and genotype (F (1,30) =0.046, p = 0.307,

Figure 3.6) were not significant. Moreover, the overall interaction was not significant (F (1,30) =2.196, p = 0.149, Figure 3.6). The partial correlation analysis is done to see the correlation between body weights. Pearson's correlation revealed that there is no significant correlation between body weights and PSD-95 (r(30) = -0.126 p = 0.492).

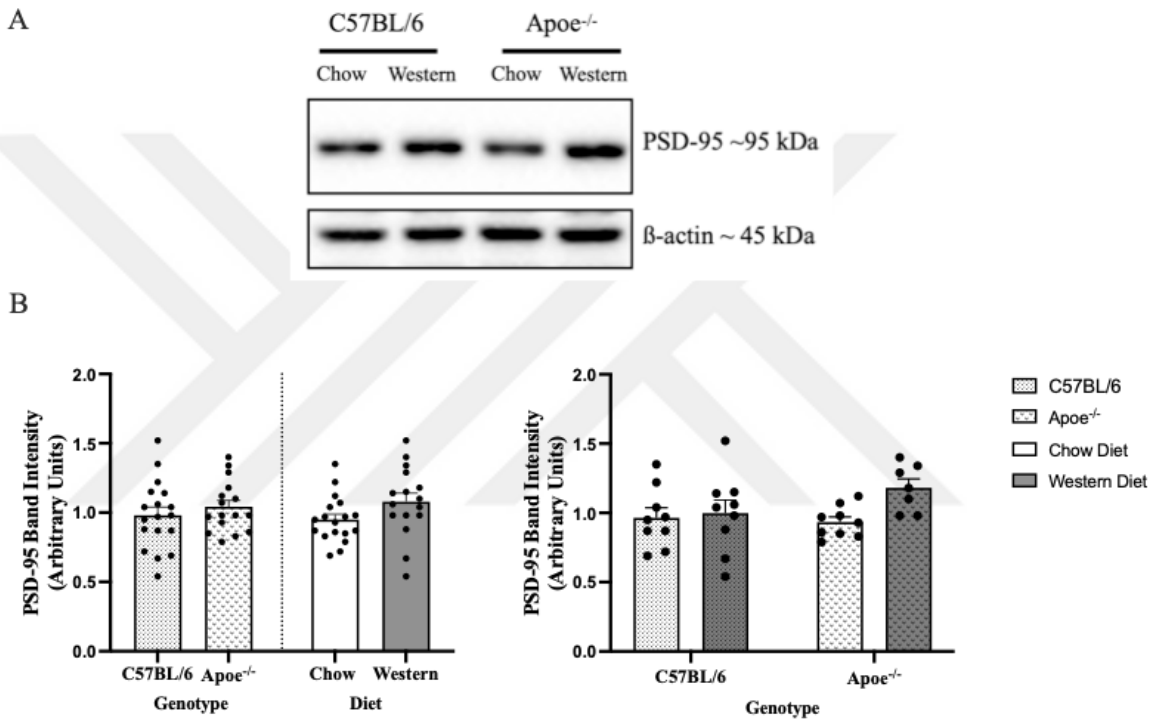

Figure 3.6. Observed Bands and Expression of PSD-95 Across Diet and Genotype. The A part shows the representative images of PSD-95 and ß-actin. The B part shows the graphs of the normalized quantified bands for PSD-95. The expression of PSD-95 did not significantly change with the genotype, and diet. There is also no significant interaction effect. The error bars represent mean +1 SEM and statistical significance was set at p < 0.05. n=9 for C57BL/6 fed with Chow, Western diet and Apoe$^{-/-}$ fed with chow diet, and n=7 for Apoe$^{-/-}$ Western groups.

3.2.3.2. Gephyrin

The normality tests were done using the Shapiro-Wilk test, and the homogeneity was checked using the Levene's Test. Assumptions of the two-way ANOVA test were not met. The Kruskal-Wallis test has been performed. It has shown that there is no significant effect of genotype (H (1) =0.019 p = 0.890, Figure 3.7) or diet (H (1) =0.430 p = 0.512, Figure 3.7) on Gephyrin expression. The partial correlation analysis is done to see the correlation between body weights. Spearman's correlation revealed that there is no significant correlation between body weights and Gephyrin (r(30) = 0.109 p = 0.553).

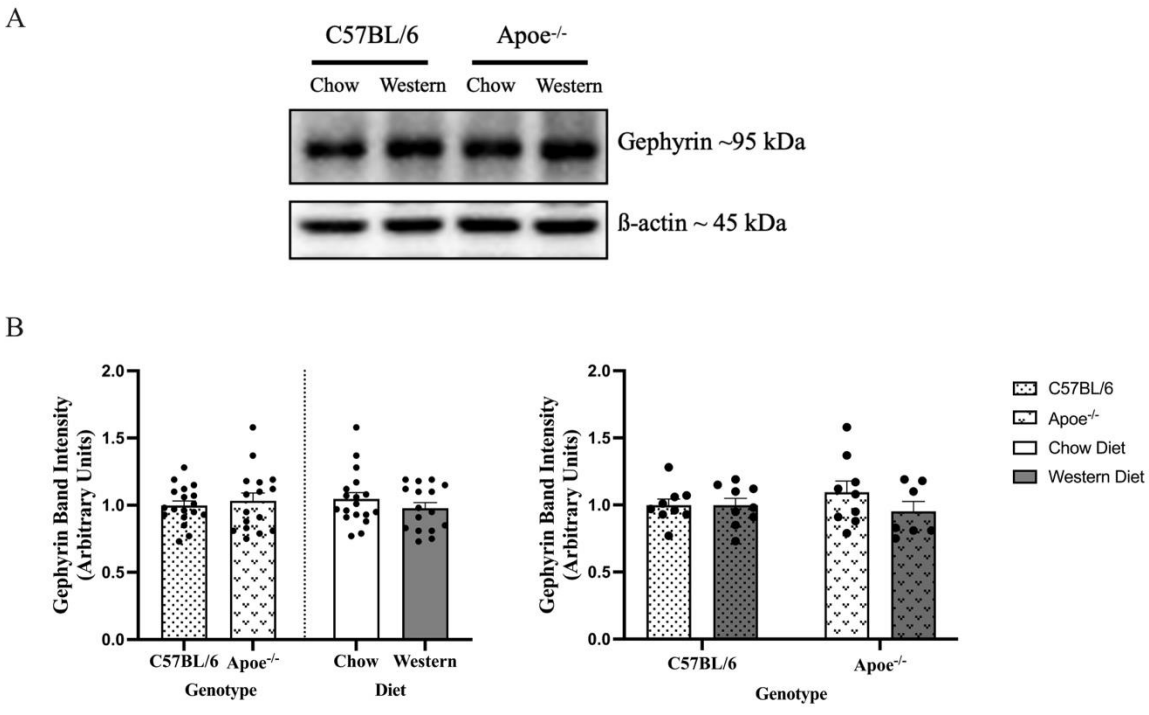

Figure 3.7. Observed Bands and Expression of Gephyrin Across Diet and Genotype. The A part shows the representative images of Gephyrin and ß-actin. The B part shows the graphs of the normalized quantified bands for Gephyrin. The expression of Gephyrin did not significantly change with the genotype and diet. The error bars represent mean +1 SEM

and statistical significance was set at $p < 0.05$. n=9 for C57BL6 Chow group and Western groups, and Apoe$^{-/-}$ Chow, and n=7 for Apoe$^{-/-}$ Western groups.

3.2.3.3. Synaptophysin

The normality tests were done using the Shapiro-Wilk test, and the homogeneity was checked using the Levene's Test. Assumptions of the two-way ANOVA test were not met. The Kruskal-Wallis test has been performed. It has shown that there is no significant effect of genotype (H (1) =0.233 p = 0.629, Figure 3.8) or diet (H (1) = 0.233 p = 0.629, Figure 3.8) on Synaptophysin expression. The partial correlation analysis is done to see the correlation between body weights. Spearman's correlation revealed that there is no significant correlation between body weights and Synaptophysin (r(30) = -0.240 p = 0.185).

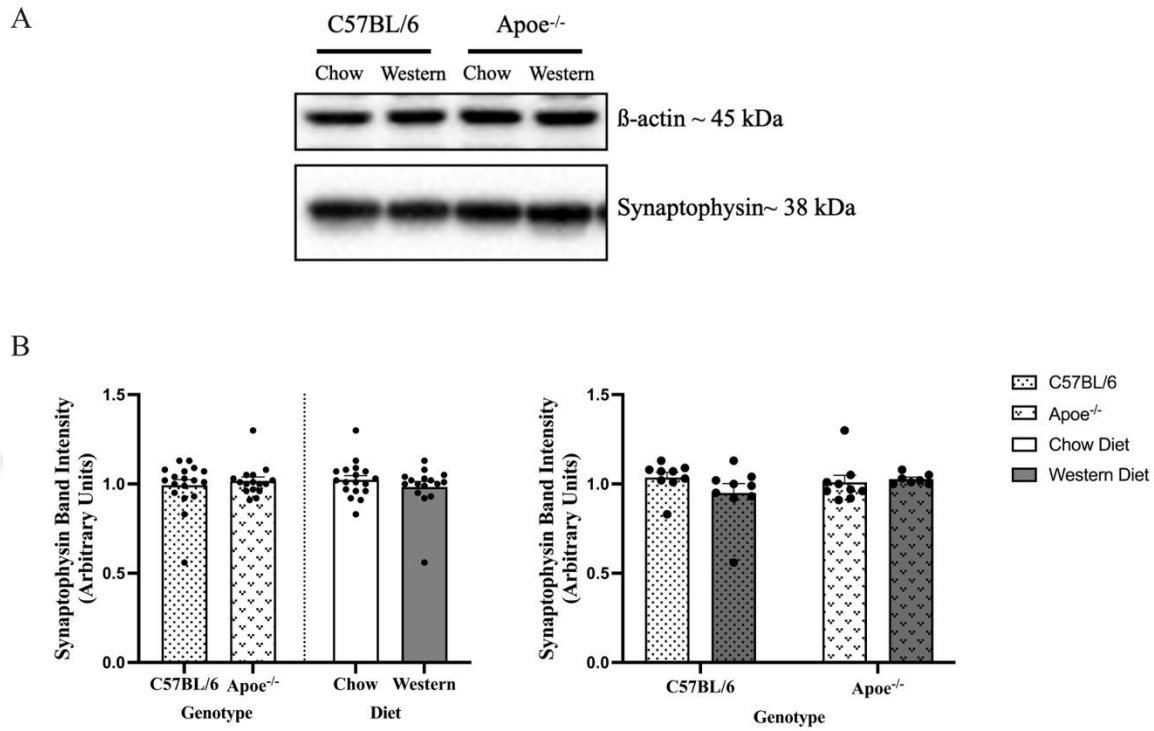

Figure 3.8. Observed Bands and Expression of Synaptophysin Across Diet and Genotype. The A part shows the representative images of Synaptophysin and ß-actin. The B part shows the graphs of the normalized quantified bands for Synaptophysin. The expression of Synaptophysin did not significantly change with the genotype and diet. The error bars represent mean +1 SEM and statistical significance was set at $p < 0.05$. n=9 for C57BL6 Chow group and Western groups, and Apoe$^{-/-}$ Chow, and n=7 for Apoe$^{-/-}$ Western groups.

3.3. PERK Pathway Inhibition on the Mouse Cerebral Cortex

3.3.1. ER Stress – The PERK Pathway

To investigate the PERK pathway inhibition following markers have been used for Western blot analysis; p-PERK and p-eIF2α. And the following markers have been used for RT-qPCR analysis; ATF4 and CHOP.

3.3.1.1. p-PERK

The normality tests were done using the Shapiro-Wilk test, and the homogeneity was checked using the Levene's Test. The Mann-Whitney U Test has revealed that the expression of p-PERK did not change with the injection of Trans-ISRIB (U (8) =28, p = 0.674, Figure 3.9) and GSK2606414 (U (4) =6, p = 0.564, Figure 3.9). The partial correlation analysis is done to see the correlation between body weights. Spearman's correlation revealed that there is no significant correlation between body weight and p-PERK/PERK ratio for both Trans-ISRIB (r(13) = -0.084 p = 0.765) and GSK2606414 (r(5) = -0.569 p = 0.182).

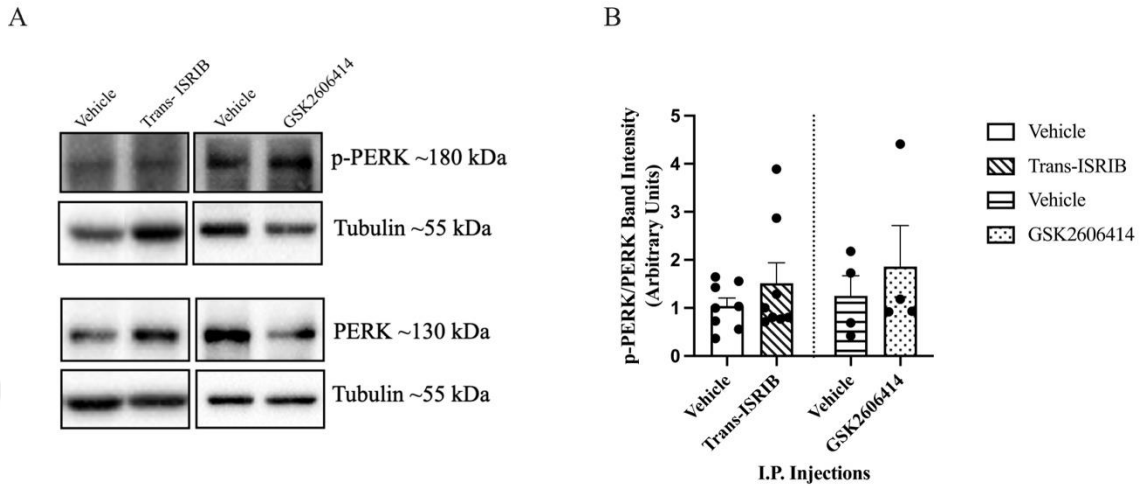

Figure 3.9 Observed Bands and Expression of p-PERK In Trans-ISRIB and GSK2606414 Injected Animals. The A part of the image shows the representative band image for p-PERK, PERK, and Tubulin. The B part shows the graphs of the quantified bands for the p-PERK/PERK ratio normalized to Tubulin. The expression of p-PERK did not significantly change with Trans-ISRIB and GSK2606414 injections. The error bars represent mean +1 SEM and statistical significance was set at $p < 0.05$. n =8 for Trans-ISRIB and its control group, n=4 for GSK2606414 and its control group.

3.3.1.2. p-eIF2α

The normality tests were done using the Shapiro-Wilk test, and the homogeneity was checked using the Levene's Test. The student t-test has revealed that the expression of p-eIF2α did not change with the injection of Trans-ISRIB (t (14) =0.773, p = 0.319, Figure 3.10). Also, there is no significant change with the injection of GSK2606414 (t (6) =-0.789, p = 0.087, Figure 3.10). The partial correlation analysis is done to see the correlation between body weights. Pearson's correlation (for Trans-ISRIB) and Spearman's

correlation (For GSK2606414) revealed that there is no significant correlation between body weight and p-eIF2α/eIF2α ratio for both Trans-ISRIB ($r(13) = 0.172$ $p = 0.541$) and GSK2606414 ($r(5) = 0.054$ $p = 0.908$).

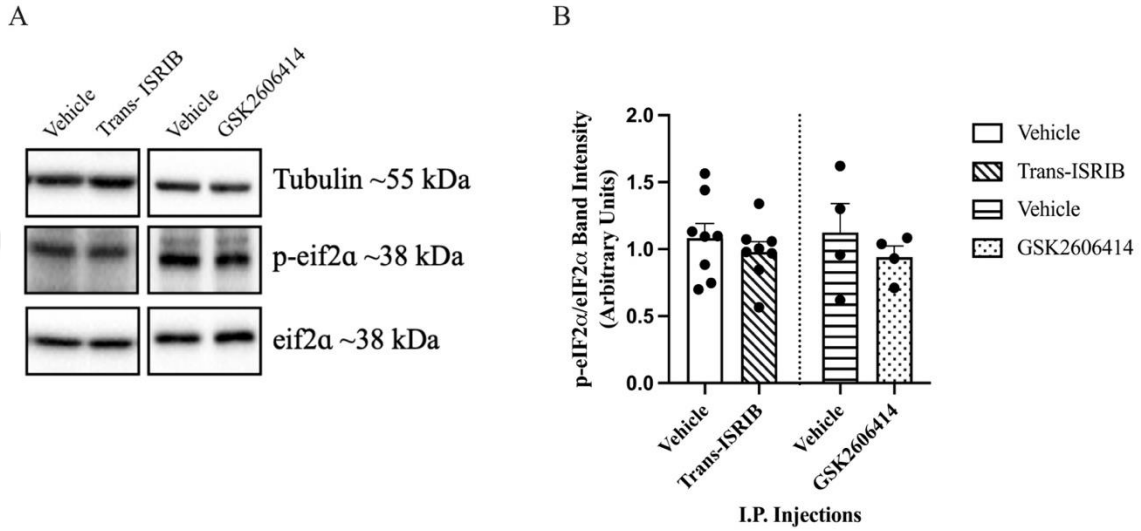

Figure 3.10 Observed Bands and Expression of p-eIF2α In Trans-ISRIB and GSK2606414 Injected Animals. The A part shows the representative images of p-eIF2α, eIF2α and tubulin. The B part shows the graphs of the normalized quantified bands for the p-eIF2α/eIF2α ratio. The expression of p-eIF2α did not significantly change with Trans-ISRIB and GSK2606414 injections. The error bars represent mean +1 SEM and statistical significance was set at $p < 0.05$. n =8 for Trans-ISRIB and its control group, n=4 for GSK2606414 and its control group.

3.3.1.3. ATF4

The normality tests were done using the Shapiro-Wilk test, and the homogeneity was checked using the Levene's Test. The student t-test has revealed that the expression of ATF4 did not change with the injection of Trans-ISRIB (t (4) =0.434, p = 0.687, Figure

3.11) and The Mann-Whitney U Test revealed that GSK2606414 (U (6) =2, p = 0.275, Figure 3.11). The partial correlation analysis is done to see the correlation between body weights. Pearson's correlation (for Trans-ISRIB) and Spearman's correlation (For GSK2606414) revealed that there is no significant correlation between body weight and ATF4 for both Trans-ISRIB (r(3) = -0.853 p = 0.066) and GSK2606414 (r(3) = -0.146 p = 0.814).

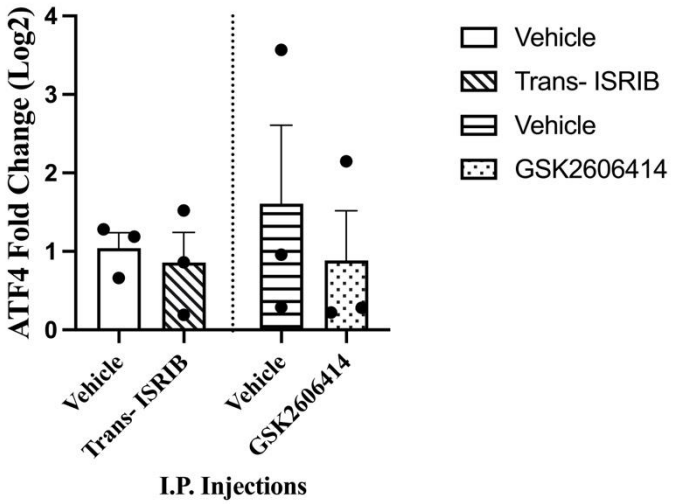

Figure 3.11. ATF4 mRNA Expression Levels in Trans-ISRIB and GSK2606414 Injected Animals. The figure shows the graph of the mRNA expression levels of ATF4 when the animals are injected with PERK pathway inhibitors. The left side shows the effect of Trans-ISRIB compared to its vehicle, and the right side shows the effect of GSK2606414 compared to its vehicle. The expression of ATF4 did not change significantly with injections of Trans-ISRIB or GSK2606414. The error bars represent mean +1 SEM, and statistical significance was set at $p < 0.05$. n=3 for all groups.

3.3.1.4 CHOP

The normality tests were done using the Shapiro-Wilk test, and the homogeneity was checked using the Levene's Test. The student t-test has revealed that the expression of CHOP did not change with the injection of Trans-ISRIB (t (4) = 0.224, p = 0.833, Figure 3.12). Also, there is no significant change with the injection of GSK2606414 (t (4) =0.886, p = 0.426, Figure 3.12). The partial correlation analysis is done to see the correlation between body weights. Pearson's correlation revealed that for Trans-ISRIB, there is significant negative correlation between CHOP and body weight (r(3) = -0.884 p = 0.047). For GSK2606414, Spearman's correlation revealed that there is no significant correlation between body weight and CHOP (r(3) = -0.568 p = 0.318).

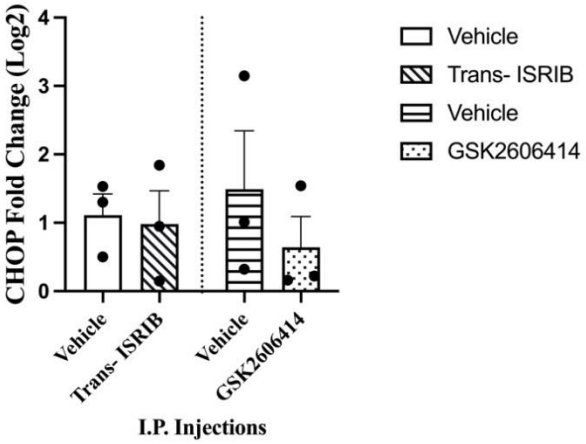

Figure 3.12. CHOP mRNA Expression Levels in Trans-ISRIB and GSK2606414 Injected Animals. The figure shows the graph of the mRNA expression levels of CHOP when the animals are injected with PERK pathway inhibitors. The left side shows the effect of Trans-ISRIB compared to its vehicle, and the right side shows the effect of GSK2606414 compared to its vehicle. The expression of CHOP did not change significantly with

injections of Trans-ISRIB or GSK2606414. The error bars represent mean +1 SEM and statistical significance was set at $p < 0.05$. n=3 for all groups.

3.3.2. Blood-Brain Barrier Integrity

To investigate how the PERK pathway inhibition affected the blood-brain barrier integrity, the following markers have been used for Western blot analysis: Claudin-5 and Occludin. For the RT-qPCR analysis vegf has been used.

3.3.2.1. Claudin-5

The normality tests were done using the Shapiro-Wilk test, and the homogeneity was checked using the Levene's Test. The student t-test has revealed that the expression of Claudin-5 did not change with the injection of Trans-ISRIB (t (14) = -1.883, p = 0.081, Figure 3.13). Also, there is no significant change with the injection of GSK2606414 (t (6) =0.286, p = 0.785, Figure 3.13). The partial correlation analysis is done to see the correlation between body weights. Pearson's correlation (for Trans-ISRIB) and Spearman's correlation (For GSK2606414) revealed that there is no significant correlation between body weight and Claudin-5 for both Trans-ISRIB (r(13) = 0.096 p = 0.733) and GSK2606414 (r(5) = 0.532 p = 0.219).

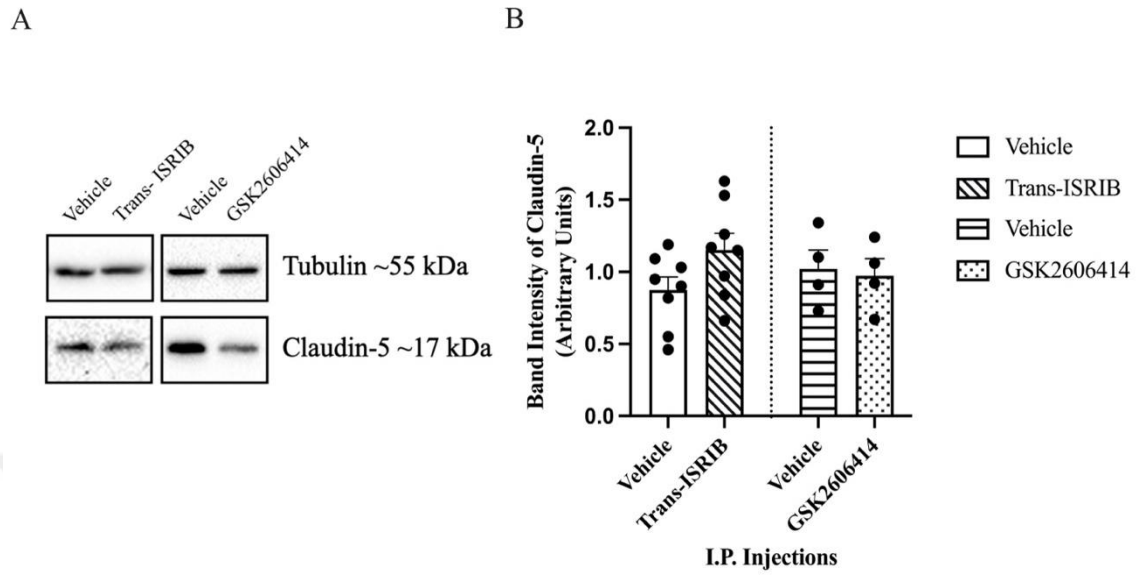

Figure 3.13. Observed Bands and Expression of Claudin-5 In Inhibitor Groups. The A part shows the representative images of Claudin-5 and Tubulin. The B part shows the graphs of the normalized quantified bands for Claudin-5. The expression of Claudin-5 did not significantly change with Trans-ISRIB injections or GSK2606414 injections. The error bars represent mean +1 SEM and statistical significance was set at $p < 0.05$. n=8 for Trans-ISRIB and its control group, n=4 for GSK2606414 and its control group.

3.3.2.2. Occludin

The normality tests were done using the Shapiro-Wilk test, and the homogeneity was checked using the Levene's Test. The student t-test has revealed that the expression of Occludin did not change with the injection of Trans-ISRIB (t (14) =0.589, p=0.953, Figure 3.14) and GSK2606414 (t (6) =-2.130, p=0.077, Figure 3.14). The partial correlation analysis is done to see the correlation between body weights. Pearson's correlation (for Trans-ISRIB) and Spearman's correlation (For GSK2606414) revealed that there is no

significant correlation between body weight and Occludin for both Trans-ISRIB ($r(13) = -0.092$ $p = 0.745$) and GSK2606414 ($r(5) = -0.245$ $p = 0.596$).

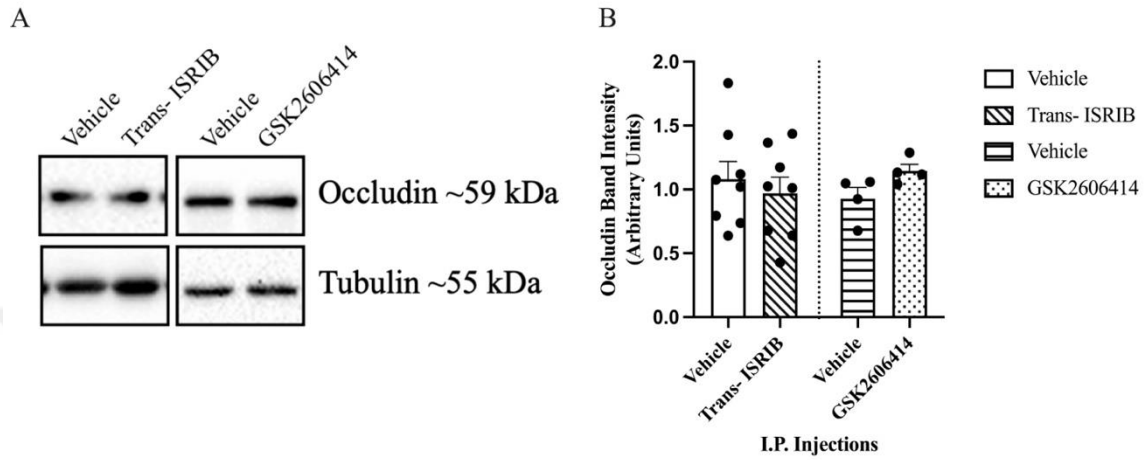

Figure 3.14. Observed Bands and Expression of Occludin in Trans-ISRIB and GSK2606414 Injected Animals. The A part shows the representative images of Occludin and tubulin. The B part shows the graphs of the normalized quantified bands Occludin. The expression of Occludin did not significantly change with Trans-ISRIB and GSK2606414 injections. The error bars represent mean +1 SEM and statistical significance was set at $p < 0.05$. n =8 for Trans-ISRIB and its control group, n=4 for GSK2606414 and its control group.

3.3.2.3. VEGF

The normality tests were done using the Shapiro-Wilk test, and the homogeneity was checked using the Levene Test. The Mann-Whitney U Test revealed that the expression of VEGF did not change with the injection of Trans-ISRIB (U (6) =4, p=0.825, Figure 3.15) and GSK2606414 (U (6) =4, p=0.827, Figure 3.15). The partial correlation analysis is done to see the correlation between body weights. Spearman's correlation revealed that for

Trans-ISRIB, there is significant negative correlation between VEGF and body weight ($r(3) = -0.880$ $p = 0.049$). For GSK2606414, there is no significant correlation between body weight and VEGF ($r(3) = -0.193$ $p = 0.756$).

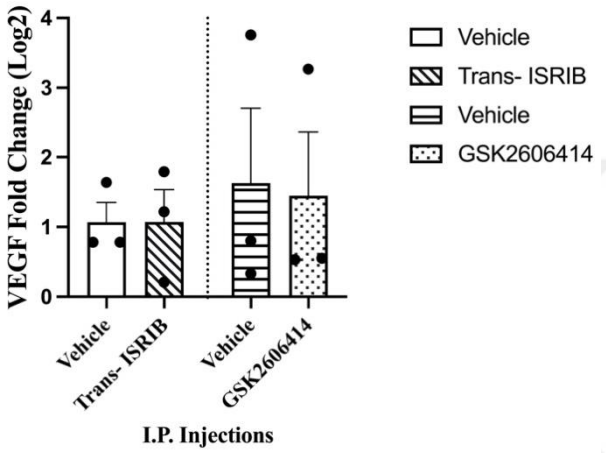

Figure 3.15. VEGF mRNA Expression Levels in Trans-ISRIB and GSK2606414 Injected Animals. The figure shows the graph of the mRNA expression levels of VEGF when the animals are injected with PERK pathway inhibitors. The left side shows the effect of Trans-ISRIB compared to its vehicle, and the right side shows the effect of GSK2606414 compared to its vehicle. The expression of VEGF did not change significantly with injections of Trans-ISRIB or GSK2606414. The error bars represent mean +1 SEM and statistical significance was set at $p < 0.05$. n=3 for all groups.

3.3.3. Synaptic Integrity

To investigate how the inhibition of PERK pathway affected the synaptic integrity, the following markers have been used for Western blot analysis: PSD-95, Gephyrin and Synaptophysin.

3.3.3.1. PSD-95

The normality tests were done using the Shapiro-Wilk test, and the homogeneity was checked using the Levene's Test. The student t-test has revealed that the expression of PSD-95 did not change with the injection of Trans-ISRIB (t (14) =0.230, p = 0.822, Figure 3.16). Also, there is no significant change with the injection of GSK2606414 (t (6) =1.261, p = 0.254, Figure 3.16). The partial correlation analysis is done to see the correlation between body weights. Pearson's correlation revealed that there is no significant correlation between body weight and PSD-95 for both Trans-ISRIB (r(13) = -0.392 p = 0.148) and GSK2606414 (r(5) = -0.155 p = 0.740).

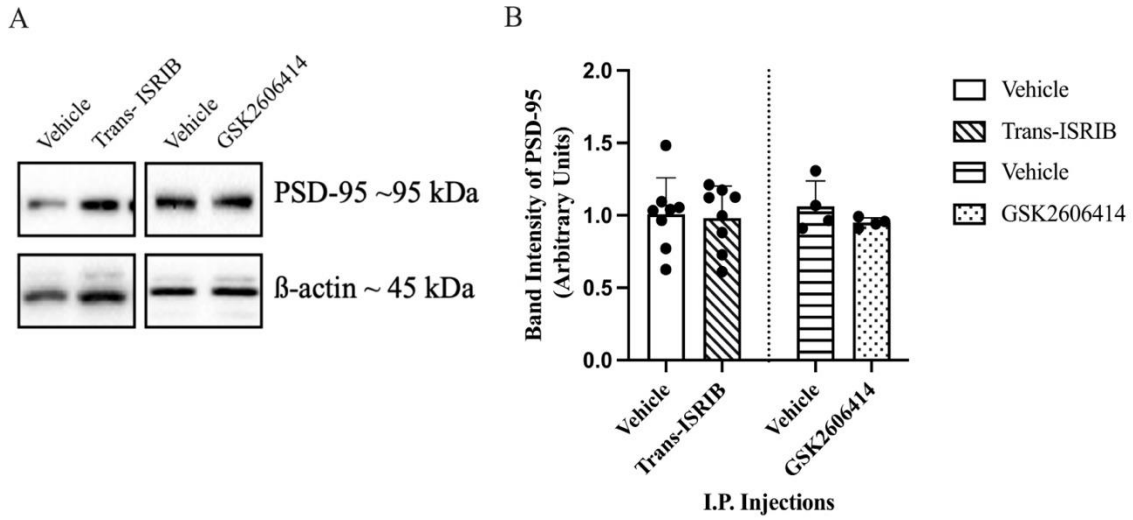

Figure 3.16. Observed Bands and Expression of PSD-95 In Inhibitor Groups. The A part shows the representative images of PSD-95 and ß-actin. The B part shows the graphs of the normalized quantified bands for PSD-95. The expression of PSD-95 did not significantly change with Trans-ISRIB injections or GSK2606414 injections. The error bars represent mean +1 SEM and statistical significance was set at $p < 0.05$. n=8 for Trans-ISRIB and its control group, n=4 for GSK2606414 and its control group.

3.3.3.2. Gephyrin

The normality tests were done using the Shapiro-Wilk test, and the homogeneity was checked using the Levene's Test. The student t-test has revealed that the expression of Gephyrin did not change with the injection of Trans-ISRIB (t (14) = -1.493, p = 0.158, Figure 3.17). Also, there is no significant change with the injection of GSK2606414 (t (6) =0.074, p = 0.943, Figure 3.17). The partial correlation analysis is done to see the correlation between body weights. Pearson's correlation revealed that there is no significant correlation between body weight and Gephyrin for both Trans-ISRIB (r(13) = 0.326 p = 0.236) and GSK2606414 (r(5) = -0.502 p = 0.251).

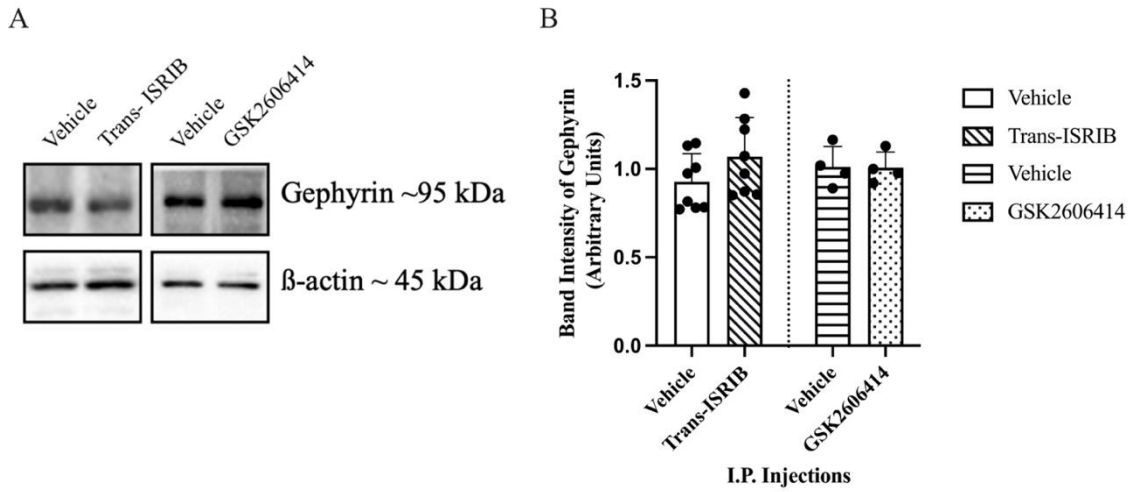

Figure 3.17. Observed Bands and Expression of Gephyrin in Inhibitor Groups. The A part shows the representative images of Gephyrin and ß-actin. The B part shows the graphs of the normalized quantified bands for Gephyrin. The expression of Gephyrin did not significantly change with Trans-ISRIB injections or GSK2606414 injections. The error bars represent mean +1 SEM and statistical significance was set at $p < 0.05$. n=8 for Trans-ISRIB and its control group, n=4 for GSK2606414 and its control group.

3.3.3.3. Synaptophysin

The normality tests were done using the Shapiro-Wilk test, and the homogeneity was checked using the Levene's Test. The student t-test has revealed that the expression of Synaptophysin did not change with the injection of Trans-ISRIB (t (14) = 1.368, p = 0.193, Figure 3.18). Also, there is no significant change with the injection of GSK2606414 (t (6) =-0.835, p = 0.436, Figure 3.18). The partial correlation analysis is done to see the correlation between body weights. Pearson's correlation revealed that there is no significant correlation between body weight and Synaptophysin for both Trans-ISRIB (r(13) = -0.385 p = 0.157) and GSK2606414 (r(5) = -0.348 p = 0.444).

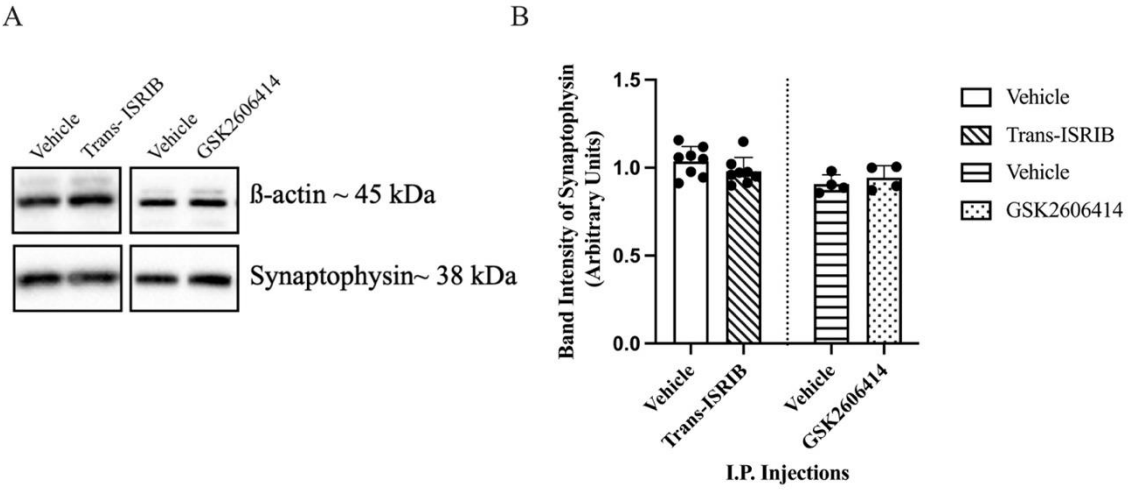

Figure 3.18. Observed Bands and Expression of Synaptophysin in Inhibitor Groups. The A part shows the representative images of Synaptophysin and ß-actin. The B part shows the graphs of the normalized quantified bands for Synaptophysin. The expression of Synaptophysin did not significantly change with Trans-ISRIB injections or GSK2606414 injections. The error bars represent mean +1 SEM and statistical significance was set at p

< 0.05. n=8 for Trans-ISRIB and its control group, n=4 for GSK2606414 and its control group.

CHAPTER 4

DISCUSSION

This thesis work is a two-part study. In the first part of the study, the aim is to understand how the high-fat diet affects the PERK pathway, blood-brain barrier integrity, and synaptic integrity in the cerebral cortex of both C57BL/6 and Apoe$^{-/-}$ subjects. The second part of the study aims to understand how the inhibition of the PERK pathway using Trans-ISRIB and GSK2606414 affects the same parameters.

For the first aim, both WT and Apoe$^{-/-}$ mouse is fed with either a standard chow diet or a high-fat diet for 16 weeks. Then, western blot and RT-qPCR analysis is performed for cerebral cortical tissues. For the ER stress, the protein levels of p-PERK and p-eIF2α are analyzed; in the meantime, to assess the BBB integrity, gene expression levels of VEGF and protein levels of Claudin-5 and Occludin are assessed. Lastly, the protein levels of PSD-95, Gephyrin, and Synaptophysin are investigated to study synaptic integrity. For the second aim, Apoe$^{-/-}$ mice fed with a high-fat diet are I.P. injected with either Trans-ISRIB or GSK2606414 for six weeks. To assess the ER stress under the inhibitors, the protein levels of p-PERK, p-eIF2α, and gene expression levels of ATF4 and CHOP are analyzed. For the BBB and synaptic integrity same parameters are checked.

Our western blot analysis shows that the p-PERK/PERK ratio is not significantly affected by either diet or genotype. Also, there is no significant interaction between these main effects. However, when it comes to the p-eIF2α/eIF2α ratio, it is significantly affected by

the genotype, as it is significantly decreased in cerebral cortical tissues of Apoe$^{-/-}$ subjects compared to WT animals. Surprisingly, the protein levels of p-eIF2α are increased in western diet-fed C57BL/6 subjects compared to chow diet given C57BL/6 mice. Furthermore, there is a significant interaction between diet and genotype, and levels of p-eIF2α are significantly less in western diet-fed Apoe$^{-/-}$ animals when compared to western diet-fed WT animals. Moreover, there is no significant correlation between body weights for either marker. This might suggest that the increase in phosphorylation levels of eIF2α independent from the body weight change.

The literature suggests that excessive nutrients as a result of hyperlipidemia are detected by ER. Detection of these excessive nutrients activates the UPR pathway by causing ER stress [88]. One of the arms of the UPR is the PERK pathway. Under stress conditions, PERK gets activated and autophosphorylates. The lack of a significant increase in the p-PERK/PERK ratio suggests no alteration in PERK pathway activation by genotype or diet. Therefore, PERK is not activated by neither the high-fat diet nor the Apoe$^{-/-}$ genotype in our subjects' cerebral cortex. The previous studies provide an input about the activated PERK pathway under high-fat diet feeding in other tissues such as the hippocampus [137],[138]. Since the PERK pathway is not activated in this thesis study in the cerebral cortex, this can point out tissue-specific differences in the PERK pathway activation in the brain. It is suggested that tissues and cells have distinct needs for ER capacity and function, and the regulation of UPR can be different as well. Moreover, different tissues activate different arms of UPR [139]. Through these suggestions, to understand our results better, it would be beneficial to investigate other branches of UPR to see whether they are

activated in the cerebral cortex rather than the PERK pathway.

eIF2 is one of the downstream elements of the PERK pathway. When PERK auto-phosphorylates, it causes the phosphorylation of eIF2 from its alpha subunit. However, in our study, there is a significant change in the phosphorylation levels of eIF2 when there is no PERK activation. In the absence of PERK activation, it is possible that another inducer caused the phosphorylation of eIF2 in WT animals fed with the western diet. Indeed, eIF2 has two other inducers apart from the PERK: Protein Kinase R (PKR) and General control nonderepressible 2 (GCN2). They respond to different stress inducers in the cell. PKR activity can be induced by excess nutrition, such as saturated fatty acids in the body [140],[141]. So, it might be possible that PKR is the reason why we saw an increased p-eIF2α in the western diet-fed wild-type mice when compared to chow-fed wild-type animals. To make better assumptions, PKR must be investigated in our subjects' cerebral cortical tissues.

Interestingly, Apoe knock-out animals do not show the same pattern in p-eIF2α. A study has shown an upregulation of BiP, which is an ER chaperone, under ER stress. They have shown that under chronic stress inducers, cells get adapted, and they get unsusceptible to further UPR activation. They suggest that, under chronic ER stress, upregulation of BiP is followed by improved protein folding, which suppresses UPR activation [142]. ApoE is responsible for the clearance of VLDL and chylomicron remnants [51]. Therefore, knocking this protein changes the lipid metabolism of the animal. As $Apoe^{-/-}$ already has a stressed metabolism due to the absence of apolipoprotein E, feeding them with a high-fat diet to further activate the ER stress by inducing hyperlipidemia might cause an adaptive

mechanism in these mice to suppress the phosphorylation of eIF2. To test this, BiP can be investigated in our experimental setup as well.

BBB protects the brain from the neurotoxins circulating in the blood. It has many components that contribute to this protection. Claudin-5 and Occludin are scaffold proteins that are found in the BBB. Hyperlipidemia affects the BBB by increasing its permeability [115]. Our western blot analysis of the Claudin-5 marker, as a part of the BBB integrity research, is significantly affected by both diet and genotype. Interestingly, it is significantly higher in $Apoe^{-/-}$ when compared to WT animals, and it is higher in western diet-fed animals when compared to chow diet-fed animals. Moreover, there is a significant interaction between diet and genotype. Claudin-5 levels are significantly higher in western diet-fed $Apoe^{-/-}$ animals when compared to western diet-fed WT animals. Additionally, western diet feeding is increased claudin-5 levels in $Apoe^{-/-}$ animals when compared to $Apoe^{-/-}$ animals fed with a chow diet. On the other hand, there are no significant effects of either diet, genotype, or interaction between these main effects on Occludin. Additionally, RT-qPCR analysis is revealed that there are no diet, genotype, or interaction effects on VEGF expression levels. Claudin-5 and Occludin are the main tight-junction proteins found in the blood-brain barrier. Also, there is no significant correlation between body weights and markers, suggesting that the increase in Claudin-5 is independent from the body weights. Previous studies showed a blood-brain barrier disruption induced by high-fat diet feeding and decreased levels of tight junction proteins [143]. However, in our study there is no decrease in Claudin-5 and Occludin upon high-fat diet feeding. Interestingly, Claudin-5 is significantly increased upon high-fat diet feeding in our experiments. In a study, they showed that low-grade inflammation causes the increased expression of various

tight junction proteins such as Occludin in the brain, suggesting that a possible protection mechanism might be in a role to restore the blood-brain barrier integrity caused by low-grade inflammation [144]. The inflammation levels of the same animals that have been used in this thesis work is checked by Fulya Kızıldağ, one of our lab members [145]. Her experiments reveales that there is an increase in inflammation markers (cleaved-caspase 1 and mature interleukin-1ß) in Apoe knock-out animals, suggesting that there might be an inflammatory response in Apoe knock-out animals. Thus, the increased levels of Claudin-5 in Apoe knock-out animals fed with a western diet might indicate a protective mechanism caused by the inflammation in these animals. Our finding of VEGF does not contradict our finding in Claudin-5. As the VEGF upregulation would cause a decreased upregulation of Claudin-5, the lack of significance in VEGF while having an increased expression of Claudin-5 fits together [146].

Although Claudin-5 is an indicator of blood-brain barrier integrity, it might not be enough to predict there is an increase in blood-brain barrier integrity. Occludin and ZO proteins regulate the Claudin-5 strands organization [147]. In studies it has been shown that knocking out Claudin-5 animals does not inhibit the tight-junction formation [148]. Moreover, in another study, they suggest that in their study blood-brain barrier disruption is not related to the degradation of Claudin-5; rather, it is its displacement that caused the disruption. So, they suggest that the linkage of Claudin-5 to actin, a process modulated by ZO proteins, is lost [149]. These findings suggest that the increase of only Claudin-5 might not be the sole and firm indicator of increased blood-brain barrier integrity. Checking the

ZO protein levels can be a good indicator of the integrity of BBB.

Two or more neurons communicate with each other through synapses. They have crucial components such as scaffold proteins PSD-95, Gephyrin or presynaptic components such as Synaptophsyin. A high-fat diet and hyperlipidemia affect the synaptic integrity by changing the expression of genes involved in synapse formation [127]. Western blot analysis of synaptic integrity investigations revealed that there is a trend towards an increase in PSD-95 of western diet-fed animals compared to chow diet-fed animals. However, there is no significant genotype effect in PSD-95. Furthermore, there is no significant interaction effect between diet and genotype. Additional to these results, there is no significant diet, genotype or interaction effect in the protein levels of Gephyrin and Synaptophysin in the cerebral cortical synaptosome. Also, there is no significant correlation between the synaptic markers and the body weights. Synaptic integrity is one of the factors that is affected by a high-fat diet [150]. Thus, investigating these markers was crucial to understand how high cholesterol levels affect the synaptic health. No change in these protein levels suggest, the presynaptic neurotransmitter release, excitatory and inhibitory synaptic strength are not affected by high-fat diet induced hyperlipidemia. However, these markers alone is not enough to comment on the synaptic integrity. A study showed a change in GABAergic signalling upon feeding with high-fat diet [151] Indeed, there are other factors that can affected rather than the scaffold proteins or abundant presynaptic protein Synaptophysin. So, understanding whether there is decline or

increased synaptic integrity requires different approaches to investigate.

The second part of the study investigates the inhibition of the PERK pathway. Under stress conditions PERK pathway is activated, thus this pathway is an important therapeutic target. Western blot analysis of the p-PERK/PERK ratio revealed that there is no significant change with either inhibitor (Trans-ISRIB and GSK2606414) compared to their respective controls. Moreover, western blot analysis showed that there is no significant change in the p-eIF2α/eIF2α ratio with Trans-ISRIB or GSK2606414 injections. There were also no significant correlation with the body weight. Furthermore, RT-qPCR analysis shows no significant change with injections of Trans-ISRIB or GSK2606414 in ATF4 and CHOP expression levels. Even though there is no significant correlation between body weights and ATF4, CHOP is significantly negatively correlated in Trans-ISRIB injected animals, suggesting an increase in body weight causes a decrease in CHOP. There is no significant correlation with body weight and either markers for GSK2606414 injected animals.

Trans-ISRIB works in a way that does not affect the phosphorylation of either PERK or eIF2. Rather it activates the eIF2B, so that global protein translation may continue. Thus, not seeing a significant change in the ratio of p-PERK/PERK or p-eIF2α/eIF2α is expected. However, there is also no change in the ATF4 and CHOP levels which we would expect a decrease when Trans-ISRIB is injected. It is important to note that the sample size was three for ATF4 and CHOP, unlike western blot analysis, which had approximately eight subjects. Therefore, the statistical power is low. This causes false negative results and reduces the finding of true results. Increasing the sample size to make more reliable assumptions would be better. GSK2606414 directly inhibits the phosphorylation of PERK, which inhibits the PERK pathway. Thus, for GSK2606414 we would expect a significant

decrease in the ER stress markers with the injections. In this case, it is important to note that an activation of the PERK pathway isn't showed by the first part of this thesis work. Moreover, there is significantly less p-eIF2α in Apoe$^{-/-}$ western-diet-fed animals. Only western diet-fed Apoe$^{-/-}$ animals is used for the injections. In this case, there might be a possibility that there is no activated PERK pathway to inhibit in the beginning.

Western blot analysis showed that there is no significant effect of Trans-ISRIB and GSK2606414 on Claudin-5 and Occludin. Moreover, RT-qPCR analysis revealed that there is no significant change in VEGF expression levels with either inhibitor. Even though there is no significant correlation between body weights and Claudin-5 and Occludin, VEGF is significantly negatively correlated in Trans-ISRIB injected animals, suggesting an increase in body weight causes a decrease in VEGF. There is no significant correlation with body weight and the markers for GSK2606414 injected animals. Lastly, western blot analysis demonstrated that there is no significant effect of Trans-ISRIB or GSK2606414 on any synaptic integrity markers: PSD-95, Gephyrin, and Synaptophysin. There is no significant correlation with body weight and the synaptic markers for both Trans-ISRIB and GSK2606414 injected animals. For the injections, a restored blood-brain barrier and synaptic integrity are aimed through the inhibition of the PERK pathway. Therefore, the lack of significance in the ER stress markers when injected with either inhibitor also suggests that there would be no change in the markers of the blood-brain barrier and synaptic integrity.

CHAPTER 5

CONCLUSIONS AND FUTURE DIRECTIONS

In the first part of this thesis work, ER stress, BBB integrity, and synaptic integrity have been investigated in the cerebral cortex of chow diet and western diet-fed C57BL/6 and Apoe-/- animals to understand the effect of a high-fat diet. In our study, a high-fat diet did not induce the phosphorylation of PERK. Therefore, no PERK pathway activation was seen in either genotype. However, p-eIF2α/eIF2α levels increased when C57BL/6 animals were fed with the western diet, and there were fewer p-eIF2α/eIF2α in Apoe knock-out animals when fed with the western diet. Our investigations on BBB integrity revealed that Claudin-5 increased in Apoe knock-out animals with a western diet, while Occludin and VEGF stayed unchanged. Also, in synaptic integrity markers remained unchanged. These results suggest that a high-fat diet and genotype have affected the ER stress markers and BBB integrity markers.

In the second part of this thesis work, the PERK pathway inhibition has been investigated. Trans-ISRIB or GSK2606414 inhibitors has been investigated on western diet-fed $Apoe^{-/-}$ animals in terms of ER stress, BBB integrity, and synaptic integrity. There were no significant results in animals injected with Trans-ISRIB or GSK2606414 in terms of ER stress, BBB integrity, and synaptic integrity.

There were a few limitations in this study, and some future studies might be added. First, ATF4 and CHOP are crucial markers for the assessment of PERK pathway activation. They were lacking in the first part of the experiments. The antibodies that have been tried were not working properly during western blot experiments. Their results are important as

they are the downstream elements of the PERK pathway, and therefore, they can give more information about the effects of a high-fat diet on the PERK pathway activation. So, just like the second part, RT-qPCR can be done on these animals for ATF4 and CHOP. Secondly, for the RT-qPCR experiments, only three animals were used to assess the effects of a high-fat diet and genotype on VEGF and later to understand the inhibition effects on VEGF, ATF4, and CHOP. Having a larger sample size in these experiments might change the results by reducing the errors. Moreover, there is no DNase treatment while doing the RNA isolation. DNase treatment is important as genomic DNA can contaminate the RNA, causing false-positive results [152]. The A260/280 values are commonly used to assess the purity of the RNA [153]. However, in this work, the A260/280 values are checked for each RNA, and furthermore, the peaks for each DNA are checked for possible DNA contamination. Moreover, the primers that are used in this work have exon-exon junctions. This avoids the amplification of genomic DNA if there is any contamination in the samples [154].

As mentioned in the discussion part, the inability to show the PERK pathway activation might be due to the cell's adaptation to the prolonged stress and resistance to further PERK pathway activation [142]. To test this theory, different feeding periods, such as two weeks and eight weeks, can be added alongside the 16-week feeding period. This way, we could see whether getting a short-term high-fat diet would cause PERK pathway activation without causing cell adaptation.

Investigating different diet processes can also be useful in how the brain is affected by the diet. For example, caloric restriction can be used to investigate whether it can change and reverse the effects of knocked-out Apoe, as caloric restriction is thought to be a good diet

for the brain [155]. Moreover, the animals that have been used in this study are dissected at their young adulthood. Seeing how different ages of mice are affected by diet intervention might provide better insights for the study. Therefore, an aged mice group, 18 to 24 months old, can be added to the studies.

For further investigation, other UPR pathways can be investigated. In a study, they have shown that even when cells are adapted to stress, they showed some ATF6 activation rather than PERK activation [138]. To see whether this is also valid for our study might be useful. Also, again, in the same study [138], they showed a BiP upregulation under prolonged stress. As BiP is an important ER chaperone that interacts with PERK, investigating BiP as well would help to interpret the results better. Moreover, to understand the pattern p-eif2α has shown, its regulators, such as PKR, can be utilized for future studies.

The Claudin-5 increase is not enough to say that an increased BBB integrity has been observed. Many BBB proteins, such as ZO proteins, especially ZO-1, interact with Claudin-5 and act as a bridge between actin molecules and the Claudins, arranging their placement on the endothelial membrane [156],[157]. Because its linkage to the cytoskeleton might still be at fault, to look more into this, ZO proteins can be studied.

As discussed in the Discussion part, there is no change in the synaptic integrity markers, but, other synaptic markers. For example, receptors such as NMDA and GABA receptors as they interact with the neurotransmitters to determine the excitation/inhibition of post synapse [158]. Also, neural cell adhesion molecules, neurexin and neuroligins, are other synaptic markers that can be looked at as they connect presynapse and postsynapse together [159], [160]. Through their important functions in the synaptic connections, they can be studied to have a better view on how synapses are affected by the interventions.

The PERK pathway inhibition was a crucial part of the study. We were unable to show the inhibition due to a lack of PERK pathway activation in the brain. Therefore, other tissues, such as the liver of these animals, can be used to confirm the effect of these inhibitors in our study. Since some tissues such as liver are more prone to develop ER stress under hyperlipidemia, showing the effect of the inhibition in these tissues would be easier [161]. Through these results, it can be suggested that the cortex remained mostly unaffected by the interventions. In the brain, there is a process called neurogenesis, which is the term used for the generation of new neurons. Each tissue has a different neurogenesis rate; some tissues, such as the hippocampus, have a higher rate of neurogenesis in adulthood, while tissues, such as the cerebral cortex, have a lower rate of adult neurogenesis [162]. This might explain the stability of the cerebral cortex tissue. Therefore, immunohistochemistry would be useful in confirming the differences between tissues and the rate of neurogenesis in the cerebral cortex.

Behavioral test are very useful to test the cognitive abilities of the mice. There are many behavioral tests, such as the Barnes maze test, can measure the animal's learning and memory [163]. Investigating how the interventions translate into the behavior of animals can provide better insights into the results.

A previous study shows that brain lipid homeostasis is affected due to APOE deficiency in human iPSC organoids. An upregulation of cholesterol biosynthesis in excitatory neurons accompanied by lipid accumulation in astrocytes is observed, and moreover, these symptoms are alleviated by ISRIB [164]. The study shows the importance of APOE and how its deficiency can be eased by ISRIB. This thesis is important in this manner; it

explores how APOE deficiency and a high-fat diet change the cerebral cortex. Moreover, this thesis provides insights on the effects of ISRIB on the cerebral cortex.

This study was important for understanding the effects of high-fat diet-induced hyperlipidemia on ER stress, BBB integrity, and synaptic integrity. These are crucial to understanding the impacts of high-fat diet-induced hyperlipidemia on the brain. The PERK pathway inhibition effects on the same parameters are also explored in this thesis.

REFERENCES

[1] P. J. H. Jones and A. H. Lichtenstein, “Lipids,” in *Present Knowledge in Nutrition*, Elsevier, 2020, pp. 51–69. doi: 10.1016/B978-0-323-66162-1.00004-4.

[2] R. A. Kreisberg and J. E. B. Reusch, “Hyperlipidemia (High Blood Fat),” *J Clin Endocrinol Metab*, vol. 90, no. 3, pp. 0–0, Mar. 2005, doi: 10.1210/jcem.90.3.9991.

[3] G. R. Thompson, “The hyperlipidaemias,” *Genetic and Metabolic Disease in Pediatrics*, pp. 211–233, Jan. 1985, doi: 10.1016/B978-0-407-02312-3.50014-4.

[4] B. Bagheri, A. Alikhani, hossein Mokhtari, and M. Rasouli, “Cholesterol Esterification and Atherogenicity The Ratio of Unesterified/esterified Cholesterol is the Major determinant of Atherogenicity of Lipoprotein Fractions,” vol. 72, no. 2, pp. 103–107, 2018, doi: 10.5455/medarh.2018.72.103-107.

[5] T. P. Burris, “Cholesterol and Other Steroids,” *Encyclopedia of Cell Biology: Volume 1-6, Second Edition*, vol. 1, pp. 233–240, Jan. 2023, doi: 10.1016/B978-0-12-821618-7.00144-9.

[6] A. V. Poznyak, D. A. Kashirskikh, V. N. Sukhorukov, V. Kalmykov, A. V. Omelchenko, and A. N. Orekhov, “Cholesterol Transport Dysfunction and Its Involvement in Atherogenesis,” *Int J Mol Sci*, vol. 23, no. 3, p. 1332, Feb. 2022, doi: 10.3390/IJMS23031332.

[7] A. Gonen and Y. I. Miller, “From Inert Storage to Biological Activity—In Search of Identity for Oxidized Cholesteryl Esters,” *Front Endocrinol (Lausanne)*, vol. 11, Nov. 2020, doi: 10.3389/FENDO.2020.602252.

[8] F. R. Maxfield and D. Wüstner, “Intracellular cholesterol transport,” *J Clin Invest*, vol. 110, no. 7, p. 891, Oct. 2002, doi: 10.1172/JCI16500.

[9] P. R. N. Viecili *et al.*, “Triglycerides Revisited to the Serial,” *Adv Clin Chem*, vol. 80, pp. 1–44, Jan. 2017, doi: 10.1016/BS.ACC.2016.11.001.

[10] H. Mu and C. E. Høy, “The digestion of dietary triacylglycerols,” *Prog Lipid Res*, vol. 43, no. 2, pp. 105–133, Mar. 2004, doi: 10.1016/S0163-7827(03)00050-X.

[11] M. H. Gordon, “FATS | Classification,” *Encyclopedia of Food Sciences and Nutrition*, pp. 2287–2292, Jan. 2003, doi: 10.1016/B0-12-227055-X/00701-X.

[12] M. Xie, “Phospholipids,” *Encyclopedia of Food Chemistry*, pp. 214–217, Jan. 2019, doi: 10.1016/B978-0-08-100596-5.21597-7.

[13] H. N. Ginsberg, “Lipoprotein physiology,” *Endocrinol Metab Clin North Am*, vol. 27, no. 3, pp. 503–519, Sep. 1998, doi: 10.1016/S0889-8529(05)70023-2.

[14] R. Zamora and F. J. Hidalgo, “Lipoproteins,” *Encyclopedia of Food and Health*, pp. 544–549, Jan. 2016, doi: 10.1016/B978-0-12-384947-2.00422-0.

[15] J. M. Ordovas, “Lipoproteins,” *Encyclopedia of Human Nutrition*, vol. 3–4, pp. 80–86, Jan. 2013, doi: 10.1016/B978-0-12-375083-9.00171-9.

[16] Y. Li *et al.*, “Apolipoproteins as potential communicators play an essential role in the pathogenesis and treatment of early atherosclerosis,” *Int J Biol Sci*, vol. 19, no. 14, p. 4493, 2023, doi: 10.7150/IJBS.86475.

[17] A. Gugliucci, “The chylomicron saga: time to focus on postprandial metabolism,” *Front Endocrinol (Lausanne)*, vol. 14, p. 1322869, Jan. 2023, doi: 10.3389/FENDO.2023.1322869/BIBTEX.

[18] M. W. Freeman and G. A. Walford, “Lipoprotein Metabolism and the Treatment of Lipid Disorders,” *Endocrinology: Adult and Pediatric*, vol. 1–2, pp. 715-736.e7, Jan. 2016, doi: 10.1016/B978-0-323-18907-1.00041-X.

[19] N. V. Bhagavan and C.-E. Ha, “Gastrointestinal Digestion and Absorption,” *Essentials of Medical Biochemistry*, pp. 97–113, Jan. 2011, doi: 10.1016/B978-0-12-095461-2.00011-4.

[20] P. O. Kwiterovich, “The metabolic pathways of high-density lipoprotein, low-density lipoprotein, and triglycerides: a current review.,” *Am J Cardiol*, vol. 86, no. 12 A, pp. 5–10, Dec. 2000, doi: 10.1016/S0002-9149(00)01461-2.

[21] P. Zarras and O. Vogl, “Polycationic salts as bile acid sequestering agents,” *Prog Polym Sci*, vol. 24, no. 4, pp. 485–516, Jul. 1999, doi: 10.1016/S0079-6700(99)00002-7.

[22] M. Chandalia and N. Abate, “Hyperlipidemia,” *Encyclopedia of Gastroenterology*, pp. 403–410, Jan. 2004, doi: 10.1016/B0-12-386860-2/00384-1.

[23] J. Chiang, “Liver Physiology: Metabolism and Detoxification,” *Pathobiology of Human Disease: A Dynamic Encyclopedia of Disease Mechanisms*, pp. 1770–1782, Jan. 2014, doi: 10.1016/B978-0-12-386456-7.04202-7.

[24] A. Dasgupta and A. Wahed, “Lipid metabolism and disorders,” *Clinical Chemistry, Immunology and Laboratory Quality Control*, pp. 105–126, Jan. 2021, doi: 10.1016/B978-0-12-815960-6.00010-8.

[25] N. F. Galeano, M. Al-Haideri, F. Keyserman, S. C. Rumsey, and R. J. Deckelbaum, “Small dense low density lipoprotein has increased affinity for LDL receptor-independent cell surface binding sites: a potential mechanism for increased atherogenicity,” *J Lipid Res*, vol. 39, no. 6, pp. 1263–1273, Jun. 1998, doi: 10.1016/S0022-2275(20)32551-7.

[26] H. Jiang *et al.*, “Mechanisms of Oxidized LDL-Mediated Endothelial Dysfunction and Its Consequences for the Development of Atherosclerosis,” *Front Cardiovasc Med*, vol. 9, p. 925923, Jun. 2022, doi: 10.3389/FCVM.2022.925923.

[27] R. Huang *et al.*, “Apolipoprotein A-I structural organization in high density lipoproteins isolated from human plasma,” *Nat Struct Mol Biol*, vol. 18, no. 4, p. 416, Apr. 2011, doi: 10.1038/NSMB.2028.

[28] E. Eren, N. Yilmaz, and O. Aydin, “High Density Lipoprotein and it’s Dysfunction,” *Open Biochem J*, vol. 6, no. 1, p. 78, Aug. 2012, doi: 10.2174/1874091X01206010078.

[29] M. Alves-Bezerra and D. E. Cohen, “Triglyceride metabolism in the liver,” *Compr Physiol*, vol. 8, no. 1, p. 1, Dec. 2017, doi: 10.1002/CPHY.C170012.

[30] R. A. Cox and M. R. García-Palmieri, “Cholesterol, Triglycerides, and Associated Lipoproteins,” *Clinical Methods: The History, Physical, and Laboratory Examinations*, 1990, Accessed: Jun. 10, 2024. [Online]. Available: https://www.ncbi.nlm.nih.gov/books/NBK351/

[31] P. M. Kris-Etherton, L. Sanders, O. Lawler, T. Riley, and K. Maki, “Hyperlipidemia,” *Encyclopedia of Human Nutrition: Volume 1-4, Fourth Edition*, vol. 1–4, pp. 361–379, Jan. 2023, doi: 10.1016/B978-0-12-821848-8.00175-X.

[32] D. Zhang *et al.*, “Important Hormones Regulating Lipid Metabolism,” *Molecules*, vol. 27, no. 20, Oct. 2022, doi: 10.3390/MOLECULES27207052.

[33] D. Lent-Schochet and I. Jialal, “Biochemistry, Lipoprotein Metabolism,” *StatPearls*, Jan. 2023, Accessed: Jun. 10, 2024. [Online]. Available: https://www.ncbi.nlm.nih.gov/books/NBK553193/

[34] A. Blanco and G. Blanco, “Lipid metabolism,” *Med Biochem*, pp. 359–400, Jan. 2022, doi: 10.1016/B978-0-323-91599-1.00014-6.

[35] M. Ouimet, T. J. Barrett, and E. A. Fisher, “HDL and Reverse Cholesterol Transport,” *Circ Res*, vol. 124, no. 10, pp. 1505–1518, May 2019, doi: 10.1161/CIRCRESAHA.119.312617.

[36] Z. Li *et al.*, “Distribution of lipid levels and prevalence of hyperlipidemia: data from the NHANES 2007–2018,” *Lipids Health Dis*, vol. 21, no. 1, Dec. 2022, doi: 10.1186/S12944-022-01721-Y.

[37] G. W. Go and A. Mani, “Low-Density Lipoprotein Receptor (LDLR) Family Orchestrates Cholesterol Homeostasis,” *Yale J Biol Med*, vol. 85, no. 1, p. 19, Mar. 2012, Accessed: Jun. 10, 2024. [Online]. Available: /pmc/articles/PMC3313535/

[38] D. Bhatnagar, J. Schofield, and H. Soran, “Genetic disorders of lipoprotein metabolism,” *Clinical Molecular Medicine: Principles and Practice*, pp. 245–265, Jan. 2020, doi: 10.1016/B978-0-12-809356-6.00014-9.

[39] P. W. Siri-Tarino, Q. Sun, F. B. Hu, and R. M. Krauss, “Saturated Fatty Acids and Risk of Coronary Heart Disease: Modulation by Replacement Nutrients,” *Curr Atheroscler Rep*, vol. 12, no. 6, p. 384, Nov. 2010, doi: 10.1007/S11883-010-0131-6.

[40] R. Shahid *et al.*, “Neurocognitive Impairment in Cardiovascular Disease Patients Taking Statins Versus Proprotein Convertase Subtilisin/Kexin Type 9 (PCSK9) Inhibitors: A Systematic Review,” *Cureus*, vol. 14, no. 10, Nov. 2022, doi: 10.7759/CUREUS.30942.

[41] A. A. Miller and S. J. Spencer, “Obesity and neuroinflammation: A pathway to cognitive impairment,” *Brain Behav Immun*, vol. 42, pp. 10–21, Nov. 2014, doi: 10.1016/J.BBI.2014.04.001.

[42] H. M. Melo, L. E. Santos, and S. T. Ferreira, “Diet-Derived Fatty Acids, Brain Inflammation, and Mental Health,” *Front Neurosci*, vol. 13, p. 439762, Mar. 2019, doi: 10.3389/FNINS.2019.00265/BIBTEX.

[43] C. P. Canales and K. Walz, “The Mouse, a Model Organism for Biomedical Research,” *Cellular and Animal Models in Human Genomics Research*, pp. 119–140, Jan. 2019, doi: 10.1016/B978-0-12-816573-7.00006-7.

[44] C. Bancells *et al.*, “Proteomic analysis of electronegative low-density lipoprotein,” *J Lipid Res*, vol. 51, no. 12, pp. 3508–3515, Dec. 2010, doi: 10.1194/jlr.M009258.

[45] S. M. Gordon, H. Li, X. Zhu, A. S. Shah, L. J. Lu, and W. S. Davidson, “A Comparison of the Mouse and Human Lipoproteome: Suitability of the Mouse Model for Studies of Human Lipoproteins,” *J Proteome Res*, vol. 14, no. 6, pp. 2686–2695, Jun. 2015, doi: 10.1021/acs.jproteome.5b00213.

[46] C. A. Hogarth, A. Roy, and D. L. Ebert, “Genomic evidence for the absence of a functional cholesteryl ester transfer protein gene in mice and rats,” *Comparative Biochemistry and Physiology - B Biochemistry and Molecular Biology*, vol. 135, no. 2, pp. 219–229, Jun. 2003, doi: 10.1016/S1096-4959(03)00046-0.

[47] A. R. Tall, “Functions of cholesterol ester transfer protein and relationship to coronary artery disease risk,” *J Clin Lipidol*, vol. 4, no. 5, pp. 389–393, Sep. 2010, doi: 10.1016/j.jacl.2010.08.006.

[48] S. Chantepie, A. E. Bochem, M. J. Chapman, G. K. Hovingh, and A. Kontush, “High-Density Lipoprotein (HDL) Particle Subpopulations in Heterozygous Cholesteryl Ester Transfer Protein (CETP) Deficiency: Maintenance of Antioxidative Activity,” *PLoS One*, vol. 7, no. 11, p. e49336, Nov. 2012, doi: 10.1371/journal.pone.0049336.

[49] Y. Zhao, H. Qu, Y. Wang, W. Xiao, Y. Zhang, and D. Shi, “Small rodent models of atherosclerosis,” *Biomedicine & Pharmacotherapy*, vol. 129, p. 110426, Sep. 2020, doi: 10.1016/J.BIOPHA.2020.110426.

[50] S. Fazio and M. F. Linton, “Mouse models of hyperlipidemia and atherosclerosis.,” *Front Biosci*, vol. 6, no. 3, pp. 515–525, Mar. 2001, doi: 10.2741/FAZIO/PDF.

[51] G. S. Getz and C. A. Reardon, “ApoE knockout and knockin mice: the history of their contribution to the understanding of atherogenesis,” 2016, doi: 10.1194/jlr.R067249.

[52] G. S. Getz and C. A. Reardon, “Apoprotein E as a lipid transport and signaling protein in the blood, liver, and artery wall,” *J Lipid Res*, vol. 50, no. Suppl, p. S156, Apr. 2009, doi: 10.1194/JLR.R800058-JLR200.

[53] M. C. Phillips, “Apolipoprotein E isoforms and lipoprotein metabolism,” *IUBMB Life*, vol. 66, no. 9, pp. 616–623, Sep. 2014, doi: 10.1002/IUB.1314.

[54] A. A. Pendse, J. M. Arbones-Mainar, L. A. Johnson, M. K. Altenburg, and N. Maeda, "Apolipoprotein E knock-out and knock-in mice: atherosclerosis, metabolic syndrome, and beyond," *J Lipid Res*, vol. 50, no. SUPPL., pp. S178–S182, Apr. 2009, doi: 10.1194/JLR.R800070-JLR200.

[55] D. S. Schwarz and M. D. Blower, "The endoplasmic reticulum: structure, function and response to cellular signaling," *Cellular and Molecular Life Sciences*, vol. 73, no. 1, pp. 79–94, Jan. 2016, doi: 10.1007/s00018-015-2052-6.

[56] I. Braakman and N. J. Bulleid, "Protein Folding and Modification in the Mammalian Endoplasmic Reticulum," *Annu Rev Biochem*, vol. 80, no. 1, pp. 71–99, Jul. 2011, doi: 10.1146/annurev-biochem-062209-093836.

[57] I. Braakman and D. N. Hebert, "Protein Folding in the Endoplasmic Reticulum," *Cold Spring Harb Perspect Biol*, vol. 5, no. 5, pp. a013201–a013201, May 2013, doi: 10.1101/cshperspect.a013201.

[58] S. A. Oakes and F. R. Papa, "The Role of Endoplasmic Reticulum Stress in Human Pathology," *Annual Review of Pathology: Mechanisms of Disease*, vol. 10, no. 1, pp. 173–194, Jan. 2015, doi: 10.1146/annurev-pathol-012513-104649.

[59] H. Zeeshan, G. Lee, H.-R. Kim, and H.-J. Chae, "Endoplasmic Reticulum Stress and Associated ROS," *Int J Mol Sci*, vol. 17, no. 3, p. 327, Mar. 2016, doi: 10.3390/ijms17030327.

[60] L. Krshnan, M. L. van de Weijer, and P. Carvalho, "Endoplasmic Reticulum–Associated Protein Degradation," *Cold Spring Harb Perspect Biol*, p. a041247, Aug. 2022, doi: 10.1101/cshperspect.a041247.

[61] A. Lopata, A. Kniss, F. Löhr, V. V. Rogov, and V. Dötsch, "Ubiquitination in the ERAD Process," *Int J Mol Sci*, vol. 21, no. 15, p. 5369, Jul. 2020, doi: 10.3390/ijms21155369.

[62] X. Chen, C. Shi, M. He, S. Xiong, and X. Xia, "Endoplasmic reticulum stress: molecular mechanism and therapeutic targets," *Signal Transduct Target Ther*, vol. 8, no. 1, p. 352, Sep. 2023, doi: 10.1038/s41392-023-01570-w.

[63] A. Ajoolabady *et al.*, "Endoplasmic reticulum stress in liver diseases," *Hepatology*, vol. 77, no. 2, pp. 619–639, Feb. 2023, doi: 10.1002/hep.32562.

[64] C. Hetz, K. Zhang, and R. J. Kaufman, “Mechanisms, regulation and functions of the unfolded protein response,” *Nat Rev Mol Cell Biol*, vol. 21, no. 8, pp. 421–438, Aug. 2020, doi: 10.1038/s41580-020-0250-z.

[65] D. Senft and Z. A. Ronai, “UPR, autophagy, and mitochondria crosstalk underlies the ER stress response,” *Trends Biochem Sci*, vol. 40, no. 3, pp. 141–148, Mar. 2015, doi: 10.1016/j.tibs.2015.01.002.

[66] S. A. Oakes and F. R. Papa, “The Role of Endoplasmic Reticulum Stress in Human Pathology,” *Annual Review of Pathology: Mechanisms of Disease*, vol. 10, no. 1, pp. 173–194, Jan. 2015, doi: 10.1146/annurev-pathol-012513-104649.

[67] A. Read and M. Schröder, “The Unfolded Protein Response: An Overview,” *Biology (Basel)*, vol. 10, no. 5, p. 384, Apr. 2021, doi: 10.3390/biology10050384.

[68] C. Hetz, “The unfolded protein response: controlling cell fate decisions under ER stress and beyond,” *Nat Rev Mol Cell Biol*, vol. 13, no. 2, pp. 89–102, Feb. 2012, doi: 10.1038/nrm3270.

[69] Z. Liu, Y. Lv, N. Zhao, G. Guan, and J. Wang, “Protein kinase R-like ER kinase and its role in endoplasmic reticulum stress-decided cell fate,” *Cell Death & Disease 2015 6:7*, vol. 6, no. 7, pp. e1822–e1822, Jul. 2015, doi: 10.1038/cddis.2015.183.

[70] A. A. Komar and W. C. Merrick, “A Retrospective on eIF2A—and Not the Alpha Subunit of eIF2,” *Int J Mol Sci*, vol. 21, no. 6, p. 2054, Mar. 2020, doi: 10.3390/ijms21062054.

[71] M. D. Jennings and G. D. Pavitt, “A new function and complexity for protein translation initiation factor eIF2B,” *Cell Cycle*, vol. 13, no. 17, p. 2660, Sep. 2014, doi: 10.4161/15384101.2014.948797.

[72] Y. Gordiyenko, C. Schmidt, M. D. Jennings, D. Matak-Vinkovic, G. D. Pavitt, and C. V. Robinson, “eIF2B is a decameric guanine nucleotide exchange factor with a γ2ε2 tetrameric core,” *Nature Communications 2014 5:1*, vol. 5, no. 1, pp. 1–12, May 2014, doi: 10.1038/ncomms4902.

[73] R. C. Wek, T. G. Anthony, and K. A. Staschke, “Surviving and Adapting to Stress: Translational Control and the Integrated Stress Response,” *Antioxid Redox Signal*, vol. 39, no. 4–6, pp. 351–373, Aug. 2023, doi: 10.1089/ARS.2022.0123.

[74] S. Bond, C. Lopez-Lloreda, P. J. Gannon, C. Akay-Espinoza, and K. L. Jordan-Sciutto, "The Integrated Stress Response and Phosphorylated Eukaryotic Initiation Factor 2α in Neurodegeneration," *J Neuropathol Exp Neurol*, vol. 79, no. 2, pp. 123–143, Feb. 2020, doi: 10.1093/jnen/nlz129.

[75] A. M. Bogorad, K. Y. Lin, and A. Marintchev, "Novel mechanisms of eIF2B action and regulation by eIF2α phosphorylation," *Nucleic Acids Res*, vol. 45, no. 20, p. 11962, Nov. 2017, doi: 10.1093/NAR/GKX845.

[76] W. Rozpedek, D. Pytel, B. Mucha, H. Leszczynska, J. A. Diehl, and I. Majsterek, "The Role of the PERK/eIF2α/ATF4/CHOP Signaling Pathway in Tumor Progression During Endoplasmic Reticulum Stress," *Curr Mol Med*, vol. 16, no. 6, pp. 533–544, Jun. 2016, doi: 10.2174/1566524016666160523143937.

[77] H. Malhi and R. J. Kaufman, "Endoplasmic reticulum stress in liver disease," *J Hepatol*, vol. 54, no. 4, pp. 795–809, Apr. 2011, doi: 10.1016/j.jhep.2010.11.005.

[78] R. C. Wek, "Role of eIF2α Kinases in Translational Control and Adaptation to Cellular Stress," *Cold Spring Harb Perspect Biol*, vol. 10, no. 7, Jul. 2018, doi: 10.1101/CSHPERSPECT.A032870.

[79] S. K. Young and R. C. Wek, "Upstream Open Reading Frames Differentially Regulate Gene-specific Translation in the Integrated Stress Response," *Journal of Biological Chemistry*, vol. 291, no. 33, pp. 16927–16935, Aug. 2016, doi: 10.1074/JBC.R116.733899.

[80] C. Hetz and F. R. Papa, "The Unfolded Protein Response and Cell Fate Control," *Mol Cell*, vol. 69, no. 2, pp. 169–181, Jan. 2018, doi: 10.1016/j.molcel.2017.06.017.

[81] K. Pakos-Zebrucka, I. Koryga, K. Mnich, M. Ljujic, A. Samali, and A. M. Gorman, "The integrated stress response," *EMBO Rep*, vol. 17, no. 10, pp. 1374–1395, Oct. 2016, doi: 10.15252/embr.201642195.

[82] E. A. V. Beilankouhi, M. A. Sajadi, I. Alipourfard, P. Hassani, M. Valilo, and R. Safaralizadeh, "Role of the ER-induced UPR pathway, apoptosis, and autophagy in colorectal cancer," *Pathol Res Pract*, vol. 248, p. 154706, Aug. 2023, doi: 10.1016/j.prp.2023.154706.

[83] H. H. Chen and W. Y. Tarn, “uORF-mediated translational control: recently elucidated mechanisms and implications in cancer,” *RNA Biol*, vol. 16, no. 10, p. 1327, 2019, doi: 10.1080/15476286.2019.1632634.

[84] S. Chipurupalli, U. Samavedam, and N. Robinson, “Crosstalk Between ER Stress, Autophagy and Inflammation,” *Front Med (Lausanne)*, vol. 8, Nov. 2021, doi: 10.3389/fmed.2021.758311.

[85] A. Merighi and L. Lossi, “Endoplasmic Reticulum Stress Signaling and Neuronal Cell Death,” *Int J Mol Sci*, vol. 23, no. 23, p. 15186, Dec. 2022, doi: 10.3390/ijms232315186.

[86] D. Hicks, K. Giresh, L. A. Wrischnik, and D. C. Weiser, “The PPP1R15 Family of eIF2-alpha Phosphatase Targeting Subunits (GADD34 and CReP),” *Int J Mol Sci*, vol. 24, no. 24, p. 17321, Dec. 2023, doi: 10.3390/ijms242417321.

[87] L. Wang *et al.*, “Endoplasmic Reticulum Stress and the Unfolded Protein Response in Cerebral Ischemia/Reperfusion Injury,” *Front Cell Neurosci*, vol. 16, May 2022, doi: 10.3389/fncel.2022.864426.

[88] R. Ghemrawi and M. Khair, “Endoplasmic Reticulum Stress and Unfolded Protein Response in Neurodegenerative Diseases,” *Int J Mol Sci*, vol. 21, no. 17, pp. 1–25, Sep. 2020, doi: 10.3390/IJMS21176127.

[89] I. L. Lemmer, N. Willemsen, N. Hilal, and A. Bartelt, “A guide to understanding endoplasmic reticulum stress in metabolic disorders,” *Mol Metab*, vol. 47, May 2021, doi: 10.1016/J.MOLMET.2021.101169.

[90] W. Zheng, “Neurotoxicology of the Brain Barrier System: New Implications,” *J Toxicol Clin Toxicol*, vol. 39, no. 7, p. 711, 2001, doi: 10.1081/CLT-100108512.

[91] H. L. McConnell and A. Mishra, “Cells of the Blood-brain Barrier: an Overview of the Neurovascular Unit in Health and Disease,” *Methods Mol Biol*, vol. 2492, p. 3, 2022, doi: 10.1007/978-1-0716-2289-6_1.

[92] M. D. Sweeney, S. Ayyadurai, and B. V. Zlokovic, “Pericytes of the neurovascular unit: Key functions and signaling pathways,” *Nat Neurosci*, vol. 19, no. 6, p. 771, May 2016, doi: 10.1038/NN.4288.

[93] Y. Wu *et al.*, “Biology and function of pericytes in the vascular microcirculation,” *Animal Model Exp Med*, vol. 6, no. 4, p. 337, Aug. 2023, doi: 10.1002/AME2.12334.

[94] M. Rodríguez-Giraldo, R. E. González-Reyes, S. Ramírez-Guerrero, C. E. Bonilla-Trilleras, S. Guardo-Maya, and M. O. Nava-Mesa, "Astrocytes as a Therapeutic Target in Alzheimer's Disease–Comprehensive Review and Recent Developments," *Int J Mol Sci*, vol. 23, no. 21, Nov. 2022, doi: 10.3390/IJMS232113630.

[95] H. Kadry, B. Noorani, and L. Cucullo, "A blood–brain barrier overview on structure, function, impairment, and biomarkers of integrity," *Fluids and Barriers of the CNS 2020 17:1*, vol. 17, no. 1, pp. 1–24, Nov. 2020, doi: 10.1186/S12987-020-00230-3.

[96] S. M. Stamatovic, A. M. Johnson, R. F. Keep, and A. V. Andjelkovic, "Junctional proteins of the blood-brain barrier: New insights into function and dysfunction," *Tissue Barriers*, vol. 4, no. 1, Jan. 2016, doi: 10.1080/21688370.2016.1154641.

[97] N. Wibbe and K. Ebnet, "Cell Adhesion at the Tight Junctions: New Aspects and New Functions," *Cells*, vol. 12, no. 23, Dec. 2023, doi: 10.3390/CELLS12232701.

[98] A. Gonçalves, A. F. Ambrósio, and R. Fernandes, "Regulation of claudins in blood-tissue barriers under physiological and pathological states," *Tissue Barriers*, vol. 1, no. 3, p. e24782, Jul. 2013, doi: 10.4161/TISB.24782.

[99] C. M. Van Itallie, A. J. Tietgens, and J. M. Anderson, "Visualizing the dynamic coupling of claudin strands to the actin cytoskeleton through ZO-1," *Mol Biol Cell*, vol. 28, no. 4, pp. 524–534, Feb. 2017, doi: 10.1091/MBC.E16-10-0698.

[100] H. Wen, D. D. Watry, M. C. G. Marcondes, and H. S. Fox, "Selective Decrease in Paracellular Conductance of Tight Junctions: Role of the First Extracellular Domain of Claudin-5," *Mol Cell Biol*, vol. 24, no. 19, p. 8408, Oct. 2004, doi: 10.1128/MCB.24.19.8408-8417.2004.

[101] C. Greene, N. Hanley, and M. Campbell, "Claudin-5: gatekeeper of neurological function," *Fluids Barriers CNS*, vol. 16, no. 1, Jan. 2019, doi: 10.1186/S12987-019-0123-Z.

[102] S. C. Ma *et al.*, "Claudin-5 regulates blood-brain barrier permeability by modifying brain microvascular endothelial cell proliferation, migration, and adhesion to prevent lung cancer metastasis," *CNS Neurosci Ther*, vol. 23, no. 12, p. 947, Dec. 2017, doi: 10.1111/CNS.12764.

[103] J. J. Lochhead, J. Yang, P. T. Ronaldson, and T. P. Davis, "Structure, Function, and Regulation of the Blood-Brain Barrier Tight Junction in Central Nervous System

Disorders," *Front Physiol*, vol. 11, p. 558491, Aug. 2020, doi: 10.3389/FPHYS.2020.00914/BIBTEX.

[104] S. Yuan, K. J. Liu, and Z. Qi, "Occludin regulation of blood–brain barrier and potential therapeutic target in ischemic stroke," *Brain Circ*, vol. 6, no. 3, p. 152, 2020, doi: 10.4103/BC.BC_29_20.

[105] S. Dithmer, I. E. Blasig, P. A. Fraser, Z. Qin, and R. F. Haseloff, "The Basic Requirement of Tight Junction Proteins in Blood-Brain Barrier Function and Their Role in Pathologies," *Int J Mol Sci*, vol. 25, no. 11, p. 5601, Jun. 2024, doi: 10.3390/IJMS25115601/S1.

[106] W. Y. Liu, Z. Bin Wang, L. C. Zhang, X. Wei, and L. Li, "Tight Junction in Blood-Brain Barrier: An Overview of Structure, Regulation, and Regulator Substances," *CNS Neurosci Ther*, vol. 18, no. 8, p. 609, Aug. 2012, doi: 10.1111/J.1755-5949.2012.00340.X.

[107] C. M. Van Itallie, A. Aponte, A. J. Tietgens, M. Gucek, K. Fredriksson, and J. M. Anderson, "The N and C Termini of ZO-1 Are Surrounded by Distinct Proteins and Functional Protein Networks," *J Biol Chem*, vol. 288, no. 19, p. 13775, May 2013, doi: 10.1074/JBC.M113.466193.

[108] D. Wu, Q. Chen, X. Chen, F. Han, Z. Chen, and Y. Wang, "The blood–brain barrier: structure, regulation, and drug delivery," *Signal Transduction and Targeted Therapy 2023 8:1*, vol. 8, no. 1, pp. 1–27, May 2023, doi: 10.1038/s41392-023-01481-w.

[109] S. R. Archie, A. Al Shoyaib, and L. Cucullo, "Blood-Brain Barrier Dysfunction in CNS Disorders and Putative Therapeutic Targets: An Overview," *Pharmaceutics*, vol. 13, no. 11, Nov. 2021, doi: 10.3390/PHARMACEUTICS13111779.

[110] J. L. Mikitsh and A. M. Chacko, "Pathways for Small Molecule Delivery to the Central Nervous System Across the Blood-Brain Barrier," *Perspect Medicin Chem*, vol. 6, no. 6, p. 11, Apr. 2014, doi: 10.4137/PMC.S13384.

[111] D. S. Miller, "Regulation of ABC Transporters at the Blood-Brain Barrier," *Clin Pharmacol Ther*, vol. 97, no. 4, p. 395, Apr. 2015, doi: 10.1002/CPT.64.

[112] M. Fernandez *et al.*, "Strategies for Drug Delivery into the Brain: A Review on Adenosine Receptors Modulation for Central Nervous System Diseases Therapy,"

Pharmaceutics, vol. 15, no. 10, Oct. 2023, doi: 10.3390/PHARMACEUTICS15102441.

[113] P. Dewangan *et al.*, "Drug delivery: The conceptual perspectives and therapeutic applications," *Polymer-Drug Conjugates: Linker Chemistry, Protocols and Applications*, pp. 1–38, Jan. 2023, doi: 10.1016/B978-0-323-91663-9.00010-2.

[114] A. Weiler, A. Volkenhoff, H. Hertenstein, and S. Schirmeier, "Metabolite transport across the mammalian and insect brain diffusion barriers," *Neurobiol Dis*, vol. 107, pp. 15–31, Nov. 2017, doi: 10.1016/J.NBD.2017.02.008.

[115] C. Li *et al.*, "High-fat diet exacerbates lead-induced blood–brain barrier disruption by disrupting tight junction integrity," *Environ Toxicol*, vol. 36, no. 7, pp. 1412–1421, Jul. 2021, doi: 10.1002/TOX.23137.

[116] Y. Chen, Y. He, J. Han, W. Wei, and F. Chen, "Blood-brain barrier dysfunction and Alzheimer's disease: associations, pathogenic mechanisms, and therapeutic potential," *Front Aging Neurosci*, vol. 15, 2023, doi: 10.3389/FNAGI.2023.1258640.

[117] M. J. Caire, V. Reddy, and M. Varacallo, "Physiology, Synapse," *StatPearls*, Mar. 2023, Accessed: Jun. 20, 2024. [Online]. Available: https://www.ncbi.nlm.nih.gov/books/NBK526047/

[118] R. Crupi, D. Impellizzeri, and S. Cuzzocrea, "Role of metabotropic glutamate receptors in neurological disorders," *Front Mol Neurosci*, vol. 12, p. 413597, Feb. 2019, doi: 10.3389/FNMOL.2019.00020/BIBTEX.

[119] C. El Khoueiry *et al.*, "GABAA and Glycine Receptor-Mediated Inhibitory Synaptic Transmission onto Adult Rat Lamina IIi PKCγ-Interneurons: Pharmacological but Not Anatomical Specialization," *Cells*, vol. 11, no. 8, Apr. 2022, doi: 10.3390/CELLS11081356.

[120] T. C. Südhof, "Calcium Control of Neurotransmitter Release," *Cold Spring Harb Perspect Biol*, vol. 4, no. 1, 2012, doi: 10.1101/CSHPERSPECT.A011353.

[121] S. Kirischuk, "Keeping Excitation–Inhibition Ratio in Balance," *Int J Mol Sci*, vol. 23, no. 10, May 2022, doi: 10.3390/IJMS23105746.

[122] A. Becher, A. Drenckhahn, I. Pahner, M. Margittai, R. Jahn, and G. Ahnert-Hilger, "The Synaptophysin–Synaptobrevin Complex: a Hallmark of Synaptic Vesicle

Maturation," *The Journal of Neuroscience*, vol. 19, no. 6, p. 1922, Mar. 1999, doi: 10.1523/JNEUROSCI.19-06-01922.1999.

[123] A. M. Stranahan, "Models and mechanisms for hippocampal dysfunction in obesity and diabetes," *Neuroscience*, vol. 309, pp. 125–139, Nov. 2015, doi: 10.1016/J.NEUROSCIENCE.2015.04.045.

[124] M. Sheng and E. Kim, "The Postsynaptic Organization of Synapses," *Cold Spring Harb Perspect Biol*, vol. 3, no. 12, 2011, doi: 10.1101/CSHPERSPECT.A005678.

[125] C. Bats, L. Groc, and D. Choquet, "The interaction between Stargazin and PSD-95 regulates AMPA receptor surface trafficking," *Neuron*, vol. 53, no. 5, pp. 719–734, Mar. 2007, doi: 10.1016/J.NEURON.2007.01.030.

[126] J. N. Levinsoni *et al.*, "Neuroligins mediate excitatory and inhibitory synapse formation: involvement of PSD-95 and neurexin-1beta in neuroligin-induced synaptic specificity," *J Biol Chem*, vol. 280, no. 17, pp. 17312–17319, Apr. 2005, doi: 10.1074/JBC.M413812200.

[127] S. Y. Cheon, "Impaired Cholesterol Metabolism, Neurons, and Neuropsychiatric Disorders," *Exp Neurobiol*, vol. 32, no. 2, p. 57, Apr. 2023, doi: 10.5607/EN23010.

[128] G. Choii and J. Ko, "Gephyrin: a central GABAergic synapse organizer," *Experimental & Molecular Medicine 2015 47:4*, vol. 47, no. 4, pp. e158–e158, Apr. 2015, doi: 10.1038/emm.2015.5.

[129] R. Pizzarelli *et al.*, "Tuning GABAergic Inhibition: Gephyrin Molecular Organization and Functions," *Neuroscience*, vol. 439, p. 125, Jul. 2020, doi: 10.1016/J.NEUROSCIENCE.2019.07.036.

[130] A. Więckowska-Gacek, A. Mietelska-Porowska, M. Wydrych, and U. Wojda, "Western diet as a trigger of Alzheimer's disease: From metabolic syndrome and systemic inflammation to neuroinflammation and neurodegeneration," *Ageing Res Rev*, vol. 70, p. 101397, Sep. 2021, doi: 10.1016/J.ARR.2021.101397.

[131] S. Sharma, "High fat diet and its effects on cognitive health: alterations of neuronal and vascular components of brain," *Physiol Behav*, vol. 240, p. 113528, Oct. 2021, doi: 10.1016/J.PHYSBEH.2021.113528.

[132] Y. Liu, J. Yu, Y. C. Shi, Y. Zhang, and S. Lin, “The role of inflammation and endoplasmic reticulum stress in obesity-related cognitive impairment,” *Life Sci*, vol. 233, p. 116707, Sep. 2019, doi: 10.1016/J.LFS.2019.116707.

[133] J. A. Moreno *et al.*, “Oral treatment targeting the unfolded protein response prevents neurodegeneration and clinical disease in prion-infected mice,” *Sci Transl Med*, vol. 5, no. 206, Oct. 2013, doi: 10.1126/SCITRANSLMED.3006767/SUPPL_FILE/5-206RA138_SM.PDF.

[134] X. Yu, L. Dang, R. Zhang, and W. Yang, “Therapeutic Potential of Targeting the PERK Signaling Pathway in Ischemic Stroke,” *Pharmaceuticals 2024, Vol. 17, Page 353*, vol. 17, no. 3, p. 353, Mar. 2024, doi: 10.3390/PH17030353.

[135] M. Halliday *et al.*, “Partial restoration of protein synthesis rates by the small molecule ISRIB prevents neurodegeneration without pancreatic toxicity,” *Cell Death & Disease 2015 6:3*, vol. 6, no. 3, pp. e1672–e1672, Mar. 2015, doi: 10.1038/cddis.2015.49.

[136] U. I. Onat *et al.*, “Intercepting the Lipid-Induced Integrated Stress Response Reduces Atherosclerosis,” *J Am Coll Cardiol*, vol. 73, no. 10, pp. 1149–1169, Mar. 2019, doi: 10.1016/j.jacc.2018.12.055.

[137] S. C. B. R. Nakandakari *et al.*, “Short-term high-fat diet modulates several inflammatory, ER stress, and apoptosis markers in the hippocampus of young mice,” *Brain Behav Immun*, vol. 79, pp. 284–293, Jul. 2019, doi: 10.1016/J.BBI.2019.02.016.

[138] J. C. Moraes *et al.*, “High-Fat Diet Induces Apoptosis of Hypothalamic Neurons,” *PLoS One*, vol. 4, no. 4, p. e5045, Apr. 2009, doi: 10.1371/JOURNAL.PONE.0005045.

[139] A. M. van Ziel and W. Scheper, “The UPR in Neurodegenerative Disease: Not Just an Inside Job,” *Biomolecules*, vol. 10, no. 8, pp. 1–22, Aug. 2020, doi: 10.3390/BIOM10081090.

[140] J. Humeau, M. Leduc, G. Cerrato, F. Loos, O. Kepp, and G. Kroemer, “Phosphorylation of eukaryotic initiation factor-2α (eIF2α) in autophagy,” *Cell Death Dis*, vol. 11, no. 6, Jun. 2020, doi: 10.1038/S41419-020-2642-6.

[141] S. Gal-Ben-Ari, I. Barrera, M. Ehrlich, and K. Rosenblum, "PKR: A kinase to remember," *Front Mol Neurosci*, vol. 11, p. 425641, Jan. 2019, doi: 10.3389/FNMOL.2018.00480/BIBTEX.

[142] D. T. Rutkowski *et al.*, "Adaptation to ER Stress Is Mediated by Differential Stabilities of Pro-Survival and Pro-Apoptotic mRNAs and Proteins," *PLoS Biol*, vol. 4, no. 11, p. e374, Nov. 2006, doi: 10.1371/JOURNAL.PBIO.0040374.

[143] G. C. de Paula *et al.*, "Hippocampal Function Is Impaired by a Short-Term High-Fat Diet in Mice: Increased Blood–Brain Barrier Permeability and Neuroinflammation as Triggering Events," *Front Neurosci*, vol. 15, p. 734158, Nov. 2021, doi: 10.3389/FNINS.2021.734158/BIBTEX.

[144] O. Guillemot-Legris, J. Masquelier, A. Everard, P. D. Cani, M. Alhouayek, and G. G. Muccioli, "High-fat diet feeding differentially affects the development of inflammation in the central nervous system," *J Neuroinflammation*, vol. 13, no. 1, pp. 1–11, Aug. 2016, doi: 10.1186/S12974-016-0666-8/FIGURES/5.

[145] F. Kızıldağ, "Investigating Hyperlipidemia-Driven Organelle Stress and Neuroinflammation On The Mouse Cerebral Cortex: Insights Into The Intervention Of PERK Pathway," Thesis (MSc), Bilkent University, Ankara, 2024.

[146] A. T. Argaw, B. T. Gurfein, Y. Zhang, A. Zameer, and G. R. John, "VEGF-mediated disruption of endothelial CLN-5 promotes blood-brain barrier breakdown," *Proc Natl Acad Sci U S A*, vol. 106, no. 6, p. 1977, Feb. 2009, doi: 10.1073/PNAS.0808698106.

[147] S. M. Stamatovic, A. M. Johnson, R. F. Keep, and A. V. Andjelkovic, "Junctional proteins of the blood-brain barrier: New insights into function and dysfunction," *Tissue Barriers*, vol. 4, no. 1, Jan. 2016, doi: 10.1080/21688370.2016.1154641.

[148] S. M. Stamatovic, R. F. Keep, and A. V. Andjelkovic, "Tracing the endocytosis of claudin-5 in brain endothelial cells," *Methods Mol Biol*, vol. 762, pp. 303–320, 2011, doi: 10.1007/978-1-61779-185-7_22.

[149] P. R. Clark, R. K. Kim, J. S. Pober, and M. S. Kluger, "Tumor Necrosis Factor Disrupts Claudin-5 Endothelial Tight Junction Barriers in Two Distinct NF-κB-Dependent Phases," *PLoS One*, vol. 10, no. 3, p. e0120075, Mar. 2015, doi: 10.1371/JOURNAL.PONE.0120075.

[150] X. Wang and H. Li, “Chronic high-fat diet induces overeating and impairs synaptic transmission in feeding-related brain regions,” *Front Mol Neurosci*, vol. 15, Sep. 2022, doi: 10.3389/FNMOL.2022.1019446/FULL.

[151] L. T. Seabrook *et al.*, “Short- and Long-Term High-Fat Diet Exposure Differentially Alters Phasic and Tonic GABAergic Signaling onto Lateral Orbitofrontal Pyramidal Neurons,” *The Journal of Neuroscience*, vol. 43, no. 50, p. 8582, Dec. 2023, doi: 10.1523/JNEUROSCI.0831-23.2023.

[152] I. Dotti and S. Bonin, “DNase Treatment of RNA,” *Guidelines for Molecular Analysis in Archive Tissues*, pp. 87–90, 2011, doi: 10.1007/978-3-642-17890-0_18.

[153] W. W. Wilfinger, K. Mackey, and P. Chomczynski, “Effect of pH and Ionic Strength on the Spectrophotometric Assessment of Nucleic Acid Purity,” *Biotechniques*, vol. 22, no. 3, pp. 474–481, Mar. 1997, doi: 10.2144/97223st01.

[154] P. Monfort-Lanzas *et al.*, “ExonSurfer: a web-tool to design primers at exon–exon junctions,” *BMC Genomics*, vol. 25, no. 1, p. 594, Jun. 2024, doi: 10.1186/s12864-024-10456-2.

[155] L. Zhang, H. Xu, N. Ding, X. Li, X. Chen, and Z. Chen, “Beneficial Effects on Brain Micro-Environment by Caloric Restriction in Alleviating Neurodegenerative Diseases and Brain Aging,” *Front Physiol*, vol. 12, p. 715443, Nov. 2021, doi: 10.3389/FPHYS.2021.715443.

[156] H. Bauer, J. Zweimueller-Mayer, P. Steinbacher, A. Lametschwandtner, and H. C. Bauer, “The Dual Role of Zonula Occludens (ZO) Proteins,” *J Biomed Biotechnol*, vol. 2010, pp. 1–11, 2010, doi: 10.1155/2010/402593.

[157] W. Liu, Z. Wang, L. Zhang, X. Wei, and L. Li, “Tight Junction in Blood-Brain Barrier: An Overview of Structure, Regulation, and Regulator Substances,” *CNS Neurosci Ther*, vol. 18, no. 8, pp. 609–615, Aug. 2012, doi: 10.1111/j.1755-5949.2012.00340.x.

[158] J. R. Chalifoux and A. G. Carter, “GABAB receptor modulation of synaptic function,” *Curr Opin Neurobiol*, vol. 21, no. 2, pp. 339–344, Apr. 2011, doi: 10.1016/J.CONB.2011.02.004.

[159] R. Zhang, H. Jiang, Y. Liu, and G. He, “Structure, function, and pathology of Neurexin-3,” *Genes Dis*, vol. 10, no. 5, pp. 1908–1919, Sep. 2023, doi: 10.1016/j.gendis.2022.04.008.

[160] T. C. Südhof, “Synaptic Neurexin Complexes: A Molecular Code for the Logic of Neural Circuits,” *Cell*, vol. 171, no. 4, pp. 745–769, Nov. 2017, doi: 10.1016/j.cell.2017.10.024.

[161] X. Liu and R. M. Green, “Endoplasmic reticulum stress and liver diseases,” *Liver Res*, vol. 3, no. 1, pp. 55–64, Mar. 2019, doi: 10.1016/j.livres.2019.01.002.

[162] M. Bitar *et al.*, “Identifying gene expression profiles associated with neurogenesis and inflammation in the human subependymal zone from development through aging,” *Scientific Reports 2022 12:1*, vol. 12, no. 1, pp. 1–12, Jan. 2022, doi: 10.1038/s41598-021-03976-4.

[163] K. Gawel, E. Gibula, M. Marszalek-Grabska, J. Filarowska, and J. H. Kotlinska, “Assessment of spatial learning and memory in the Barnes maze task in rodents-methodological consideration”, doi: 10.1007/s00210-018-1589-y.

[164] J. Zhao *et al.*, “RESEARCH Open Access APOE deficiency impacts neural differentiation and cholesterol biosynthesis in human iPSC-derived cerebral organoids,” *Stem Cell Res Ther*, vol. 14, p. 214, 2023, doi: 10.1186/s13287-023-03444-y.

[165] P. K. Kamat, A. Kalani, and N. Tyagi, “Method and validation of synaptosomal preparation for isolation of synaptic membrane proteins from rat brain,” *MethodsX*, vol. 1, no. 1, pp. 102–107, Jan. 2014, doi: 10.1016/J.MEX.2014.08.002.

[166] S. Rajkumar, T. M. Böckers, and A. Catanese, “Fast and efficient synaptosome isolation and post-synaptic density enrichment from hiPSC-motor neurons by biochemical sub-cellular fractionation,” *STAR Protoc*, vol. 4, no. 1, p. 102061, Mar. 2023, doi: 10.1016/J.XPRO.2023.102061.

[167] A. Simiczyjew, A. J. Mazur, A. Popow-Woźniak, M. Malicka-Błaszkiewicz, and D. Nowak, “Effect of overexpression of β- and γ-actin isoforms on actin cytoskeleton organization and migration of human colon cancer cells,” *Histochem Cell Biol*, vol. 142, no. 3, p. 307, 2014, doi: 10.1007/S00418-014-1199-9.

APPENDICES

A.1. Synaptosome Isolation Confirmation

To confirm the synaptosome isolation, NMDAR-2B (LS-C25797, LSBio, Washington, USA) has been used as a synaptic marker. Synaptosomes contain synaptic proteins and receptors. As such, NMDAR is used to assess the synaptic fraction during synaptosome isolations [165]. In cytosol, we do not expect to see any band, while we expected a clear band in synaptosome. As for synaptophysin, it is a synaptic cytosol protein, it is present in both synaptic and cytosolic fraction [166]. And ß-actin is a ubiquitous protein, it should be present in every fraction [167].

A.1.1. Synaptosome Isolation Confirmation for Diet and Genotype Western Blot Analysis

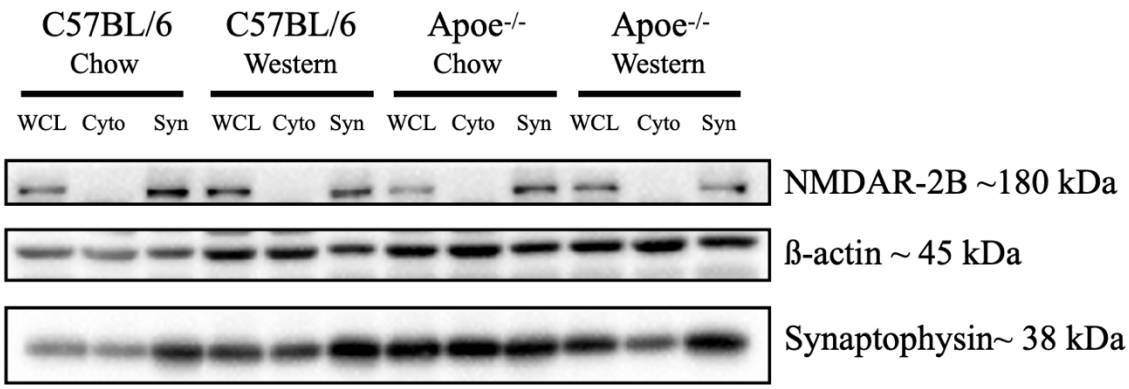

Figure A.1. Observed Band Images for Synaptosome Isolation Confirmation. The figure shows the blot images for brains of animals used to investigate diet and genotype relationship. NMDAR-2B is a post-synaptic receptor, and it is used as synaptic marker. As expected, it is present in synaptosome while absent in cytosol. Synaptophysin as it is synaptic cytosol protein it is present in every fraction. ß-actin as ubiquitous protein present

in all fractions. WCL: Whole Cell Lysate, Cyto: Cytosol, Syn: Synaptosome Chow: Chow Diet, Western: Western Diet

A.1.2. Synaptosome Isolation Confirmation for the PERK Pathway Inhibitor Injection Western Blot Analysis

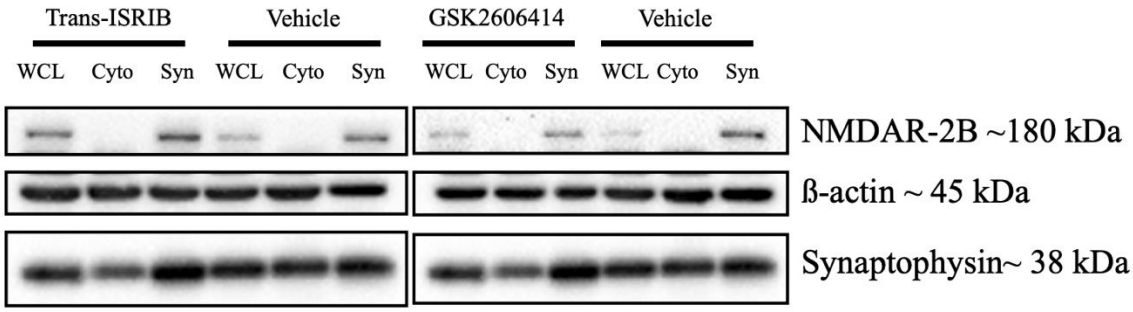

Figure A.2. Observed Band Images for Synaptosome Isolation Confirmation. The figure shows the confirmation experiments for inhibitor injected animals. NMDAR-2B is a post-synaptic receptor, and it is used as synaptic marker. As expected, it is present in synaptosome while absent in cytosol. Synaptophysin as it is synaptic cytosol protein it is present in every fraction. ß-actin as ubiquitous protein present in all fractions. WCL: Whole Cell Lysate, Cyto: Cytosol, Syn: Synaptosome